

THE DETECTION AND FUNCTIONAL CONTRIBUTION OF ALCAM
IN CANCER PROGRESSION

By

Amanda Georgia Hansen

Dissertation

Submitted to the Faculty of the
Graduate School of Vanderbilt University
in partial fulfillment of the requirements

for the degree of

DOCTOR OF PHILOSOPHY

in

Cancer Biology

August, 2013

Nashville, Tennessee

Approved:

Simon Hayward, Ph.D.

Andries Zijlstra, Ph.D.

Harold Moses, M.D.

Barbara Fingleton, Ph.D.

Amy Major, Ph.D.

To my parents and family, whose love and encouragement
have inspired me throughout.

ACKNOWLEDGEMENTS

I am especially thankful to my mentor, Dr. Andries Zijlstra. Through your patience and inquisition, you have played an integral role in my development as an independent scientist. I really admire your tireless efforts, and genuine zeal for science. I must also thank the other members of my committee, Simon Hayward, Hal Moses, Barbara Fingleton, and Amy Major for challenging me and providing guidance through my graduate training. I am thankful for the opportunity to learn from these exceptional researchers.

I would also like to thank all the members of the Zijlstra Lab, past and present. You have made my time in the lab one to cherish. Thanks goes to Trenis Palmer, a dear science buddy, the man with a super-memory. You always had an encouraging word mixed with humor. You helped through the many ups and downs of graduate school. Thanks to Celeste Jones-Paris, the calm, creative presence in lab; Will Ashby, the patient tech guru; Shanna Arnold, an endless resource who has progressed my work in clinical research; Kate Hebron, the spritely new member; and Tatiana Ketova, the force that keeps the lab running.

This work would not have been possible without the invaluable knowledge and assistance from members of the Bone Center, especially Dr. Julie Sterling and Alyssa Merkel. Another group of scientists I need to thank, is to the members of the Moses Lab, you have been integral in providing reagents and support.

Also, thanks to Tracy Cooper at the Vanderbilt Antibody and Protein Resource (VAPR) and the staff at the Epithelial Biology Center Imaging Resource. Thanks also goes to the entire administrative staff of both the Department of Cancer Biology and the Department of Pathology, Immunology and Microbiology. Whit Adams has made PMI my home away from home. Tracy Tveit keeps me motivated and ensures no form goes unsigned. The work in this dissertation was performed in the Department of Cancer Biology at Vanderbilt University from 2007-2013. This work was funded by the following grants: US Public Health Services grants CA120711-01 and CA143081-01 (to A.Z.), T32 HL007751 and P50 CA098131.

Finally, I have a special indebtedness to my friends and family, for these people have invested in ensuring my success and happiness. I am extremely grateful for the friendships I have made through this experience, I would not have traversed this passage in life without all of you. Thank you Mom for being my emotional rock and Dad, for your sarcastic humor. Together, you have been a constant source of sanity, comic relief, love and encouragement. Most importantly, I would like to thank my husband, Nick. Our adventures have been endless and your support unrelenting. To my littlest wonder, Hazel. I am amazed and thankful everyday by your wit and seemingly endless love.

TABLE OF CONTENTS

DEDICATION.....	ii
ACKNOWLEDGEMENTS.....	iii
LIST OF FIGURES.....	vii
LIST OF TABLES.....	ix
ABBREVIATIONS.....	x
Chapter	
I. INTRODUCTION.....	1
Cell Adhesion and Tumor Metastasis.....	1
General Introduction to ALCAM and Cellular Functions.....	4
ALCAM in Hematopoietic Cells.....	8
Role in Development.....	9
Expression in Multipotent & Stem Cells.....	9
ALCAM in the Neural Network.....	10
Interactions with Ligands and Other Proteins.....	10
Expression in the Bone Marrow Microenvironment.....	12
Sub-cellular Localization and Regulation.....	12
ALCAM Shedding.....	13
ALCAM in Cancer.....	14
Summary.....	17
II. ALCAM IS A TGF β RESPONSIVE MARKER AND FUNCTIONAL REGULATOR OF PROSTATE METASTASIS TO BONE.....	20
Introduction.....	20
Materials and Methods.....	23
Results.....	30
ALCAM Gene Expression in Advanced Prostate Cancer and Patient Outcome.....	30
TGF β induces ALCAM Expression and Shedding.....	32
<i>In Vivo</i> Tumor Progression Correlates with ALCAM Shedding.....	35

ALCAM Shedding Mediated by ADAM17.....	39
Knockdown of ALCAM Impairs <i>in vitro</i> TGFβ-mediated Migration & <i>In Vivo</i> Dissemination to Bone.....	42
ALCAM Expression Contributes to Tumor Cell Survival in the Bone Microenvironment.....	45
Discussion.....	49
III. ELEVATED ALCAM SHEDDING IN COLORECTAL CANCER CORRELATES WITH POOR PATIENT OUTCOME.....	56
Introduction.....	56
Material and Methods.....	59
Results.....	68
Correlation of ALCAM and ADAM17 mRNA Expression with Survival of colorectal cancer patients.....	68
Production and Validation of an Antibody Specific for the Cytoplasmic Domain of ALCAM.....	73
Dual Staining of ALCAM in Normal and Tumor Tissue.....	76
Quantitative Analysis of ALCAM Shedding.....	78
ALCAM Shedding Corresponds with Reduced Patient Survival....	81
Discussion.....	85
IV. CONCLUSIONS.....	90
Significance.....	90
Preliminary Data and Future Directions.....	91
Concluding Remarks.....	111
REFERENCES.....	113

LIST OF FIGURES

Figure

1.	ALCAM adhesion and proteolytic regulation.....	6
2.	ALCAM is overexpressed in metastatic prostate cancer and correlates with patient survival.....	31
3.	ALCAM shedding not associated with microparticles.....	33
4.	Expression and shedding of ALCAM is increased in response to TGF β	34
5.	ALCAM shedding correlates with tumor burden.....	36
6.	ALCAM serum half-life in mice.....	37
7.	Immune response modulation does not effect serum ALCAM.....	38
8.	Ectodomain shedding of ALCAM is mediated by ADAM17 <i>in vitro</i> and <i>in vivo</i>	40
9.	Compound 32/ADAM17 Inhibitor dosing <i>in vivo</i>	41
10.	Tumor-derived ALCAM mediates TGF β -induced migration and skeletal metastasis, but not primary growth in the prostate.....	43
11.	Tumor-derived ALCAM impacts metastatic growth, but not incidence after intratibial injection.....	46
12.	Tumor-derived ALCAM impacts tumor survival and proliferation in the bone microenvironment of intratibial bone tumor model.....	47
13.	Tumor-induced osteolysis not affected by decreased ALCAM expression..	48
14.	Effect of ALCAM knockdown on <i>in vitro</i> proliferation.....	53
15.	Multi-species sequence alignment of ALCAM.....	65
16.	ALCAM expression in colorectal carcinoma and its correlation to patient outcome.....	69
17.	ALCAM expression in continuous cancer cell lines.....	70
18.	Lack of cytoplasmic ALCAM corresponds with poor patient outcome.....	72
19.	The specificity of anti-ALCAM ICD antibody confirmed by analysis of ALCAM in ALCAM ^{-/-} mice.....	74

20. Screening and validation of an antibody specific to the cytoplasmic domain of ALCAM.....	75
21. Detection of ALCAM shedding in cancers of the stomach and colon.....	77
22. Quantitative analysis of ALCAM shedding in CRC.....	79
23. The image processing pipeline implemented using FUJI.....	80
24. ALCAM shedding in CRC correlates with poor survival.....	83
25. ALCAM mRNA, protein and shedding in colorectal cancer.....	88
26. ALCAM cytoplasmic domain has a distinct distribution compared to extra-cellular domain.....	93
27. Reduced ALCAM expression results in enhance apoptosis.....	94
28. <i>In vivo</i> inhibition of TGF β does not decrease circulating serum tumor-derived ALCAM.....	100
29. Elevated baseline ALCAM shedding and decreased sensitivity to TGF β in PC3 bone metastatic clones.....	101
30. Bone microenvironment-associated soluble factors provoke ALCAM shedding.....	102
31. Skeletal metastasis of PC3-luc tumor cells in Rag1 ^{-/-} mice after intracardiac injection.....	104
32. Analysis of bone lesions formed by PC3 in Rag1 ^{-/-} after intracardiac injection.....	105
33. ALCAM shedding correlates with bone lesion number and area.....	107
34. Shedding of tumor-derived ALCAM shedding is detectable and responsive to zoledronate in tumor-bearing animals.....	108

LIST OF TABLES

1.	Summary involvement of Immunoglobulin Superfamily (Ig-SF) cell adhesion molecules in the metastatic cascade.....	3
2.	Summary ALCAM antibodies and constructs used for mechanistic studies.....	16
3.	Depiction of ALCAM immunoreactivity for HPA10926.....	63
4.	Comparison of High and Low ALCAM shedding colon cancer.....	82

ABBREVIATIONS

ALCAM	Activated Leukocyte Cell Adhesion Molecule
ANOVA	Analysis of Variance
BMP	Bone Morphogenic Protein
cDNA	Complementary DNA
CAM	Cell Adhesion Molecule
CD	Cluster of Differentiation
CM	Conditioned Media
CRC	Colorectal Cancer
CT	Computed Tomography
DAPI	"4',6-diamidino-2-phenylindole"
DMEM	Dulbecco's Modified Eagle Medium
DMSO	Dimethyl Sulfoxide
DNA	Deoxyribonucleic Acid
ECD	Extracellular Domain
ECM	Extracellular Matrix
EGFR	Epidermal Growth Factor Receptor
ELISA	Enzyme-linked immunosorbant assay
EMT	Epithelial to Mesenchymal Transition
FGFR	Fibroblast Growth Factor Receptor
FBS	Fetal Bovine Serum
GADPH	Glyceraldehyde 3-phosphate Dehydrogenase
ICAM-1	Intercellular Cell Adhesion Molecule
ICD	Intracellular Domain
Ig-SF	Immunoglobulin Super Family
IRB	Institutional Review Board
JNK	c-Jun N-terminal kinases
kDa	kiloDalton
LOH	Loss of Heterozygosity
LPS	Lipopolysaccharide
MCAM	Melanoma Cell Adhesion Molecule
MMP	Matrix Metalloproteinase
mRNA	Messenger RNA
NCAM	Neural Cell Adhesion Molecule
NF- κ B	Nuclear Factor Kappa-light-chain-enhancer of Activated B Cells
OD	Optical Density
PARP	Poly ADP-Ribose Polymerase
PBST	Phosphate Buffered Saline/0.5%Tween-20
PCR	Polymerase Chain Reaction
PDGF	Platelet Derived Growth Factor
PECAM-1	Platelet Endothelial Cell Adhesion Molecule
PKC- α	Protein Kinase C alpha

PMA	Phorbol Myristate Acetate
PMSF	Phenylmethylsulfonyl Fluoride
PSA	Prostate Specific Antigen
PTHrP	Parathyroid Hormone-related Protein
PVDF	Polyvinylidene Difluoride
qPCR	Quantitative Polymerase Chain Reaction
qRT-PCR	Quantitative Reverse Transcriptase PCR
RANKL	Receptor Activator of Nuclear Factor-KappaB Ligand
RNA	Ribonucleic Acid
ROC	Receiver Operating Characteristic
SBE	Smad-binding Element
Scid	Severe Combined Immunodeficient
SDS	Sodium Dodecyl Sulfate
SDS-PAGE	Sodium Dodecyl Sulfate Polyacrylamide Gel Electrophoresis
SEM	Standard Error of the Mean
shRNA	Short Hairpin RNA
siRNA	Small Interfering RNA
SRCR	Scavenger Receptor Cysteine Rich Domain
TGF β	Transforming Growth Factor Beta
TNF α	Tumor Necrosis Factor Alpha
TNM	Tumor Node Metastasis
TRAP	Tartrate-resistant acid phosphatase
VCAM-1	Vascular Cell Adhesion Molecule
VE-cadherin	Vascular Endothelial Cadherin
Δ	Deletion

CHAPTER I

INTRODUCTION

Cell Adhesion and Metastasis

It is estimated that 25% of all deaths in the United States are attributed to cancer-related events (1). Despite significant advances in cancer therapy, the primary cause of morbidity and mortality of cancer is attributable to the departure of tumor cells from their primary site to distant sites and the resistance of these metastatic tumors to current therapies. In the process of tumor cell dissemination to distant sites, tumor cells assimilate normal cell migration processes (2). Modulation of cell adhesion molecules is a key functional component involved in the metastatic process, a complex cascade involving: 1) detachment from the primary site 2) invasion of the extracellular matrix, 3) intravasation and dissemination via haematogenous or lymphatic routes 4) extravasation and migration to target tissues and 5) establishment of a tumor at a secondary site (3). In the early steps of tumor cell detachment from the primary site, epithelial tumor cells undergo dramatic changes leading to the acquisition of a motile phenotype through epithelial-to-mesenchymal transition (EMT) and subsequent changes in intracellular adhesion (4). Tumor cell migration is dependent on a dynamic regulation of adhesion and de-adhesion, reiterating the requirement cellular plasticity of adhesion molecules to facilitate metastatic dissemination (5).

Cell adhesions predominantly function through three main types of cell adhesion molecules (CAMs): cadherins, claudins and immunoglobulin-like cell adhesion molecules (Ig-CAM). Of the three classes of adhesion molecules, the Ig-CAMs are likely to regulate the most diverse array of cellular functions critical to tumor progression and metastasis (Table I; (6)). Ig-CAMs are characterized by a variable number of extracellular immunoglobulin domains and fibronectin type III repeats (7). While most contain a single-pass transmembrane domain and cytoplasmic tail, some are linked to the cell surface through a glycosylphosphatidylinositol anchor (8). Family members include melanoma cell adhesion molecule (MCAM), L1CAM, activated leukocyte CAM (ALCAM), intercellular CAM-1, neural CAM (NCAM), vascular CAM-1 (VCAM-1) and platelet endothelial CAM-1 (PECAM-1). These comprise a diverse group of adhesive receptors fundamental to biological functions ranging from maintaining tissue architecture, establishing homeostasis, controlling cell differentiation, and mediating intracellular communication (6). Consequently, they participate in almost every physiology and pathology including neural development, cellular migration, and tumor cell biology. Not only do immunoglobulin superfamily (Ig-SF) cell adhesion molecules exert their functions through cell-cell and cell-matrix adhesion, they are also able to elicit signals that function in tumor progression. Neural cell adhesion molecule (NCAM) is known for its role in neurite outgrowth, axonal guidance and long term potentiation (9). This prototypical immunoglobulin superfamily cell adhesion molecule (Ig-SF CAM) is known to initiate intracellular communication through activation of fibroblast growth factor receptor (FGFR) or through direct interaction

Stages in Metastasis	Involvement of IgSF Members	
	Known Role	Potential Role
(1) Cell Proliferation in Primary Tumor		
(i) Apoptotic Evasion	NCAM, ALCAM, PECAM-1, ICAM-1	MCAM
(ii) Angiogenesis	PECAM-1, ICAM-1	VCAM
(2) Local Cell Invasion		
(i) Cell-Cell Interactions	MCAM, L1CAM, ALCAM	
(ii) Directional Cell Migration & Polarity	MCAM	ICAM, VCAM, PECAM-1, NCAM, MCAM, L1CAM
(iii) Matrix Degradation	MCAM, NCAM	ALCAM
(3) Invasion and Dissemination		MCAM, ALCAM
(4) Extravasation		MCAM, ALCAM, NCAM, L1CAM, PECAM-1
(5) Colonization and Proliferation	As for (1) and (2)	As for (1) and (2)
(6) Immunological Escape		MCAM, ALCAM, NCAM

Adapted from Wong *et al.*, International Journal of Cell Biology 2012

Table 1. Summary involvement of Immunoglobulin Superfamily (Ig-SF) cell adhesion molecules in the metastatic cascade.

with its cytoplasmic domain with tyrosine kinases, Fyn and Fak (10), resulting in sustained MAPK activation and cell migration (11). Not only is NCAM-dependent FGFR signaling required for *in vitro* epithelial ovarian cancer cell migration and invasion, NCAM expression is clinically correlated with advanced epithelial ovarian cancer tumor grade (12). Studies in endothelial cells overexpressing the Ig-SF CAM, PECAM-1, have shown a reduction in migration. In contrast, expression of the nonphosphorylatable PECAM-1 increased endothelial cell migration, suggesting divergent functions of the intra- and extracellular domains. PECAM-1 intracellular domain associates with SHP-2, a tyrosine phosphatase, to signal changes in phosphorylation of cytoskeletal and focal contact components, highlighting the non-adhesive functions of Ig-CAMs in modulating cellular and molecular behavior (13). On a clinical level, a number of Ig-SF members have been identified as biomarkers of advanced tumor progression, thus understanding the molecular interactions of cell adhesion molecules are critical to understanding metastatic tumor progression.

General Introduction to ALCAM and its cellular functions

Activated Leukocyte Cell Adhesion Molecule (ALCAM)

ALCAM (activated leukocyte cellular adhesion molecule) is a cell surface glycoprotein and immunoglobulin superfamily (Ig-SF) member frequently referred to by its cluster of differentiation (CD) annotation, CD166. Major sites of ALCAM expression include most epithelial cells, hematopoietic cell populations (particularly activated T-cells), the central nervous system, endothelial cells, and most

stem cell populations. ALCAM belongs to a small subgroup of the Ig-SF, defined by five extracellular immunoglobulin-like domains, including two variable (V) and three constant (C) domains (VVC2C2C2). The membrane distal variable region is the ligand-binding domain while the membrane proximal constant regions are responsible for homotypic oligomerization (Fig. 1) (14). ALCAM is a cell–cell adhesion protein that can engage in homophilic (ALCAM–ALCAM), and heterophilic interactions with CD6 (ALCAM–CD6). Although initially identified and primarily expressed in activated leukocytes as the only known ligand for CD6, ALCAM is in fact broadly expressed in human tissues and cells, including neuronal, immune, epithelial, and stem cells of hematopoietic and mesenchymal origin. ALCAM participates in a number of cellular response mechanisms, including T-cell activation and proliferation, angiogenesis, hematopoiesis, and axon fasciculation. Pathologically, ALCAM expression and function have been associated with a number of cancers, including melanoma, prostate cancer, breast cancer, and colorectal carcinoma. The broad biological impact of ALCAM has led to various alternate names, including MEMD, SC-1, DM-GRASP, BEN and CD166. While its capability as an adhesion molecule is clear, the molecular mechanism and function of ALCAM remain unclear. Recent studies in models of tumors and neuron development suggest that it has roles in cell differentiation and vascularization, as well as invasion and migration.

On the cell surface in the blood–brain barrier endothelium, ALCAM is concentrated in cholesterol-enriched microdomains, or lipid rafts (15). In highly specialized lung microvascular endothelial cells, ALCAM is localized to the adherens

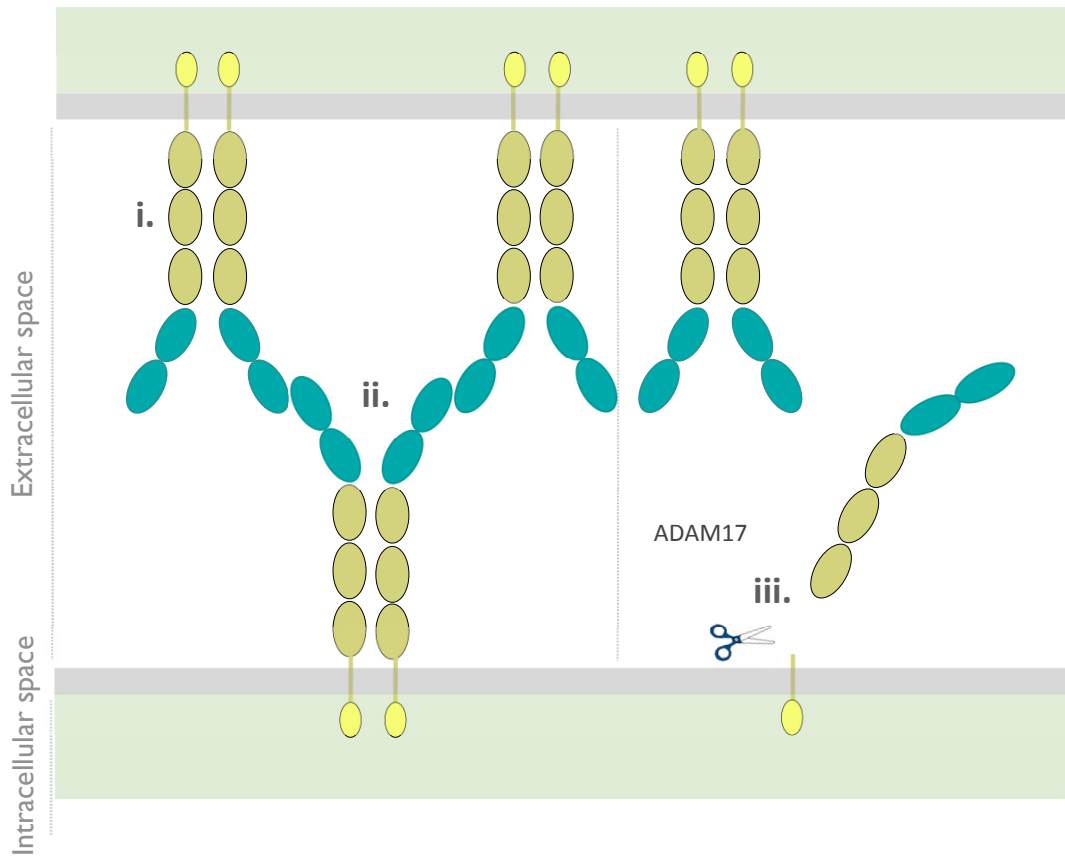


Figure 1. ALCAM adhesion and proteolytic regulation. (i) Oligomerization domain of ALCAM is located at the D3-5 membrane proximal region (ii). Homotypic interactions are mediated through engagement of the terminal amino-D1 domain (iii) ADAM17/TACE is an metalloprotease involved in the processing of ALCAM resulting in the cleavage and release of extracellular ALCAM

junctions, and participates in a complex containing vascular endothelial (VE) cadherin and neural (N) cadherin (16). ALCAM is continuously recycled through endocytic pathways and is readily detectable in early endosomes. On the cell surface, ALCAM co-localizes with clathrin, but not caveolin-1 (17). In several neoplasia, ALCAM overexpression is associated with diffuse cytoplasmic staining (18-20).

ALCAM functions as a cell–cell adhesion molecule and engages in homotypic (ALCAM–ALCAM) and heterotypic (ALCAM–CD6) interactions between adjacent cells. These interactions are mediated through its most amino-terminal V domain (D1). In ALCAM-ALCAM interactions this seems to be a D1–D1 interaction (21,22), while in ALCAM–CD6 interactions the ALCAM D1 domain binds to the membrane-proximal scavenger receptor cysteine rich (SRCR) domain of CD6 (Bowen et al., 1996). ALCAM is also capable of oligomerizing through lateral interactions between adjacent ALCAM molecules in the same cell. These interactions occur through the D3–D5 domains proximal to the membrane (22). ALCAM expression is most apparent at areas of cell–cell contact, where it may interact with other cell–cell adhesion molecules. In fact, upon reconstitution of the α -catenin/E-cadherin complex by α -N-catenin transfection, ALCAM relocalizes to the cell membrane and co-localizes with E-cadherin at the cell membrane in prostate cancer cells. In addition, these cells reverted to an epithelial-like morphology (23) further defining a functional role for ALCAM in cell–cell adhesion. The amino-terminal V-type Ig domain is required for cell–cell adhesive interactions and is, in fact, expressed as an isolated, alternatively spliced isoform (24).

While the participation of ALCAM in several biological processes has been verified, the exact molecular mechanism remains unclear. The highly conserved nature of the short cytoplasmic domain suggests that ALCAM functions, in part, by conveying extracellular signals to the cytoplasm. In spite of the participation of ALCAM in many biological processes, ALCAM knockout mice have been generated and are viable, fertile. These mice exhibit no defects in fertility, nor any outward physiological defects, and have normal organ development and a normal lifespan (25). However, upon detailed analysis, an axon fasciculation defect and a neuromuscular synapse defect have been identified (26). It seems that ALCAM is required for targeting retinal axons to their termination zones in two brain targets: the superior colliculus and the lateral geniculate nucleus (26).

ALCAM in hematopoietic cells

ALCAM received this name when it was identified in activated leukocytes as the only known ligand for CD6 (27), and the ALCAM–CD6 interaction is required for optimal activation of T-cells (28-31). *In vitro* affinity and kinetic binding analysis revealed a 100-fold weaker homophilic interaction compared to CD6–ALCAM heterotypic interaction. Moreover, ALCAM plays a critical role in mediating the transmigration of T-cells and monocytes across the blood–brain barrier (15,32). Through its heterotypic interaction with CD6, ALCAM seems to be important for formation of the immunological synapse at the T-cell:antigen-presenting cell (APC) interface during antigen presentation (33). In fact, optimal T-cell activation requires CD6–ALCAM engagement (29,34). Moreover, unlike other adhesion

molecules in the immunological synapse, ALCAM is required for the whole process of T-cell activation (31).

Role in Development

ALCAM is expressed in human blastocysts, but not in embryos at the 8-cell or morula stages. ALCAM expression reappears in most developing tissues (35-38). Nevertheless, the adhesive role of ALCAM is apparent in development, where the loss of ALCAM function results in loss of cell adhesion and cardiac morphogenesis in the *Xenopus* model system (39). Using injection of morpholinos targeting ALCAM into zebrafish, coupled with rescue experiments expressing ALCAM mRNA, Choudhry and colleagues determine that ALCAM is essential for ventral cartilage development (40). In this same study, endothelin-1, a known mitogenic peptide in several cancers, was able to modulate ALCAM expression through stabilization and prevention of proteosomal degradation. ALCAM functions in hematopoietic and endothelial development and is highly associated with hematopoiesis and vasculogenesis (41). Neuronal outgrowth studies in chick and zebra fish further define ALCAM as a guidance protein for cellular migration and neuronal outgrowth during development (35,42,43).

Expression in multipotent and stem cells

Although ALCAM was initially used to delineate hematopoietic stem cells (44), the molecule has been used broadly as a surface marker (under the name CD166) in a panel of markers (including CD44, CD90, CD105, CD73, CD29 and

CD133) to define multipotent cells from a variety of tissues, including umbilical cord blood (45), bone marrow (46), testes (47), fetal lung (48), intervertebral disc (49), and dental pulp (50). More recently, the expression of CD166 as a marker of cancer stem cells has become of significant interest (51-54). While ALCAM is clearly a defining feature of stem cells, it is unclear if there is a functional contribution to the multipotent capacity of these cells.

ALCAM in the neural network

The abundance of ALCAM in neuronal tissue is reflected in its sequential discovery in neurons and related tissues from various species as DM-GRASP (55), SC-1 (21), neurolin (56), and BEN (57). ALCAM controls the extension of axons (43,58-60) and is involved in axonal guidance and mapping (26,61). While ALCAM knockout mice are outwardly normal in appearance, they do have physiological deficiencies, including a delay in maturation of neuromuscular junctions and defects in axon fasciculation (25,26). ALCAM-blocking antibodies induce aberrant branching in zebra fish motor axons during development (43). During *in vitro* experiments axon outgrowth can be guided by ALCAM-coated surfaces, thereby providing conclusive evidence of ALCAM as a migration-guiding factor (58,59).

Interactions with Ligands and other proteins

In addition to the well established homophilic interactions, ALCAM was identified as the only known ligand for CD6, a member of the SRCR protein su-

perfamily (22,27). In contrast with the relatively weak and transient homophilic ALCAM–ALCAM interactions, ALCAM–CD6 interactions are robust and persistent (34,62). These interactions are thought to be important for T-cell proliferation and maturation (31). In both instances it is the amino-terminal V domain that is engaged in the protein–protein interactions. For neuronal guidance, ALCAM has been suggested to interact with L1CAM (L1-cellular adhesion molecule, also known by the chick homolog NgCAM). This interaction seems to target retinal axons during development (26,58,63).

ALCAM co-localizes with E-cadherin through an α -catenin-dependent process, although no direct interaction has been confirmed (23). ALCAM also requires active protein kinase C alpha (PKC- α) for ALCAM-mediated cell adhesion (64). While no physical association between these proteins has been confirmed, ectopic expression of in K562 leukemic cells activates PKC, leading to cell clustering (65). Association with the actin cytoskeleton is confirmed and regulates ALCAM clustering. Though interactions that connect ALCAM to the cytoskeleton are unknown (62,66), preliminary findings from Sawhney *et al.* (19) suggest the scaffolding proteins 14-3-3 ζ and 14-3-3 σ may be involved.

Though little is known about the cytoplasmic tail, it has been shown to be ubiquitinated. Ubiquitination seems to control ALCAM endocytosis and thereby affect its role in axon navigation (67). ALCAM was also shown to interact with EGFR (68); however, this observation was made in an epidermoid carcinoma cell line (A431) and has not been confirmed elsewhere. Recently, ALCAM was shown to specifically bind galectin-8 sequestered in the extracellular matrix (69). This

interaction influenced endothelial cell migration and tubule morphogenesis. Anti-ALCAM antibody studies suggest that this interaction involves the same domain that is required for homotypic ALCAM–ALCAM, as well as CD6, binding.

ALCAM in the bone marrow

ALCAM was defined initially as a hematopoietic cell antigen present in bone marrow (70,71). Indeed, ALCAM is a surface marker of the earliest hematopoietic precursor populations, the mesenchymal stem cells, and stromal cell populations present in the bone (72-74). Along with CD90 and CD105, ALCAM defines a multipotent progenitor cell population capable of chondrogenic, osteogenic and adipogenic differentiation (75-77). Early observations by Bruder et al. indicated a functional role for ALCAM in the bone marrow. They determined that anti-ALCAM fragment, antigen binding (Fab) fragments promote osteogenic differentiation (72). Indeed ALCAM delineates subpopulations of the endosteal niche, where its expression defines populations of mature osteoblasts and mesenchymal stem cells (74,78,79). In particular, Chitteti et al. defined mature osteoblasts specifically as CD45⁻CD31⁻Ter119⁻Sca1⁻ALCAM⁺ (79).

Subcellular localization and Regulation of Activity

On the cell surface in the blood–brain barrier endothelium, ALCAM is concentrated in cholesterol-enriched microdomains, or lipid rafts (15). In highly specialized lung microvascular endothelial cells, ALCAM is localized to the adherens junctions, and participates in a complex containing vascular endothelial (VE)

cadherin and neural (N) cadherin (16). ALCAM is continuously recycled through endocytic pathways and is readily detectable in early endosomes. On the cell surface, ALCAM co-localizes with clathrin, but not caveolin-1 (17). In several neoplasias, ALCAM overexpression is associated with diffuse cytoplasmic staining (18-20).

Since cell–cell adhesion is the primary activity of ALCAM, adhesive interactions can be regulated by its availability and ability to bind to proximal partners. ALCAM is dysregulated in a number of cancers, including, but not limited to, melanoma, colorectal, breast and prostate. Immunohistochemical analysis showed that ALCAM was overexpressed in low-grade carcinoma. However, in some high grade carcinomas ALCAM was either localized to the cytoplasm or lost altogether (18,80-82). Although there is differential ALCAM expression in cancer, the mechanism by which it is regulated is unknown.

At the subcellular level, cytoskeleton disruption, via chemical treatment in erythroleukemic K562 cells with cytochalasin D, promotes lateral movement of ALCAM and promotes ALCAM-mediated adhesion regulated through cytoskeleton-dependent clustering (66), This effect suggests ALCAM clustering is necessary to form stable cell adhesion complexes (14,22).

ALCAM Shedding

Similar to other cell adhesion molecules, ALCAM can be proteolytically shed from the cell surface. Currently ADAM17, a member of the disintegrin and metalloproteinase family, is the only known protease able to cleave ALCAM (Fig.

1; (83)). ADAM17, initially identified as the enzyme cleaving TNF α from its transmembrane precursor form (84), is a promiscuous “shedase” involved in cleavage of many other immunoglobulin superfamily cell surface proteins including ICAM-1 (85), VCAM-1 (86), NCAM (87), and L1CAM (88). Cleavage of ALCAM is thought to occur at the membrane proximal region, generating a soluble ALCAM component containing the five extracellular domains and a truncated membrane-bound ALCAM containing the transmembrane and cytoplasmic domains. Proteolytic release of ALCAM can be induced by non-specific agents, including phorbol myristate acetate (PMA) or ionomycin, and through epidermal growth factor receptor stimulation (89). It has been reported that inhibition of ADAM17 with CGS27023A inhibitor in TPC-1 cells results in a dose-dependent decrease in shed ALCAM in culture media (90). Interestingly, the expression of the soluble D1 domain (sALCAM, the most amino-terminal V domain) (24) could potentially disrupt the interaction between full-length membrane-anchored ALCAM molecules (14), however it is currently unclear how shed ALCAM can compete with *cis* or *trans* ALCAM-ALCAM interactions. ALCAM concentrations in the cell can be regulated by expression, endocytosis, and shedding from the cell surface. The studies presented here are some of the first to investigate the parameters that change ALCAM shedding and connect this biology with patient outcome.

ALCAM in cancer

Cancer-associated ALCAM was first identified as MEMD in melanoma cell lines (91). ALCAM has subsequently been found to be expressed in almost all

cancers, although it is distinctly absent in myeloma. Even though the pathological function of ALCAM is not fully understood, *in vivo* mouse studies demonstrate its participation in cancer progression (92-94). Truncation of ALCAM can be achieved by ADAM17 and may facilitate migration (89). Indeed the upregulation of truncated ALCAM that lacks the D1 domain (Δ N-ALCAM) promotes metastasis, while the ectopic expression of soluble amino-terminal D1 (V) domain inhibits metastasis (Table 2, (14,93). The distinct up regulation of ALCAM in some cancers but down-regulation in others has created a paradox in terms of its contribution to cancer progression (95). Histological analysis has emphasized that the cytoplasmic localization of ALCAM correlates more strongly with cancer progression than the overall expression level (18,19,81,96). Although somewhat contradictory, recent research using blocking antibodies confirms that the presence of ALCAM can contribute to the metastatic process (96,97), while expression analysis illustrates that the absence of ALCAM can convey resistance to treatment (98). It is likely that the role of ALCAM in cancer is context-dependent and its function is influenced by tissue from which the tumor originated.

In recent years ALCAM expression has been used as a biomarker of cancer progression in prostate cancer (99), colorectal cancer (20), breast cancer (98,100-102), oral cancers (19), pancreatic cancer (96,103), neuroblastoma (104), ovarian cancer (81), gastric cancer (105) and melanoma (106). Serum levels of ALCAM have also been explored as a diagnostic tool for cancer (107-112). The studies presented within this thesis explore the relationship between

	Description	Function	Known Activity
anti-ALCAM Neutralizing mAb	ALCAM Neutralizing mAb	Block ALCAM binding ability	Inhibits migration
wALCAM	Intact WT protein	Engage in cell-cell binding	Regulation of migration
sALCAM	Soluble ALCAM (sALCAM).	Natural, soluble antagonist	Inhibits Metastasis
ΔNALCAM	Truncated ALCAM (ΔNALCAM)	Unknown	Promotes Metastasis

Table 2. Summary ALCAM antibodies and constructs used for mechanistic studies

ALCAM expression and ALCAM shedding while correlating these parameter to patient outcome (113).

Summary of Dissertation

The dissemination of prostate cancer to bone is a common, incurable aspect of advanced disease. Prevention and treatment of this terminal phase of prostate cancer requires improved molecular understanding of this process as well as markers indicative of molecular progression. The goal of my dissertation research was to investigate the contribution of tumor-derived ALCAM in prostate tumorigenesis *in vivo*, and the clinical application of intratumoral ALCAM shedding in colorectal cancer progression.

In Chapter II, I demonstrate, using biochemical analyses and *in vivo* loss-of-function studies that the cell adhesion molecule ALCAM is actively shed from metastatic prostate cancer cells by the sheddase ADAM17 in response to TGF β . Not only is this post-translational modification of ALCAM a marker of prostate cancer progression, the molecule is also required for effective metastasis to bone. Biochemical analysis of prostate cancer cell lines reveal that ALCAM expression and shedding is elevated in response to TGF β signaling. Both *in vitro* and *in vivo* shedding are mediated by ADAM17. Longitudinal analysis of circulating ALCAM in tumor-bearing mice revealed that shedding of tumor, but not host-derived ALCAM is elevated during growth of the cancer. Gene-specific knock-down of ALCAM in bone-metastatic PC3 cells greatly diminished both skeletal dissemination and tumor growth in bone. The reduced growth of ALCAM knock-

down cells corresponded to an increase in apoptosis and decreased proliferation. Together these data demonstrate that the ALCAM is both a functional regulator as well as marker of prostate cancer progression.

In Chapter III, we introduce the concept that molecular biomarkers of cancer are needed to assist histological staging in the selection of treatment, outcome risk stratification, and patient prognosis. This is particularly important for patients with early-stage disease. We demonstrate that shedding of the extracellular domain of ALCAM (Activated Leukocyte Cell Adhesion Molecule) is prognostic for outcome in patients with colorectal cancer (CRC). Previous reports on the prognostic value of ALCAM expression in CRC have been contradictory and inconclusive. This work clarifies the prognostic value of ALCAM by visualizing ectodomain shedding using a dual stain that detects both the extracellular and the intracellular domains in formalin-fixed tissue. Using this novel assay, 105 primary colorectal cancers patients and 12 normal mucosa samples were evaluated. ALCAM shedding, defined as detection of the intracellular domain in the absence of the corresponding extracellular domain, was significantly elevated in CRC patients and correlated with reduced survival. Conversely, retention of intact ALCAM was associated with improved survival, thereby confirming that ALCAM shedding is associated with poor patient outcome. Importantly, analysis of stage II CRC patients demonstrated that disease-specific survival is significantly reduced for patients with elevated ALCAM shedding ($p=0.01$, HR 3.0) suggesting that ALCAM shedding can identify patients with early stage disease at risk of rapid progression.

The current data relating to ALCAM in tumorigenesis span a little over a decade, however future studies will likely provide more mechanistic insight into the paradoxical function of cell adhesion molecules in cancer. ALCAM participates in a number of diverse roles in human pathology including stem cell maintenance, cellular migration, and suppression of apoptosis, all properties that can be co-opted by tumor cells to facilitate cancer progression. The ultimate goal of this dissertation was to gain a better understanding of ALCAM's role in tumor cell invasion and metastasis. Together, our data and previously published literature, strongly suggest ALCAM to be a contributor to cancer progression. Future studies using intratumoral ALCAM shedding as a biomarker would advance early stage screening for aggressive disease, potentially leading to the identification of high risk patients and providing an opportunity for effective treatments.

CHAPTER II

ALCAM/CD166 IS A TGF β RESPONSIVE MARKER AND FUNCTIONAL REGULATOR OF PROSTATE CANCER METASTASIS TO BONE

INTRODUCTION

Morbidity and mortality among prostate cancer patients is frequently a result of metastatic dissemination to bone (114,115). To date there is no curative treatment for skeletal metastasis, and this growth of tumor in bone results in bone loss, fractures, and pain (116). Even for patients with organ-confined disease, the method and rigor of clinical intervention is defined in large part by the risk of disease progression. For patients with skeletal events, survival from the time of diagnosis to time of death is approximately 3-5 years (117). Thus, clinical intervention would greatly benefit from further understanding of the molecular mechanisms that drive skeletal metastasis as well as molecular indicators that identify patients at risk of disease progression. Since cell motility is an important contributor to metastasis, the activation state of migratory mechanisms could be suitable for both therapeutic intervention as well as a biomarker of metastatic behavior.

Tumor cell metastasis to distant sites, including bone, is a multi-step process. Cancer cells must first detach from the primary tumor site and migrate locally to invade blood vessels. Thereafter, tumor cells intravasate into the bloodstream and are attracted to preferred sites of metastasis through site-specific cel-

lular and microenvironmental interactions (5,118). Activated Leucocyte Cell Adhesion Molecule (ALCAM) is a cell adhesion molecule that engages in homotypic and heterotypic cell adhesion in a calcium-independent manner (22). It has been implicated in a number of adhesive and migratory behaviors including axonal guidance, leukocyte homing and cancer metastasis. It has been demonstrated that ALCAM can be proteolytically cleaved at the cell surface by ADAM17 causing the ectodomain to be shed. ALCAM shedding can be induced by ionomycin, PMA, and epidermal growth factors (89). Proteolytic cleavage/shedding of cell surface proteins is a common regulatory mechanism which can alter the function and localization of transmembrane proteins such as cell adhesion molecules, growth factors and growth factor receptors. This regulation can weaken cell adhesion and destabilize adherens junctions as in the case of E-cadherin, through the loss of homotypic cell adhesion molecular interactions (119). The soluble shed ectodomain can act as an antagonist, thereby competing for membrane-bound receptors or cell adhesion molecules. While these processes are important in development, they have also been associated with tumorigenesis. Functionally, expression of the truncated, trans-membrane fragment of ALCAM in BLM melanoma cells results in increased lung metastasis *in vivo*, while overexpression of a soluble extracellular ligand-binding fragment diminished metastases (for review see (94) and (120)). Previous studies from our lab and others have investigated the clinical relevance of ALCAM expression and shedding in a variety of human malignancies, including colorectal, breast, ovarian, thyroid and prostate

cancer, however its role in tumorigenesis remains unclear (80,81,90,113,121,122).

Elevated ALCAM expression in aggressive prostate cancer (99) together with its putative role in cell adhesion/migration (93,94) suggests that ALCAM is a molecular participant in prostate cancer metastasis. We hypothesized that ecto-domain shedding of ALCAM is induced by cytokines present in the tumor microenvironment and that its detection can be a marker of tumor progression. This work herein investigates ALCAM expression and shedding by ADAM17 in response to cytokine stimulation through biochemical analyses while its contribution to skeletal metastasis is determined in a series of orthotopic, and experimental metastasis models. We have identified transforming growth factor-beta (TGF β), a pleiotropic cytokine that regulates growth, cell motility, development and differentiation, as a driver of ALCAM expression and shedding. TGF β signaling is frequently dysregulated in prostate cancer and is considered instrumental in the tumor microenvironment whereby it influences both tumor progression and metastasis (123-126). Findings from these investigations provide important insight not only into the molecular correlation between ALCAM and prostate cancer progression but also demonstrate that ALCAM is a key functional contributor to metastatic growth in the bone.

MATERIALS AND METHODS

Reagents, cell culture. Full-length purified recombinant porcine TGF β was obtained from R&D Systems . Antibodies against ALCAM were obtained from R&D Systems (Clone 105902). The following tumor cell lines were obtained from American Type Culture Collection (Manassas, VA) and maintained according to the American Type Culture Collection's recommendations: DU145, LNCaP, PC3 (prostate metastasis). PC3-luciferase (PC3-luc) cells (Dr. Ken Pienta, University of Michigan) were cultured in RPMI/10%FBS.

SDS-PAGE and immunoblotting. Cells (2.5×10^5) were plated in 6-well dishes. After 24 h, cells were serum starved in Opti-MEM for 16 h and then treated in the presence or absence of indicated growth factors or inhibitors, for 48 h. After that, the cells were lysed in TNE Lysis Buffer (20 mM Tris-Cl [pH 7.4], 0.5 mM EDTA, 1% Triton X-100, 150 mM NaCl, protease inhibitor cocktail (Sigma), 1 mM phenylmethylsulfonyl fluoride (PMSF). Total protein in the lysates was quantified using BCA assay (BioRad). Conditioned media samples were concentrated with microcon centrifugal filters (Millipore) following manufacturers protocol, which were eluted directly in 5X sample buffer for Western blot analysis. Protein loading for conditioned-medium samples for Western blot analysis was adjusted according to the total protein in cell lysates. Conditioned media and total protein was subjected to SDS-PAGE and electrophoretic transfer to polyvinylidene difluoride

membranes (Immobilon P, Millipore, Inc., Bedford, MA). Immunodetection was by conventional chemiluminescence.

Quantitative PCR. The mRNA samples were prepared from tumor cells lysed in TRI Reagent (Ambion) and purified using phenol extraction, followed by real-time polymerase chain reaction (RT-PCR). The following qPCR primers were used ALCAM, TCAAGGTGTTCAAGCAACCA (forward) and CTGAAATGCAGT-CACCCAAC (reverse); ADAM17, ATGTTTCACGTTTGCAGTCTCCA (forward) and CATGTATCTGTAGAAGCGATGATCTG (reverse); and glyceraldehyde-3-phosphate dehydrogenase, ATCTTCTTTTGCGTCGCCAG (forward) and TTCCCATGGTGTCTGAGC (reverse).

ShRNA Knockdown. To establish cell lines in which ALCAM expression is stably knocked down cells were transduced with ALCAM-specific “Mission” shRNA (Sigma) lentivirus. Following transduction, cells were selected in 10 μ g/ml of puromycin. Transduced cells were flow sorted for ALCAM expression and ALCAM knock-down cells were cultured and maintained on 5 μ g/ml of puromycin.

Migration Assay. Two-dimensional gap closure assays (formerly known as scratch assays) were conducted using magnetically attachable stencils attached to culture plates (127). In short, 250,000 cells were seeded in 6-well plates and allowed to recover overnight to form a confluent monolayer. Stencils were removed with tweezers, after which cells were rinsed with PBS to remove detached

cells. Culture medium was re-added and closure of the gap was measured at 8 and 16 hours. Gap closure was quantified using TScratch (National Institutes of Health, Bethesda, MD, USA).

Mouse models of acute inflammation. All animal handling was performed in accordance with institutional guidelines and approved by the Vanderbilt Institutional Animal Care and Use Committee. C57BL/6(SJL)-Tg(SMAD binding element [SBE]/Tk-luc)^{7Twc/J} mice (128), obtained from the laboratory of Harold Moses, MD (Vanderbilt University), were used at 16 weeks of age. These transgenic mice, referred to as SBE-Luc mice, express luciferase in response to activation of the Smad2/3-dependent signaling pathway. Mice were administered 2mg/kg of LPS to induce an acute inflammatory response and bled via saphenous vein at 0, 6, 24 hours and 1 week post-administration.

Mouse models of wound-healing Wounding was performed on mice anesthetized with isofluorane. In brief, the mouse backs were shaved, back skin and *panniculus carnosus* was pulled up, and a sterile standard biopsy punch tool was used to create two circular excisional full-thickness wounds of 6-mm diameter described previously (129). Mice were bled via saphenous vein at 0 hours (establish basal levels), 24 hours, one week and two weeks after wound initiation.

In vivo ALCAM serum half-life. Serum was harvested from ALCAM wild-type, mixed background, mice and pooled. Combined serum collected from WT mice

was injected retroorbitally in ALCAM KO mice (100 μ l/mouse). ALCAM KO mice were pre-bled via saphenous vein bleed, and then bled at 10 mins, 2 hours, 4 hours, 24 hours and 48 hours (n=2/time point; total n=10). WT pooled serum was used as ELISA control to quantitatively determine ALCAM serum half-life.

Histological analysis of mouse tissue. Tumor-bearing tissue and bones were fixed in 10% formalin. Bone specimens were decalcified in 20% EDTA pH 7.4 for 3-4 days at room temperature. Decalcified bone and tissue were dehydrated and embedded in paraffin. Tumor burden was confirmed in 5 μ m serial sections stained with H&E. Osteoclast were visualized using a standard Tartrate Resistant Acid Phosphatase (TRAP) protocol. All immunohistochemistry and immunofluorescence on tumor sections involved antigen retrieval using a standard pH 6.0 citrate buffer followed by blocking via incubation with 20% Aquablock (East Coast Bio). Immunofluorescence data was obtained using primary antibodies for ALCAM (1:1000; Leica Biosystems; Clone, MOG/07), Ki67 (1:500; Fisher, Clone SP6), Cleaved caspase-3 (1:200; CellSignaling, D175), and collagen I (1:1000; Sigma C2206) by incubation overnight at 4°C. Corresponding Alexa Fluor® secondary antibodies were used (1:1000; Invitrogen). Fluorescent imaging was completed on a Olympus BX61WI upright fluorescent microscope using Velocity Imaging Software.

ELISA of mouse serum and plasma. Blood was obtained via the saphenous vein; samples were collected in either the presence of EDTA as an anticoagulant

or a serum separator tube (Fisher Scientific) and were centrifuged at 1,500 rpm, 4°C to remove cells. Plasma and serum samples were stored at –80°C until analyzed. Samples were analyzed for soluble mouse and human ALCAM using the R&D Systems DuoSet following manufacturers instructions. Briefly, ELISA plates coated with capture antibody were incubated overnight with 100 µl of sera diluted 1:50. Capture ALCAM was detected with biotinylated antibody and peroxidase-conjugated avidin followed by colorimetric detection at 450 nm.

Mouse models of prostate cancer and in vivo quantitation of tumor growth.

All experimental protocols were approved by the Vanderbilt University Institutional Animal Care and Use Committee. Orthotopic prostate xenografts were performed according to Li et. al (130). Briefly, 5×10^4 PC3-luc cells were suspended in 30 µl of neutralized type I collagen and allowed to polymerize for 16 hrs at 37°C before implantation into the prostate of 10 week old C.B-17/lcrHsd-Prkdc scid male mice (Harlan). Tumor growth was monitored weekly by bioluminescent detection of luciferase expressing cells. For the xenograft model, sub-confluent PC3-luc cells were trypsinized, washed twice in PBS to remove serum, and then resuspended in HBSS at a concentration of 1×10^7 cells/ml. One hundred µl containing 1×10^6 PC3 cells in a 50/50 mix of PBS and growth factor-reduced Matrigel (BD Biosciences) were injected subcutaneously into the right flank of 7-week-old nude male mice (Harlan Laboratories; athymic Foxn1 nu/nu). Tumor growth was monitored weekly by caliper measurements, and tumor volume in mm³ was calculated based on the following formula: Volume = (width)² x length/2. PC3-

luciferase shControl (Vector) or PC3-luciferase shALCAM (KD2 or KD3) tumor cells (1×10^5) in a 10 μ l volume of sterile phosphate buffered saline (PBS) were injected into the tibia of anesthetized 6-week-old nude male mice (Harlan Laboratories). Skeletal metastasis was performed as previously described by Park et. al. (131). Briefly, 1×10^5 PC-3-luc cells were injected into the left heart ventricle of male nude mice (Harlan Laboratories). Skeletal metastases were monitored by bioluminescent detection of luciferase expressing cells and formation of bone lesion by X-ray. Whole animal luminescent imaging was performed with the IVIS™ system (Caliper Life Sciences, Hopkinton, MA). Luciferin (150 mg/kg in sterile PBS, Biosynth International, Itasca, IL) was delivered via intra-peritoneal injection 10 minutes prior imaging. Living Image™ software (Caliper Life Sciences) was used to quantify the luminescence intensity. Blood was obtained via the saphenous vein and collected in either the presence of EDTA as an anticoagulant or a serum separator tube (Fisher Scientific). Plasma and serum samples were stored at -80°C until analyzed.

Micro computed tomography (μ CT) analysis. For gross analysis of trabecular bone volume, formalin fixed tibiae were scanned at an isotropic voxel size of 12 μ m using a microCT40 (SCANCO Medical, Bruttisellen, Switzerland). The tissue volume (TV) was derived from generating a contour around the metaphyseal trabecular bone that excluded the cortices. The area of measurement began at least 0.2 mm below the growth plate and was extended by 0.12 mm. The bone volume (BV) included all bone tissue that had a material density greater than 438.7 mgHA/cm³.

Radiographic Analysis. Beginning 1 week after tumor cell inoculation, tumor-bearing animals were subjected to radiographic imaging. Radiographic images (Faxitron X-ray Corp, Lincolnshire, IL, USA) were obtained using an energy of 35 kV and an exposure time of 8 seconds. Osteolytic lesions were quantified bilaterally in the tibia, fibula, femora, humeri, and pelvis at the endpoint using x-ray images. Lesion area and lesion numbers were evaluated using image analysis software (Metamorph, Molecular Devices, Inc.). Data presented are the average of lesion area and lesion numbers per mouse in each group.

Statistical Analyses. Expression analysis was performed on datasets GDS1439 and GSE10645 available through the Gene Expression Omnibus (references (132) and (133) respectively). Expression data for selected genes from GDS1439 was clustered in software Cluster 3.0 and visualized with software TreeView. For survival analysis the patient population of GSE10645 (n=596) was dichotomized across upper and lower quartile of ALCAM expression. Statistics were completed using either R, SPSS or GraphPad Prism. For all standard bar and box plots the results were reported as mean and SEM unless stated otherwise in the legend. Comparisons were performed using unpaired two-sided Student's t-test, non-parametric Mann-Whitney test, or one-way ANOVA. R² and P values were reported from linear regression analysis of mouse data. All statistical tests were considered significant when $p < 0.05$ where * denotes $p < 0.05$, ** denotes $p < 0.01$ and *** denotes $p < 0.001$.

RESULTS

ALCAM gene expression is elevated in advanced prostate cancer and correlates with poor patient outcome. Changes in ALCAM expression have been linked to patient outcome for several malignancies. In prostate cancer the correlation of ALCAM expression and patient outcome are sometimes conflicting. Minner et. al. (122) conclude that reduced ALCAM expression correlates to poor patient outcome while the opposite is suggested by Kristiansen et. al. (99). We evaluated several publicly available microarray datasets to determine the relationship between ALCAM mRNA levels, patient diagnosis and outcome (Fig. 2). A comparison of benign, localized and metastatic disease revealed increased levels of ALCAM mRNA in metastatic prostate cancer (Fig. 2A, GDS1439). Elevated levels of ALCAM coincided with molecular evidence of a pro-migratory phenotype based on the decreased expression of E-cadherin and p120 concurrent with elevated expression of N-cadherin (Fig. 2B). These observations were supported by survival analysis for a cohort of 596 prostate cancer patients (GSE10645) which revealed that high levels of ALCAM mRNA corresponded with poor patient outcome. (Fig. 2C). Immunohistological staining of prostate cancer tissue microarrays available through the Human Protein Atlas (134) revealed that ALCAM is clearly evident in normal, benign and malignant disease but is frequently absent from the tumor cell surface in advanced disease (proteinatlas.org, Fig. 2D).

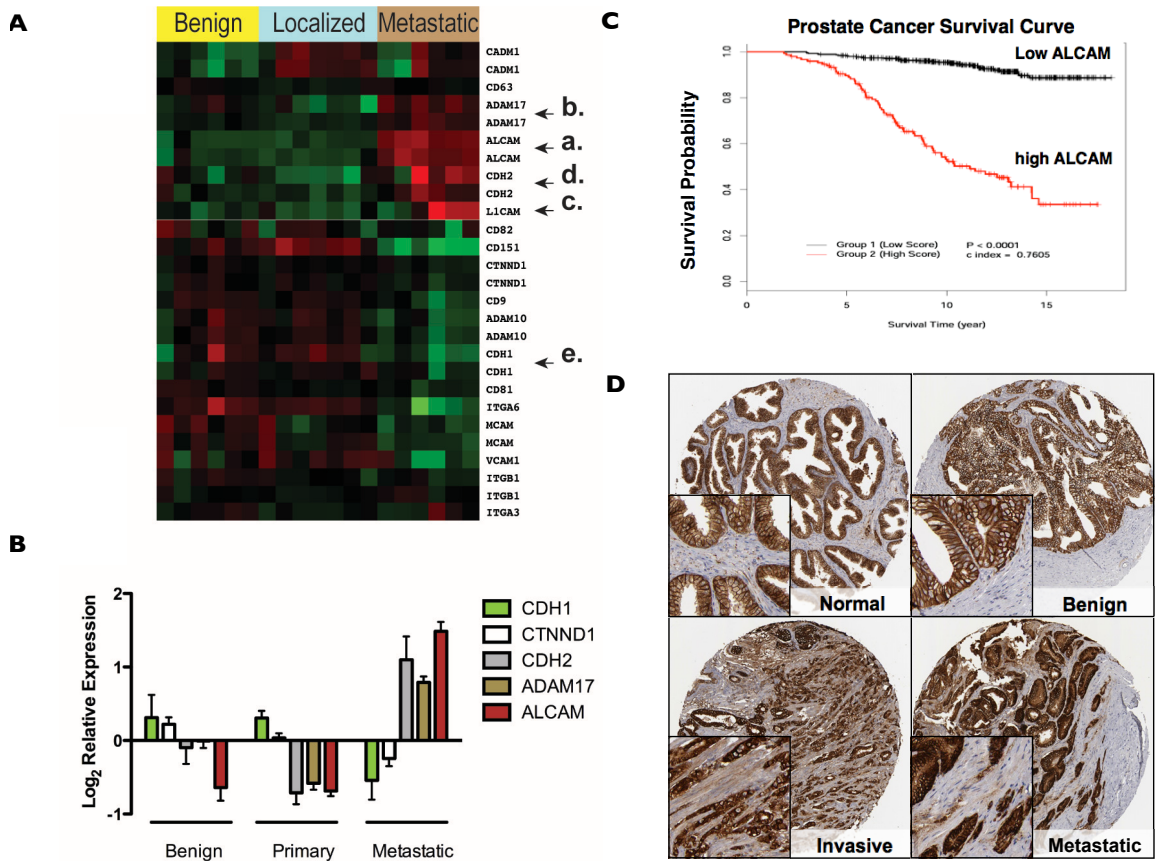


Figure 2: ALCAM is overexpressed in metastatic prostate cancer and correlates with patient survival. (A) ALCAM expression levels were analyzed in publicly available dataset (GDS1439, n=19) of prostate cancer. Heat map (A) and corresponding relative expression (B) of ADAM17 (i) ALCAM (ii) N-cadherin (iii), p120 (iv) and E-cadherin (v) indicated by arrows. (C) Correlation of ALCAM expression to overall survival in a publicly available dataset (GSE10645) composed of 596 prostate cancer patients. Kaplan-Meier survival curves represent the upper and lower quartile ALCAM expression. (D) Representative images from immunohistochemical staining of ALCAM membranous and cytoplasmic expression in benign to metastatic prostate cancer. Images obtained through The Human Protein Atlas.

TGF β induces ALCAM expression and shedding. Since ALCAM shedding is associated with disease progression, we set out to determine if cytokines associated with cancer progression could promote ALCAM shedding *in vitro*. ALCAM is proteolytically shed from PC3 cells (Fig. 3). Absence of the cytoplasmic tail confirms that the ectodomain is shed (Fig. 3A). Moreover, ALCAM is absent from PC3-derived exosomes, ensuring that the ectodomain is shed and not released with cell-derived microparticles (Fig. 3B). Since prostate cancer disseminates predominantly to bone we selected cytokines thought to be involved in this process, including TGF β . Of the 8 agents tested, only TGF β was able to promote ALCAM shedding relative to overall total protein increase (Fig. 4A). To further explore the response to exogenous stimulation with TGF β , ALCAM expression in PC3 cells was compared to ALCAM expression in LNCaP cells which are unable to respond to the cytokine possibly due to a lack in the TGF β receptor type I or mutation of the TGF β type II receptor (135) (Fig. 4B and C). Quantitative RT-PCR analysis for ALCAM demonstrates that TGF β was also able to induce ALCAM gene transcription in PC3 but not LNCaP cells (Fig. 4B). The cytokine also increased levels of ALCAM protein expression and ectodomain shedding (Fig. 4C). Conversely, LNCaP did not respond to TGF β , even though these cells express abundant ALCAM (Fig. 4C). TGF β -induced expression in PC3 cells could be abrogated with the small molecule inhibitor SB431542 (Fig. 4D, 10 μ M; Sigma) while TGF β -induced ALCAM mRNA and protein expression could be restored in LNCaP cells when the cells were transfected with dominant-active TGF β receptor type I (Fig. 4E&F).



Figure 3. ALCAM shedding in prostate tumor cells is not associated with microparticles. A) Western blot analysis of ALCAM shedding in conditioned media of LNCaP and PC3 cells treated with or without 10ng/ml of TGFβ using antibodies specifically recognizing the extracellular and intracellular domains. **B)** ALCAM shedding in response to 10ng/ml TGFβ after 48 hours as measured by Western blotting of ALCAM and CD151 (exosome marker) in PC3 tumor cell conditioned media. Conditioned media was ultracentrifuged to isolate exosome fraction; “Total CM” = total conditioned media, “CM Supernatant” = conditioned media supernatant without exosome pellet, “Exosome pellet” = exosome pellet resuspended in phosphate buffered saline.

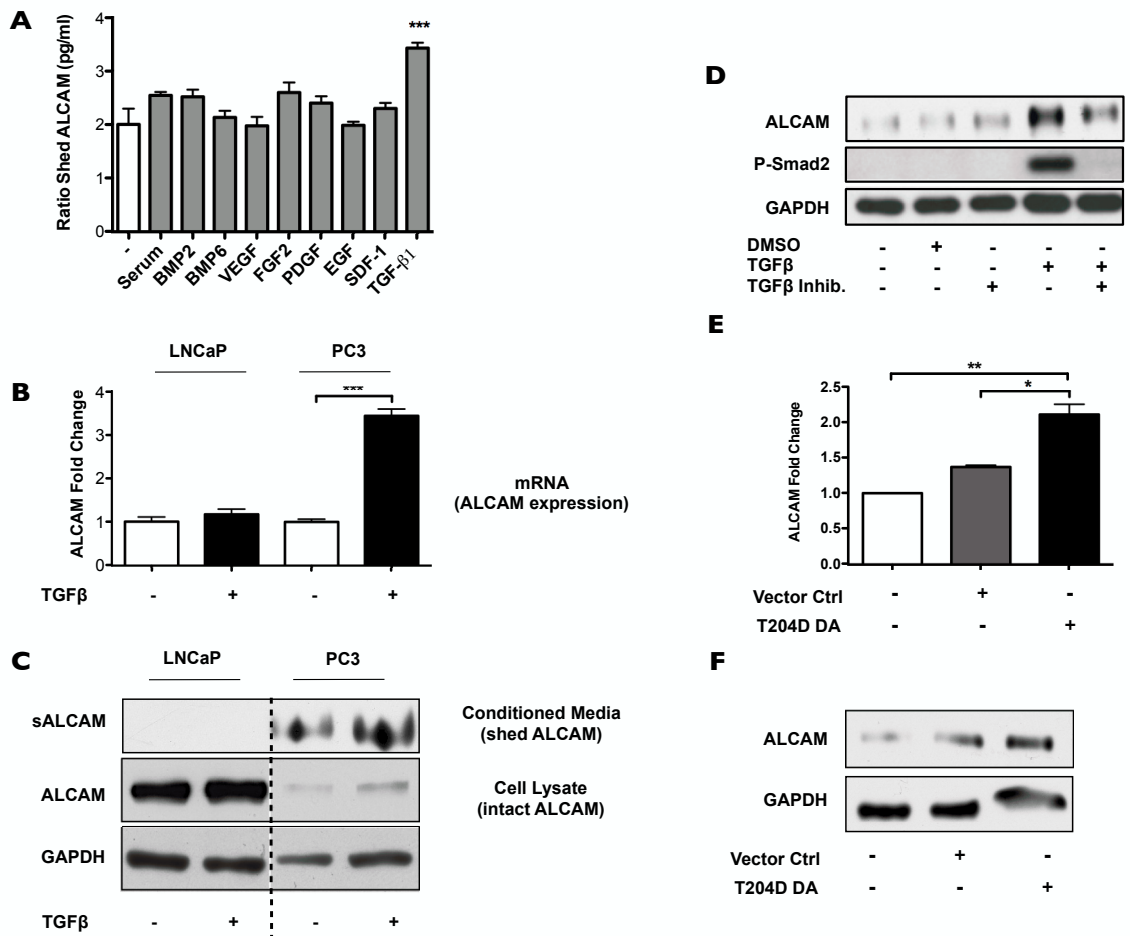
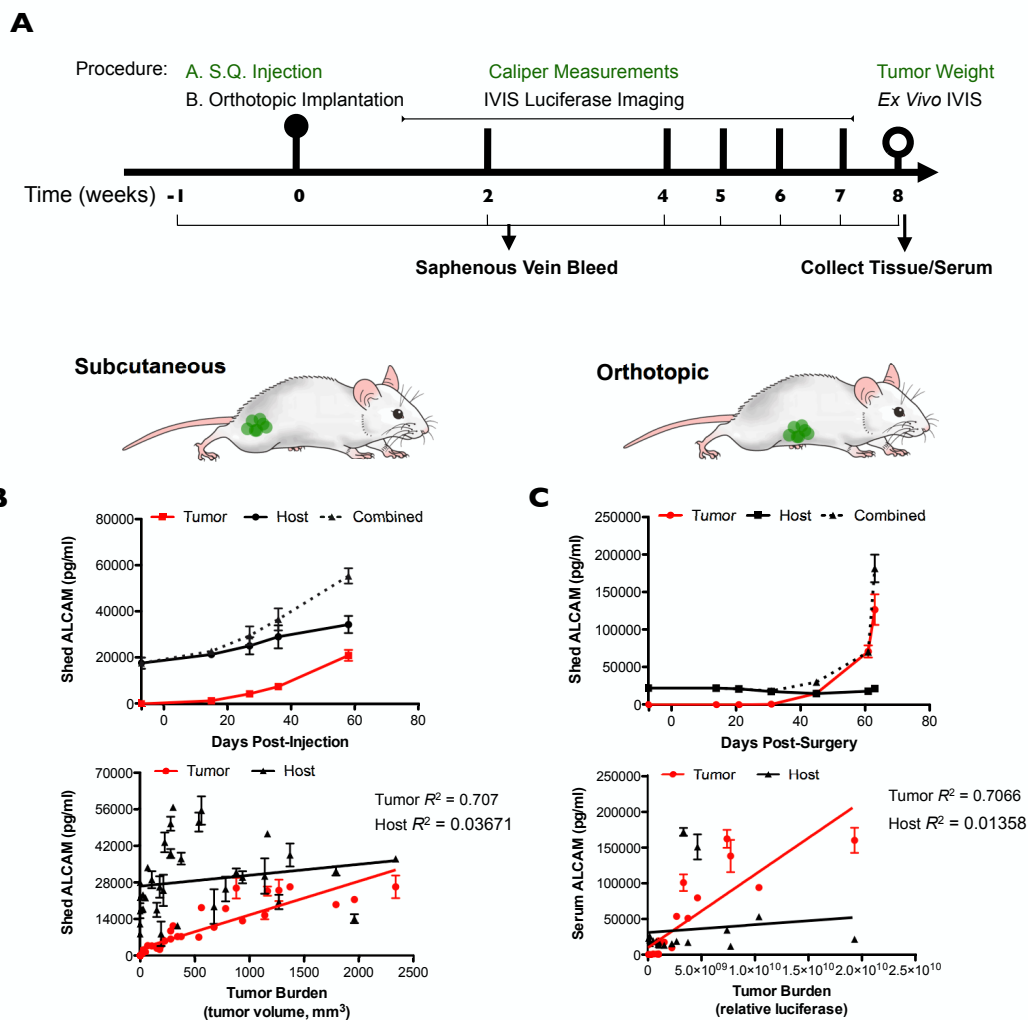


Figure 4. Expression and shedding of ALCAM is increased in response to TGFβ . (A) ELISA analysis of ALCAM shedding in concentrated conditioned media of PC3 cells treated with indicated exogenous cytokines. TGFβ, $p < 0.001$ **(B)** Expression of ALCAM by RT-PCR fold change relative to GAPDH, glyceraldehyde 3-phosphate dehydrogenase in PC3 or LNCaP cells treated with or without 10ng/ml of TGFβ for 48 hrs **(C)** Western blot analysis of shed ALCAM in the conditioned media and intact ALCAM in the cell lysate in LNCaP and PC3 cells. **(D)** Western blot detection of ALCAM and Phosphorylated-Smad2 expression in PC3 cells treated with 10ng/ml TGFβ for 48 hrs. in the presence or absence of 10μM SB431542, a TGFβ receptor tyrosine kinase inhibitor. **(E)** RT-PCR and **(F)** Western blot analysis of ALCAM expression in LNCaP cells transfected with vector control or T204D, dominant active TGFβ type I receptor; * $p < 0.05$, ** $p < 0.01$.

ALCAM shedding *in vivo* correlates with tumor progression. Published clinical studies have demonstrated that circulating levels of ALCAM are frequently elevated in cancer patients (103,110). These studies suggest that ALCAM is shed by the tumor, however, there has been no experimental comparison of tumor and host ALCAM to demonstrate definitively that the elevated levels of shed ALCAM are derived from the tumor. To determine if tumor-derived ALCAM is the source of elevated circulating ALCAM, we used species-specific antibodies to monitor circulating levels of both host (mouse) ALCAM and tumor (human) ALCAM longitudinally during orthotopic and subcutaneous growth of PC3 cells (Fig. 5). The half-life of human ALCAM in the circulation of its mouse host was determined to confirm that tumor-derived ALCAM could act as a stable biomarker *in vivo* (Fig. 6). Circulating ALCAM exhibits a 17hr half-life which is sufficient for monitoring its release from an endogenous tumor burden.

Circulating levels of ALCAM were subsequently monitored on a weekly basis (Fig. 5A) in SCID mice bearing subcutaneous (Fig. 5B, n=5) or orthotopic xenografts of PC3 (Fig. 5C, n=8). Animals were bled on a pre-determined schedule via saphenous vein puncture. Circulating ALCAM levels were detected by ELISA and a comparison to pre-grafting baseline levels allowed for the detection of any increase in host (mouse) ALCAM and the appearance of tumor (human) ALCAM in response to an increasing tumor burden. Tumor-derived ALCAM levels showed significant weekly increases in the serum of tumor-bearing mice (Fig. 5B,C, and Fig. 7; $P < 0.0001$). Regression analysis showed a direct linear relationship between circulating levels of tumor-derived ALCAM and tumor burden for



subcutaneous xenografts (Fig. 5B; tumor-derived $R^2 = 0.707$, $p < 0.0001$, $n = 4$) and orthotopic xenografts (Fig. 5C; tumor-derived $R^2 = 0.7066$, $p < 0.0001$, $n = 4$).

Figure 5: ALCAM shedding correlates with tumor burden. Circulating ALCAM levels were monitored longitudinally in mice bearing subcutaneously (S.Q.) or orthotopically implanted PC3 cells. **(A)** Schematic representation of *in vivo* strategy for S.Q. and orthotopic tumor models. **B and C)** Circulating levels of soluble host and tumor-derived ALCAM detectable in mice bearing subcutaneous injected PC3 cells **(B)** or PC3 cells orthotopically implanted into the prostate **(C)**. Levels of ALCAM are shown as a function of time (*top*) or tumor burden at the time of experiment completion (*bottom*). Each point reflects mean of duplicate measurements \pm SD. Each line and corresponding R^2 represents a best fit linear regression analysis.

Serum Half Life

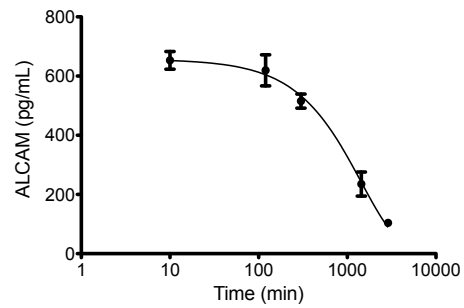


Figure 6. ALCAM serum half-life in mice. Pooled serum from ALCAM WT mice was delivered retro-orbitally into ALCAM KO mice (n=10) Circulating levels of mouse ALCAM were measured 10mins, 2, 4, 24 and 48hrs post injection. Baseline pre-bleed was used as negative control. ALCAM WT serum was used as ELISA control.

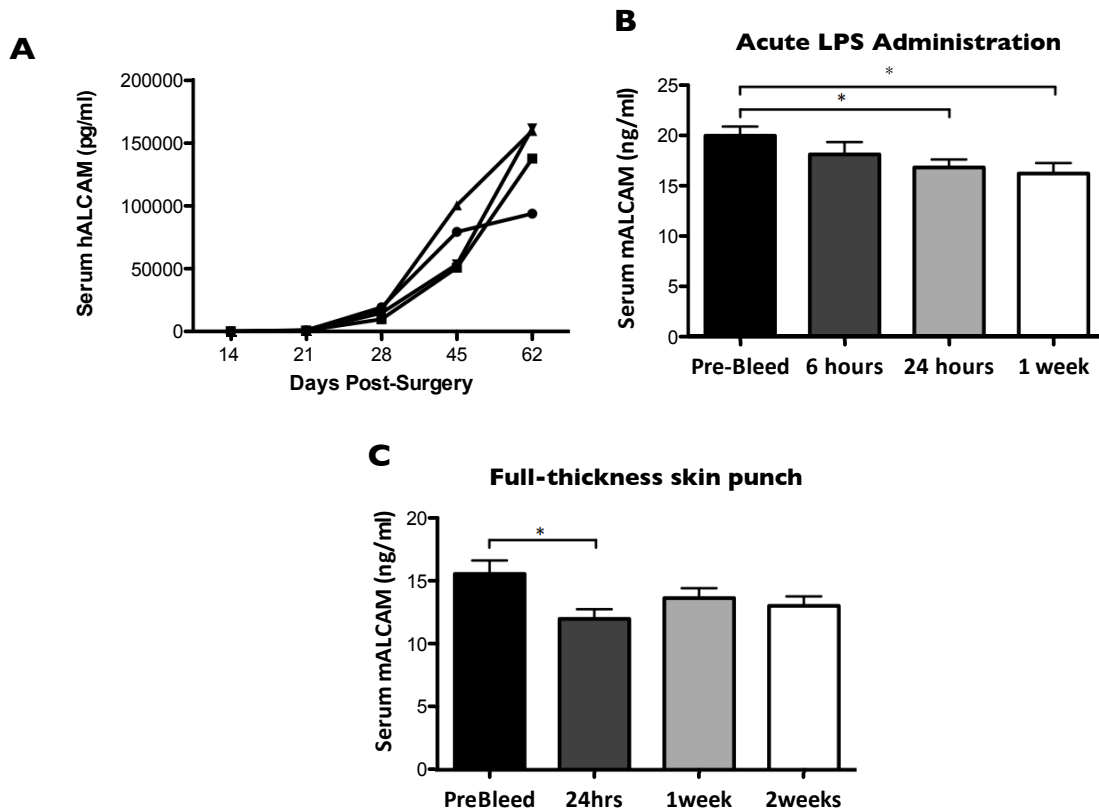


Figure 7. Immune response modulation does not affect serum ALCAM **A)** Tumor-derived (human) ALCAM serum levels in individual mice plotted longitudinally **B)** Serum levels of mouse ALCAM pre-and post-treatment with Lipopolysaccharide (LPS). Data are mean \pm SEM (n=5); *p<0.05 (One-way ANOVA; Mann-Whitney test). **C)** Serum levels of mouse ALCAM in pre-and post full thickness skin punch. Data are mean \pm SEM (n=6); *p<0.05 (One-way ANOVA; Mann-Whitney test).

In contrast to tumor-derived ALCAM, changes in host-derived ALCAM did not correspond to tumor burden (Fig. 5B; host-derived $R^2 = 0.03671$, $n = 4$ animals; Fig. 5C; host-derived $R^2 = 0.01358$, $n = 4$ animals).

ALCAM shedding is mediated by ADAM17 *in vitro* and *in vivo*. Since ALCAM is a proteolytic target of ADAM17 we hypothesized that ADAM17 was responsible for TGF β -induced cleavage of ALCAM. This hypothesis was supported by published work demonstrating that TGF β can increase ADAM17 activity by phosphorylation of the protease (136,137). Indeed, knockdown of ADAM17 using small interfering RNA (siRNA) transfection resulted in a loss of TGF β -induced ALCAM shedding (Fig. 8A). Similar results were obtained using an ADAM17-specific inhibitor (Fig. 8B, Compound-32, Bristol Meyers-Squibb) (138). These studies were extended to orthotopic models to confirm that ADAM17 was also the primary protease responsible for ALCAM shedding *in vivo* (Fig. 8C). *In vivo* inhibitor dosing and efficacy was confirmed using serum TNF-alpha (Fig. 9, n=6) which demonstrated that 50% inhibition of ADAM17 could be achieved for the duration of the ALCAM serum half-life (Fig. 6; 17hr) without signs of distress or toxicity. Mice were treated twice-daily for 3 days with 20mg/kg of the ADAM17 inhibitor (Compound-32 or vehicle DMSO control). Pre-surgery, weekly, pre- and post-treatment saphenous vein bleeds were collected. We found that inhibition of ADAM17 resulted in a significant decrease in serum levels of shed ALCAM approximating the 50% inhibition we achieved with our dosing studies (Fig. 9).

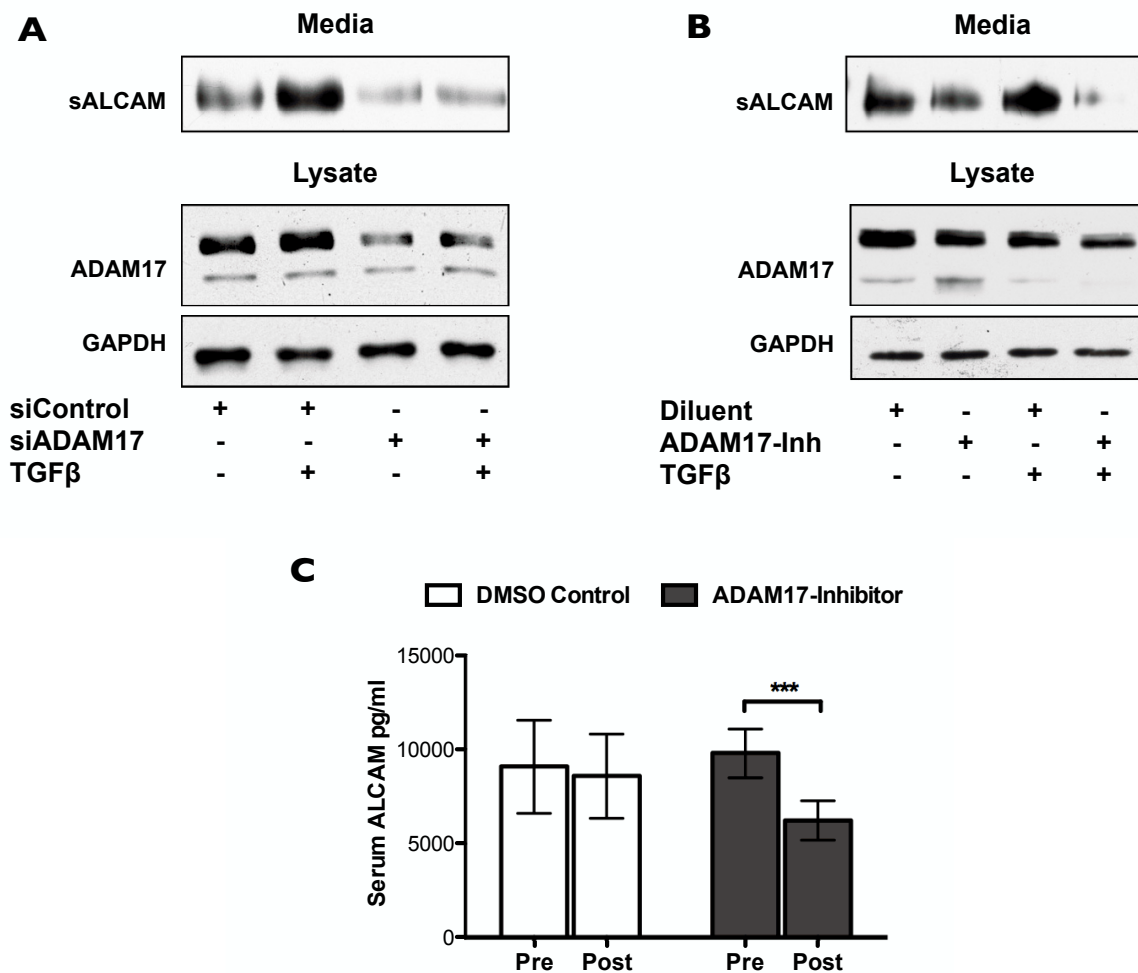


Figure 8. Ectodomain shedding of ALCAM is mediated by ADAM17 *in vitro* and *in vivo*. (A) Western blot analysis of shed ALCAM in the conditioned media and ADAM17 in the total cell lysate of PC3 transiently transfected with either scrambled siRNA or siRNA targeting ADAM17. (B) Western blot analysis of shed ALCAM in PC3 cells treated with an ADAM17-specific inhibitor (Compound-32, BMS), broad-spectrum MMP inhibitor (GM6001), or diluent control. (C) Serum levels of tumor-derived ALCAM in 10wk old SCID mice bearing PC3-luc tumors and treated with DMSO diluent or Compound-32 for three days, $p=0.0005$

Serum TNF-alpha post-1hr. LPS

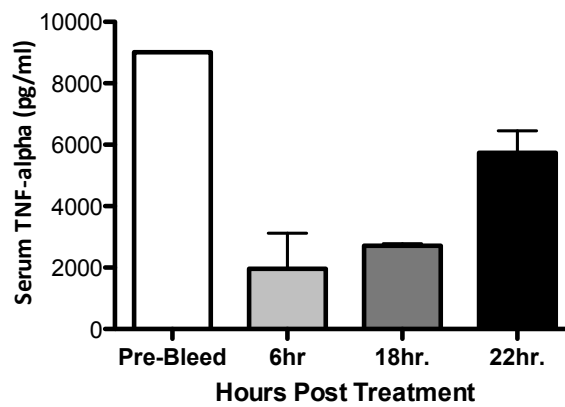


Figure 9. Compound-32/ADAM17 inhibitor dosing *in vivo*. 20mg/kg of Compound-32 (ADAM17 Inhibitor) was delivered intraperitoneally in WT C57/Bl6 (n=6) mice. Serum was collected at 6, 18 and 22hrs following one hour post-LPS injection. ELISA was used to determine serum TNF- α levels. Serum from pre-bleed prior to LPS injection was used as baseline.

Taken together these data suggest that ALCAM cell surface shedding is mediated by ADAM17 and promoted by TGF β .

Knockdown of ALCAM in PC3 cells inhibits TGF β -induced migration and *in vivo* dissemination to bone. Given TGF β is a central driver of tumor cell motility and metastasis, we sought to determine the effects of exogenous TGF β on prostate cancer cells *in vitro*. To test whether ALCAM is functionally involved in tumor cell migration and metastasis, we knocked down expression in PC3-Luc cells using viral delivery of short hairpin RNA (shRNA). Three separate stable ALCAM knockdowns were produced (ALCAM KD 1, 2 and 3). Transduced cells were selected with puromycin and subsequently subjected to flow-sorting to isolate the highest knockdown population (Fig. 10A). We pre-treated PC3-luc-ALCAM^{KD1} cells and PC3-luc-ALCAM shControl cells with 10 μ g/ml TGF β for 16hrs in serum-free conditions, followed by initiation of MATS assay (Fig. 10B) or scratch assay (data not shown). We compared both TGF β pre-treatment and treatment at the time of scratch and noted similar results. The analysis revealed a loss of TGF β -induced migration in PC3-luc-ALCAM^{KD1} cells (Fig 10B). Similar observations were made in ALCAM^{KD2} and ALCAM^{KD3} cells. Interestingly, the reduction in ALCAM expression led to a slight increase in migration, possibly due to a loss of ALCAM-ALCAM homotypic interaction on adjacent cells.

Given the critical importance of cancer cell migration in malignant tumor expansion and metastasis, we subsequently evaluated the contribution of ALCAM to primary tumor growth and bone metastasis. Primary tumor growth was

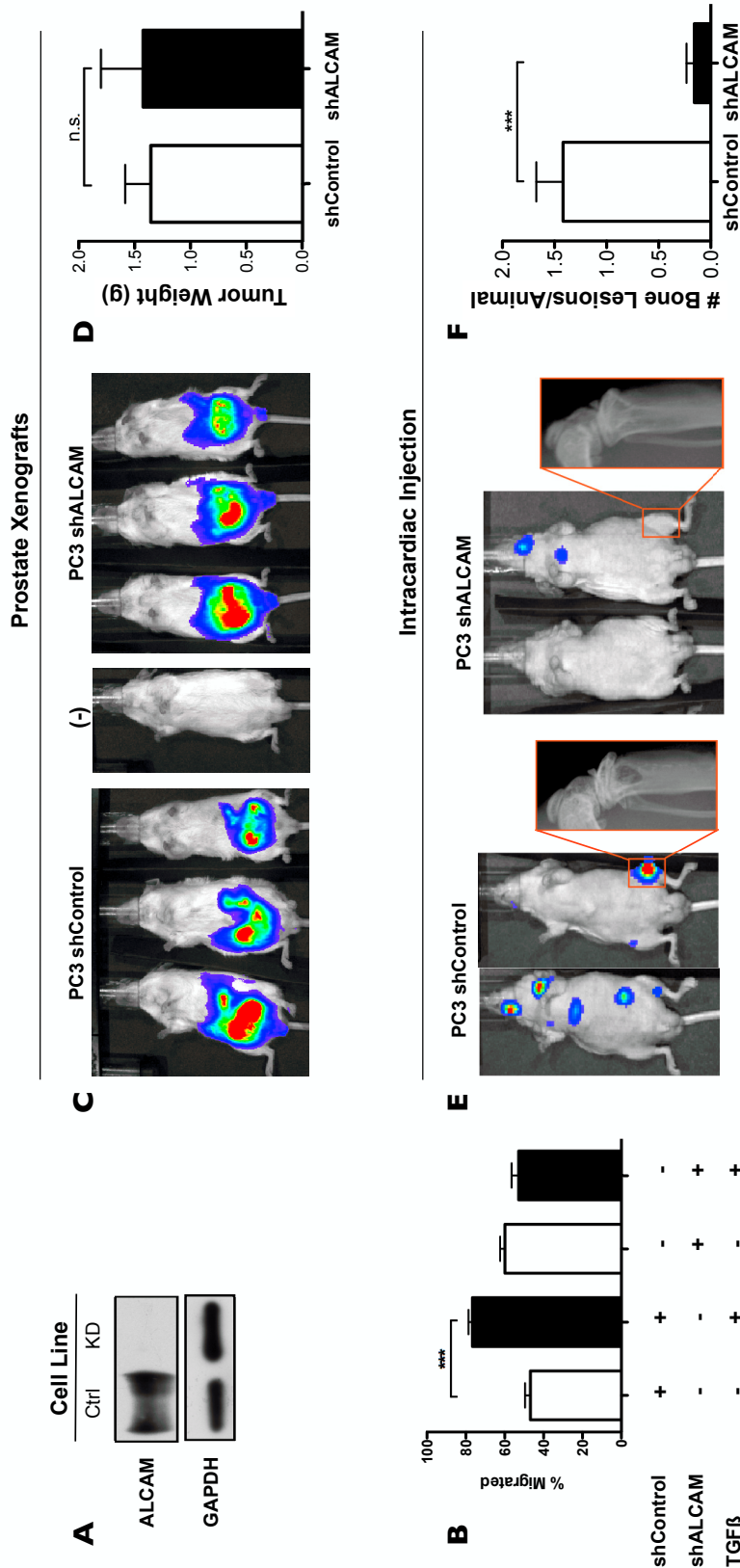


Figure 10. Tumor-derived ALCAM mediates TGFβ-induced migration and skeletal metastasis but not primary tumor growth in the prostate. (A) Western blot analysis of lysates from parental PC3-luc and PC3-luc shRNA ALCAM (KD1) knockdown cells. **(B)** Quantitative analysis of tumor cell migration in parental PC3 cells and PC3 cells with shRNA-mediated knockdown of ALCAM treated with or without 10ng/ml TGFβ. **(C)** Whole animal luciferase imaging of mice bearing orthotopic PC3-luc parental tumors or PC3-luc ALCAM knockdown tumors 6-weeks post surgery. **(D)** Primary tumor weights of orthotopic PC3-luc parental tumors (n=8) and PC3-luc ALCAM knockdown tumors (n=8) **(E)** Representative whole-animal luciferase imaging and matching x-rays 8 weeks post-intracardiac injection of PC3-luc parental (shControl) or PC3-luc ALCAM knockdown (shALCAM, KD1). **(F)** Average number of bone lesions in mice from PC3-luc (1.42 ± 0.26; n=31) or PC3-luc shRNAALCAM (KD1) knockdown cells (0.16 ± 0.07; n=25). **p<0.0001.

accomplished using an orthotopic model based on implantation of tumor cells into the anterior prostate of SCID mice (Fig. 10C, n=8 for PC3-luc-Control and PC3-luc-ALCAM^{KD1}). Skeletal metastasis was accomplished by intracardiac injection of tumor cells in nude mice (Fig. 10D, n=31 for PC3-luc-Control and n=25 for PC3-luc-ALCAM^{KD1}). Bioluminescent imaging was used to monitor tumor burden for both models at weekly intervals. Interestingly, reduced ALCAM expression did not limit tumor growth within the prostate (Fig. 10C). Whole body and *ex vivo* bioluminescent imaging of the orthotopic model upon experiment completion confirmed that both the PC3-luc-Control and PC3-luc-ALCAM^{KD1} exhibited similar tumor burden based on luciferase activity (Fig. 10C), and comparable tumor size based on weight (Fig. 10D). Local invasion and mesenteric dissemination is common in this model (139) and was not altered by reduced ALCAM expression.

In contrast to the orthotopic model, a reduction in ALCAM resulted in a significant decrease in skeletal metastasis (Fig. 10E). Both incidence and metastatic burden were reduced. Approximately 75% of mice injected with PC3-luc-Control tumor cells developed bone metastasis while only 17% of the mice injected with PC3-luc-ALCAM^{KD1} cells developed bone lesion. In addition, mice that did develop skeletal metastases formed by PC3-luc-ALCAM^{KD1}, the number of lesions per mouse was greatly reduced (0.2 events versus 1.4 events, Fig. 10F). The orthotopic and intracardiac experiments were repeated with PC3-luc-ALCAM^{KD3} and similar results obtained.

ALCAM expression contributes to tumor cell survival in the bone microenvironment. To determine the biologic importance of tumor-derived ALCAM in prostate tumor growth in the bone, PC3-luc-Control (n=8), PC3-luc-ALCAM^{KD2} (n=8) and PC3-luc-ALCAM^{KD3} (n=8) were injected into the tibia of nude mice. Following intratibial injection, luminescent and X-ray imaging was used to monitor tumor burden over time (Fig. 11A). Quantitation of the bioluminescent signal showed a markedly lower growth rate for the ALCAM KD cells (Fig 11B). At completion of the experiment 100% of control mice exhibited lesion compared to an 80% incidence in limbs bearing PC3-luc-ALCAM^{KD3} tumor cells (Fig. 11C). ALCAM^{KD} intratibial tumors continued to exhibit reduced ALCAM expression (Fig. 11D). Detailed imaging of the osteolytic lesions by microCT (Fig. 12A) further confirmed decreased lesion area and increased bone volume in the bones containing ALCAM KD cells (Fig. 12B and C). Finally, the histological visualization of bone tumors generated by control and ALCAM KD cells resulted in reduced bone tumor size upon ALCAM knockdown (Fig. 12D). Tibias in the PC3-luc-vector, PC3-luc-ALCAM^{KD2} and PC3-luc-ALCAM^{KD3} were stained for the osteoclast marker, tartrate-resistant alkaline phosphatase (Fig. 13). Both the ALCAM KD tumors induced osteolytic lesions as evidenced by osteoclast presence adjacent to tumor lesions suggesting that the ability to induce bone-remodeling was not deficient in these cells.

We then carried out immunofluorescent staining for cleaved caspase-3 (Fig. 12E, apoptosis) and Ki67 (Fig. 12F, proliferation) on intratibial bone tumors harvested at 28 days post injection. Compared to the control tumors, the bone

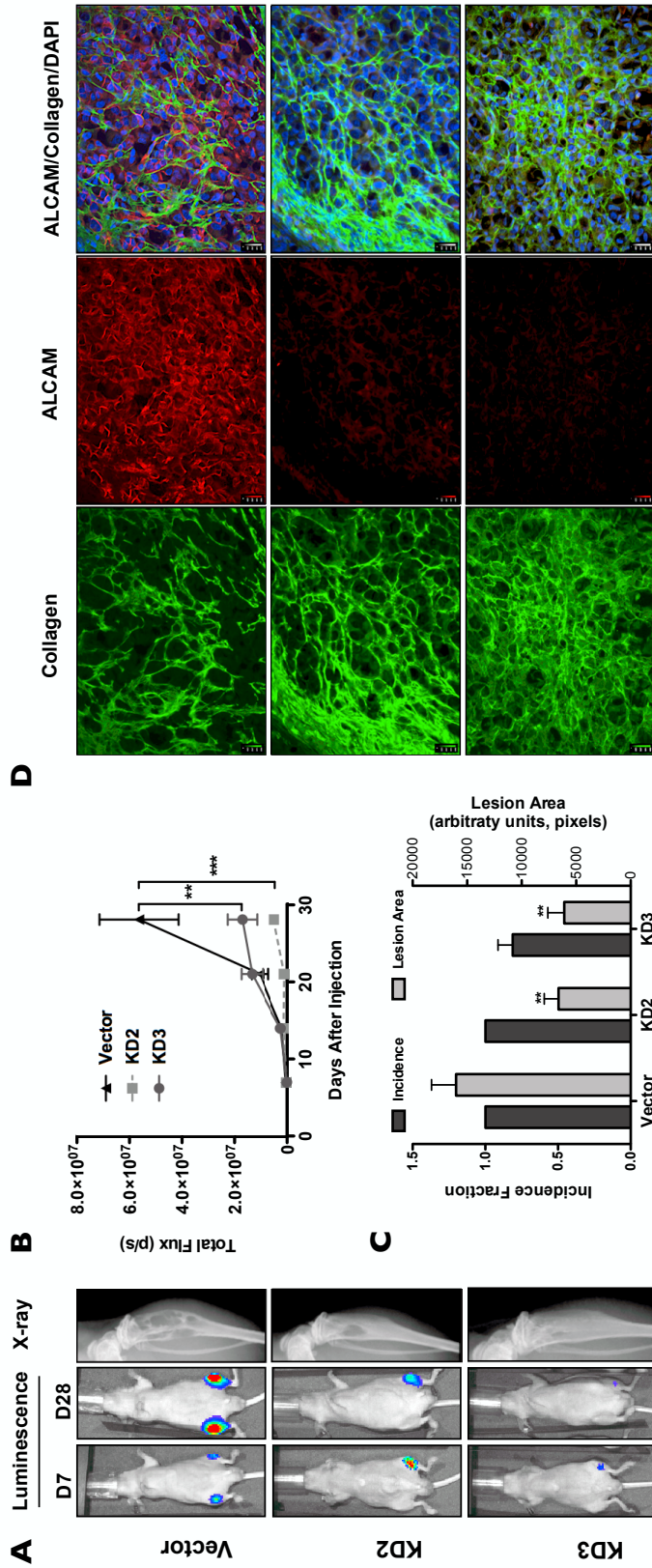


Figure 11. Tumor-derived ALCAM impacts metastatic growth but not incidence after intratibial injection. (A) Representative whole animal luciferase and x-ray imaging of mice post-intratibial injection of PC3-luc parental tumors (vector, n=8), and PC3-luc ALCAM knockdown tumor cells (KD2, n=8 & KD3, n=8). (B) Tumor incidence and average lesion area in the tibias of mice bearing PC3-luc vector, PC3-luc KD2 and KD3 tumors. Data represent the mean \pm SEM (n=8/group); **p<0.01; ***p<0.0001 (C) Bioluminescent curve of intratibial tumor development in mice bearing PC3-luc vector, PC3-luc KD2 and KD3 tumors. (Two-way ANOVA with Bonferroni post-test). (D) Collagen I and ALCAM immunofluorescence of tumor cells within the tibias of mice bearing PC3-luc vector or PC3-luc KD2 or KD3 tumors.

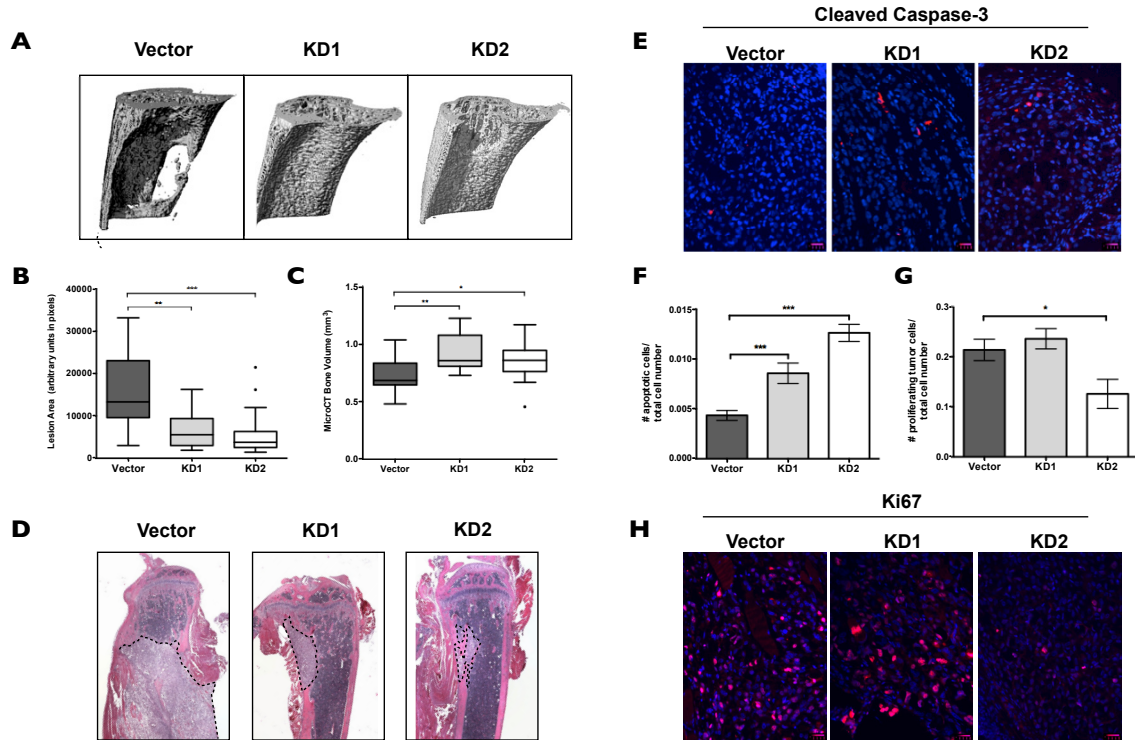


Figure 12: Tumor-derived ALCAM impacts tumor survival and proliferation in the bone microenvironment of intratibial bone tumor model. **A)** Representative three dimensional reconstitutions of microCT images from mice injected with PC3-luc-vector, PC3-luc-KD1 and PC3-luc-KD2 tumor cells **B)** Box-plots of average BV/TV (bone volume/total volume) by group for the PC3-luc-vector, PC3-luc-KD2 and PC3-luc-KD3 tumor bearing mice. Data represents quartiles with dots indicating outliers (1.5x upper or lower quartile; n=16 tibias/group) * $p < 0.05$, ** $p < 0.01$, (One-way ANOVA $p = 0.0047$. Post-hoc Mann-Whitney) **C)** A boxplot representing the lesion area calculated from end-point x-ray images from the same experiment shows dramatic decrease in the lesion area in the KD2 and KD3 tumor lesions compared to vector control (One-way ANOVA $p = 0.0003$. Post-hoc Mann-Whitney ** $p < 0.01$, *** $p < 0.0001$. n=8/group). Lesion areas were measured using arbitrary pixel unit. **D)** Representative H&E stains of osteolytic bone lesions in the hind leg of mice. Outlines indicate the osteolytic tumor lesion within the bone. **E)** Representative immunofluorescent staining of cleaved caspase-3 positive cells (red) in tibias of PC3-luc-vector, PC3-luc-KD2 and PC3-luc-KD3 tumor-bearing mice. **F)** Representative immunofluorescent staining of Ki67 proliferating cells (red) in tibias of PC3-luc-vector, PC3-luc-KD2 and PC3-luc-KD3 tumor-bearing mice. Data are mean \pm SEM (n=8/group); * $p < 0.05$, ** $p < 0.01$, *** $p < 0.005$ (One-way ANOVA; Mann-Whitney test). **G)** Apoptosis in the tumor-bone microenvironment as a function of total cell number was assessed by staining for cleaved caspase-3 in PC3-luc-vector, PC3-luc-KD2 and PC3-luc-KD3 tumor bearing tibias of mice 4 weeks post-injection. **H)** Proliferation in the tumor-bone microenvironment as a function of total cell number was assessed by staining for Ki67 in PC3-luc-vector, PC3-luc-KD2 and PC3-luc-KD3 tumor bearing tibias of mice 4 weeks post-injection.

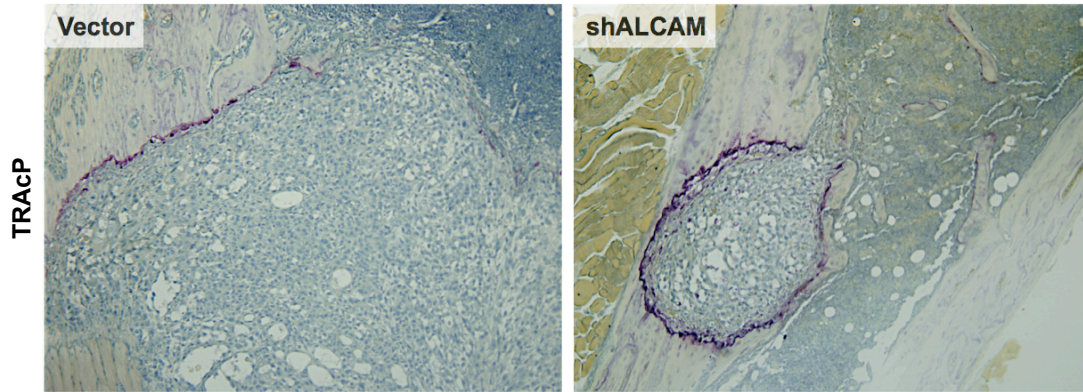


Figure 13. Tumor-induced osteolysis not affected by decreased ALCAM expression. Representative TRAP stained photomicrographs of PC3 shControl and shALCAM injected animals at day 28.

tumors created by both ALCAM KD cells exhibited elevated levels of cleaved caspase-3 suggesting that these cells are experiencing a reduced ability to survive (Fig. 12G). In addition, bone tumors from PC3-luc-ALCAM^{KD3} had significantly lower Ki67 staining suggesting that ALCAM contributes to both proliferation and survival (Fig. 12H).

DISCUSSION

We have established for the first time that ALCAM plays a role in prostate cancer establishment in the bone microenvironment. ALCAM mRNA is elevated in malignant disease yet by immunohistochemistry it is frequently absent from the tumor cell surface in advanced disease (Fig. 2D) (80,99,122). We have demonstrated recently that in colorectal cancer tissue, ectodomain shedding is responsible for the apparent loss of ALCAM immunohistochemical detection (113). This shedding is likely the cause for conflicting results reported for several malignancies (95). Indeed the protease responsible for shedding of ALCAM ectodomain, ADAM17, is elevated in advanced prostate cancer (Fig. 2B) (140). These data implies that while ALCAM gene transcription is elevated in prostate cancer, ectodomain shedding depletes the cell surface of intact protein in advanced disease. Regression analysis showed a direct linear relationship between circulating levels of (human) tumor-derived ALCAM and tumor burden in animals with subcutaneous xenografts (Fig. 5B) and orthotopic xenografts (Fig. 5C). In contrast, the host-derived ALCAM did not correspond to tumor burden (Fig. 5B&C;), demon-

strating that elevations in circulating ALCAM are tumor-specific. Consistent with this observation, host-derived ALCAM does not increase, but rather decreases slightly, in immunocompetent mice challenged with LPS (a model of acute inflammation) or full-thickness skin punch (a model for wound-healing, Fig. 7B&C, respectively). These data suggest that tumor-derived ALCAM is a marker specific of tumor burden and that host ALCAM is not significantly shed in response to the tumor burden.

The TGF β responsiveness of ALCAM (Fig. 4) together with the elevated levels of ALCAM expression and shedding observed in cancer patients (Fig. 2) (90,103,113) and experimental models (Fig. 4 &5) suggested that ALCAM could contribute to the metastatic behavior of prostate cancer cells. *In vitro* suppression of ALCAM expression by stable transfection of ALCAM targeting shRNAs significantly inhibits prostate cancer cell migration *in vitro* in response to exogenous TGF β . This pleiotropic cytokine is particularly important in establishing the vicious cycle of tumor cells in the bone microenvironment (116) and is known to be elevated in the plasma of patients with breast and prostate bone metastasis (141). These observations demonstrate that ALCAM contributes to TGF β -induced migration and skeletal metastasis, but does not influence primary tumor growth or local invasion.

The mechanism by which ALCAM participates in metastasis of prostate cancer to bone remains unclear. Recent data have shown that activation of NF- κ B in prostate cancer cells increases RANKL and PTHrP. NF- κ B proteins are an important class of transcriptional regulators in prostate cancer. Similar to inactiva-

tion of NF- κ B signaling in prostate cancer cells, our data show decreased expression of ALCAM, a downstream target of the p65/p55 subunit of NF- κ B, inhibits tumor establishment and growth in the bone microenvironment (142,143). Both the over-expression of ALCAM and nuclear p65 NF- κ B in prostate cancer cells correlates with chemoresistance, advanced stage, PSA recurrence and metastatic spread (99,107,144-147). While we did not observe a reduction in osteoclast activity by TRAP staining (Fig. 13) in ALCAM knockdown bone metastatic sites, one would suggest NF- κ B exerts additional pro-metastatic function through modulation of ALCAM expression, independent of increasing osteoclastogenesis. Intratibial tumor formation was enhanced in LNCaP cells expressing constitutively activated NF- κ B through retroviral infection with a mutant IKK2 (142). If indeed NF- κ B activation increases ALCAM expression, it is possible that ALCAM expression and ectodomain shedding can have specific, yet separate roles in tumor cell growth versus tumor establishment. This provides a rationale for further investigation into the role of ALCAM in prostate bone metastasis.

Within the metastatic cascade there are many sequential steps that can contribute to the overall success of any single metastatic lesion. Evaluation of primary tumor growth and experimental metastasis suggest that, in our model of prostate cancer, ALCAM contributes to skeletal colonization after arrival to the secondary site. Close examination of metastatic colonies from mice injected intracardially with PC3-luc-ALCAM^{KD1} and PC3-luc-ALCAM^{KD3} revealed a reduced lesion size, suggesting that ALCAM might be important for tumor growth in bone. Intratibial bone tumors composed of ALCAM knockdown cells remained small

throughout the duration of the experiment suggesting that there was not a lag in tumor growth but rather a persistent reduced ability to proliferate or, conversely, a decreased ability to survive.

Although there was no evidence of reduced proliferation *in vitro* (Fig. 14), the *in vivo* data suggest that tumor-derived ALCAM is important for growth of tumor cells in the bone. Intriguingly, PC3-luc-ALCAM^{KD2}, which retains more ALCAM expression than PC3-luc-ALCAM^{KD3} (Fig. 11A), did not exhibit reduced proliferation suggesting that the threshold of ALCAM expression that influences cell survival is different from the threshold influencing cell proliferation. These data demonstrate for the first time that tumor-derived ALCAM impacts tumor growth and expansion in the bone microenvironment by promoting cell proliferation and survival. Our results show that ALCAM expression in the bone microenvironment can have a significant impact on tumor cell survival. This is in accordance with *in vitro* data whereby ALCAM gene silencing in MCF-7 tumor cells resulted in increased cleaved caspase-7 and PARP, in addition to decreased levels of the apoptosis regulator, Bcl-2 (148). Taken together, these observations suggest a protective, anti-apoptotic role of ALCAM in tumor cell survival in the bone microenvironment. Extravasation of tumor cells is considered an important step in metastasis because tumor cells must adhere and transverse the endothelial layer before settling at a secondary site (149). Both soluble ALCAM-Fc and blocking ALCAM antibodies are able to decrease *in vitro* transendothelial migration of THP1 monocytes suggesting this may be a requirement for transendothelial migration of tumor cells (150). In our study, intracardiac injection of prostate cancer

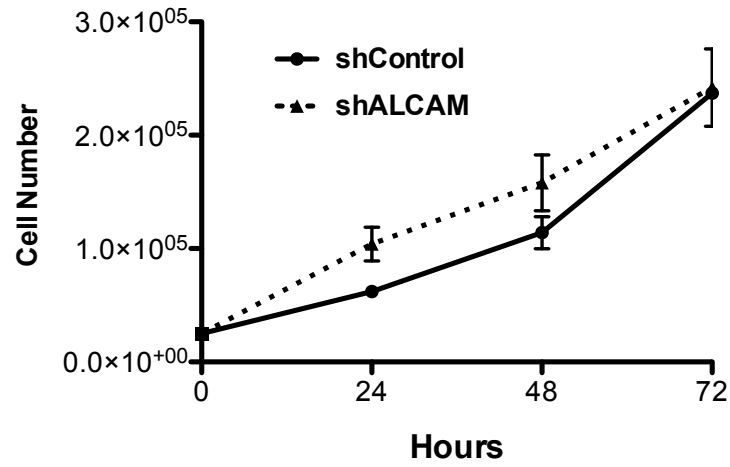


Figure 14. Effect of ALCAM knockdown on *in vitro* proliferation. Graph represents tumor cell proliferation over time as assessed by total cell counts over 72 hours.

cells with reduced ALCAM expression resulted in a dramatic reduction of tumor incidence (Fig. 10E). On the contrary, intratibial injection did not significantly impact tumor incidence (Fig. 11C), rather survival (Fig. 12F), suggesting a dual adhesive and signaling function of ALCAM whereby the intracellular signaling function of ALCAM functions to serve a protective role in apoptosis, and the extracellular adhesive function is required for extravasation and subsequent colonization at a secondary site. While we have convincing data that ALCAM expression is important in the osteotropism and survival of tumor cells in the bone, (Figure 10 & 12, respectively) further work is necessary to fully elucidate the mechanisms involved.

Here we have presented evidence that ALCAM not only serves as a longitudinal molecular indicator of tumor burden, but functionally contributes to metastasis to bone. Clinically, ALCAM may be a surrogate marker for bone metastasis in prostate cancer patients. In support of the hypothesis that ALCAM is required for tumor cell maintenance in the bone microenvironment, we show that a reduction in ALCAM expression reduces cell survival in the bone microenvironment. The relevance of ALCAM in the bone microenvironment is coupled with our data showing ALCAM expression is driven by TGF β , a known contributor of the vicious cycle in bone metastasis (151). Dissecting the molecular mechanisms that contribute to tumor cell survival and growth in the bone is critical for the development of targeted therapies and clinical biomarkers of disease progression. Further elucidation of the role of ALCAM in the bone microenvironment and clinical application ALCAM as a candidate marker of bone metastasis is warranted and

could impact detection and treatment intervention in prostate bone metastatic disease.

CHAPTER III

ELEVATED ALCAM SHEDDING IN COLORECTAL CANCER CORRELATES WITH POOR PATIENT OUTCOME

INTRODUCTION

Colorectal cancer (CRC) is the third most frequently diagnosed cancer, and second leading cause of cancer-related deaths in the US (152). Current prognosis for CRC patients predominantly rely on pathologic UICC/AJCC tumor node metastasis (TNM) staging classification (153). Although TNM staging successfully stratifies high-risk patients, there is significant variability in the rate of disease progression within each stage. Particular concern exists for early stage disease (Stage I and II) where patients can progress more rapidly than expected. It is well known that approximately 30% of stage II CRC patients die of recurrent and metastatic disease. Identification of patients at risk of recurrence/progression could inform clinicians on adjuvant chemotherapeutic treatment decisions. Biomarkers can assist in identifying those patients that require more aggressive intervention or patients at risk of relapse after initial treatment. Promising clinical tests including Oncotype DX™ and Coloprint™ evaluate possible disease progression by assessing gene expression. These tests are not yet widely applied, possibly because their epigenetic evaluation reflects gene expression which does not always reliably predict actual cellular behavior. Thus, existing prognostic tests

would be enhanced with the addition of biomarkers that report on cancer prognosis.

While clinical trials have demonstrated less than 5% 5-year survival benefit from adjuvant therapy for unselected stage II colon cancer patients (154), it is clear that a subset of these patients are at high risk for poor outcome and would likely benefit from adjuvant therapy (155,156). Those high-risk stage II patients have similar outcomes to patients with stage III tumor status (157), highlighting the need for molecular stratification parameters to identify high-risk patients with apparent early stage disease. Attempts made to stratify patients using gene expression profiles have experienced some success but have not been translated to the clinic (158,159). Molecular indicators capable of identifying subgroups of patients with poor prognosis and therapeutic benefit include microsatellite instability and 18q loss of heterozygosity (LOH), however, 18qLOH has not been translated to a useful predictive tool for clinical use (160).

ALCAM has been highlighted as a putative biomarker for the progression of many cancers, including CRC (81,90,109,110,112,161,162). ALCAM is a cell-cell adhesion protein that has been identified in a broad array of biological processes including inflammatory responses, neuronal outgrowth and epithelial migration (120). Unlike most candidate biomarkers, ALCAM expression is not tissue-restricted and it is commonly found in most epithelia and related carcinomas and contributes to tumor progression by controlling migration. Its molecular activity appears to be regulated through shedding of the extracellular domain. Conse-

quently, advanced disease tissues continue to express ALCAM but exhibit an elevated level of ALCAM shedding.

ALCAM has been evaluated for CRC in five published reports. Unfortunately, the findings from these studies are contradictory (20,52,53,109,162). In a study characterizing the expression of ALCAM in the gastrointestinal tract and colorectal cancer, ALCAM was found to be highly expressed in the colon crypts of normal tissue and heterogeneously expressed in tumor sections (53). In a study of 299 CRC patients, membranous ALCAM expression was a positive prognostic indicator for overall survival (109). Similarly, a previous study by Lugli *et al.* also found the loss of membranous ALCAM to be indicative of worse patient prognosis (162). In contrast, Weichert *et al.* reported that membranous ALCAM expression is associated with decreased patient survival (20). A subsequent study by Horst *et al.* (52) found ALCAM not to be correlated with CRC patient outcome.

Although these studies are contradictory, ALCAM has significant potential as a biomarker for CRC because it is not only readily detected in CRC but is also functionally and clinically associated with a large number of cancers including: colorectal (20,52,109,162), prostate (80,99), breast (100,112), gastric (105), thyroid (90), pancreatic (103), melanoma (94), and ovarian (81). At the clinical level, shed ALCAM is detectable in the serum of breast, thyroid, ovarian and pancreatic cancer patients, and the loss of cell surface ALCAM is associated with poor prognosis (90,107,112,163). These data suggest that the proteolytic cleavage of

ALCAM is functionally important in tumorigenesis, and detection of ALCAM shedding may function as a prognostic biomarker.

In this study, we sought to determine if ALCAM shedding in human primary colorectal cancers reflects a unique molecular progression of the tumor and consequently acts as a prognostic biomarker. For this purpose we developed a unique dual stain to detect both the extracellular and the intracellular domain of ALCAM within the same tissue. We find that ALCAM shedding in the primary tumor correlates strongly with a poor clinical outcome. This was particularly striking in stage II patients in which disease-specific survival was significantly worse when the tumor tissue exhibited high ALCAM shedding.

MATERIALS AND METHODS

Cell lines and mice. The continuous cell lines for cancer of the breast (MDA-MB-231 and MCF-7), prostate (PC3 and Du145) and colon (RKO, DLD, LOVO, LS174t, HCT116, HCA7, Scko1, Caco2, HT29, KM12c and KM12) were cultured in their appropriate basal media (DMEM or RPMI) with 10% FBS to confluence before lysis with 1% Triton-X 100 in PBS. ALCAM knockout mice (c57bl/6 ALCAM^{-/-}) were purchased from Jackson Laboratories. Mouse tissues were surgically resected, snap frozen and subsequently extracted with 1% Triton-X 100 lysis buffer.

Western Blot Analysis. SDS–PAGE under non-reducing conditions and transfer of proteins to a PVDF membrane has been described previously. After blocking with 5% skimmed milk in PBS/0.05% Tween-20, blots were probed with primary antibodies for extracellular ALCAM (Clone 105902; R&D Systems) and selected hybridoma clones, followed by peroxidase-conjugated secondary antibody and ECL (Perkin-Elmer) detection.

Lentivirus-delivered RNA Interference. Four individual constructs containing shRNAs for human ALCAM and a negative control (scrambled sequence) were purchased from Sigma (Mission shRNA). Constructs were packaged for viral production and infection and tested for target knockdown. For viral packaging, constructs were co-transfected into 293T cells using Fugene HD (Roche Applied Science). Media containing viruses were collected 48hr after transfection. PC3 cells were infected with the viruses in the presence of Polybrene (8 μ g/ml) for 24hr and then subjected to selection by 5 μ g/ml puromycin. Two constructs with \geq 90% knockdown efficiency as determined by immunoblotting and flow cytometry were used for further studies.

Human material. The protocols and procedures for this study were approved by the institutional review boards at the University of Alabama-Birmingham Medical Center, Vanderbilt Medical Center (VMC), the Veterans Administration Hospital (Nashville, TN), and the H. Lee Moffitt Cancer Center (MCC; Tampa, FL). Tissue specimens from 250 colorectal cancer patient enrolled at Vanderbilt Medical Cen-

ter (VMC, n = 55) and Moffitt Cancer Center (MCC, n = 195) were used for gene-expression microarray analyses as described previously (159). All patients had a diagnosis of colorectal adenocarcinoma. Each cancer specimen was staged according to American Joint Commission on Cancer (AJCC) guidelines (stages I-IV), and 10 normal adjacent specimens were deemed to contain only normal colonic tissue by a certified gastro-intestinal pathologist. VMC 55 includes 14 patients from the University of Alabama-Birmingham Medical Center (159). Microarray data for the NCI cell lines was obtained through the NCBI Gene Expression Omnibus (GEO data set GDS1761).

A tissue microarray containing 75 primary colorectal carcinomas and 12 normal age and sex-matched colorectal mucosa was constructed using 2mm cores in triplicate. Specimens from 69 CRC patients and 12 normal colonic mucosa were suitable to be used in the dual staining analysis. Subsequent expansion of this dataset was accomplished by selection of 36 stage II patients under IRB #120063 providing analysis for a total of 105 CRC and 12 normal mucosa with triplicate representation of each patient. Collection of serum from control (n=6), non-cancer patients (n=48) and colorectal patients immediately before surgery (pre-op, n=71) or after treatment (followup, n=20) at was accomplished at Vanderbilt Medical Center under IRB# 121365.

ALCAM Dual Immunofluorescence stain. Immunofluorescent staining for ALCAM in tissues was performed with hybridoma HPA010926 (Sigma Prestige An-

tibodies) directed against the extracellular domain and clone 1G3A1 (obtained from our fusion) directed against the intracellular domain (Table 3). Sections cut from patient tissue and tissue microarrays were deparaffinized in xylene and re-hydrated. Sections were blocked in 20% Aqua Block™ after pressure cooker antigen retrieval in citrate buffer (pH 6.0) . Samples were immunostained with mouse monoclonal intracellular ALCAM antibody, 1G3A1, (3 μ g/ml) and rabbit monoclonal extracellular ALCAM antibody, HPA010926 (1:250 dilution). The arrays were incubated with Alexa-546 Goat anti-rabbit (1:500) and Alexa-647 Goat anti-mouse secondary antibody (1:500, LifeTechnologies). The sections were counterstained with 2 μ g/ml of Hoechst for 2mins, and mounted with Prolong® Gold Anti-fade.

Image acquisition and quantitative analysis of ALCAM shedding. Tissue microarrays were imaged using the Ariol® SL-50 platform from Genetix. Image analysis and quantitation were performed using the open-source software ImageJ (FIJI). The analysis pipeline was designed as follows: a) The tumor area was selected using the free-hand selection tool. b) The color image was split into its red, green and blue component channels. c) Image thresholding was used to generate the detectable region of intracellular ALCAM staining (red channel) and extracellular ALCAM staining (green channel). d) Intact ALCAM was determined as the area of co-localized intracellular and extracellular ALCAM (red and green


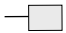
ALCAM Status	Antibody reactivity		ALCAM Schematic	
	Intracellular Domain (1G3A1)	Extracellular Domain (HPA10926)	HPA10926 ↓	1G3A1 ↓
Intact ALCAM	+	+		
ALCAM Shedding	+	-		
ALCAM Absent	-	-		

Table 3. Depiction of ALCAM immunoreactivity for HPA10926 which reacts with the extracellular domain and 1G3A1 which is specific for the intracellular domain

channel) while ALCAM shedding was determined as the area of intracellular ALCAM that lacks extracellular ALCAM (red but no green). The sum of these two represents total ALCAM expression.

Immunization and Fusion. Four A/J mice were immunized with the ALCAM C-terminal peptide sequence CKDLGNMEENKKLEENNHK (New England Peptide) based on the cytoplasmic sequence of ALCAM (Fig. 15). The peptide was conjugated to Keyhole Limpet Hemocyanin (KLH) using the N-terminal cysteine. Initial immunization was performed with 50 µg of purified antigen emulsified in 50% phosphate-buffered saline (PBS), 50% Freund's complete adjuvant (Pacific Immunology) injected subcutaneously into the nape of the neck (50%) and intramuscularly to the gluteal muscles (50%). Subsequent boosts were performed subcutaneously with incomplete Freund's adjuvant. Serum collected post injection was assayed for reactivity with the antigen by enzyme-linked immunosorbent assay (ELISA) and western blot analysis. The mouse with the highest titre was chosen for the final intraperitoneal boost followed four days later by electrofusion of spleen-derived cells by standard methods with SP2/0 myeloma cells. Fused cells were plated for under selection in semi-solid media and antigen-reactive colonies identified by solid phase ELISA were picked using a ClonePix robotic system (Genetix, Ltd.). ALCAM-specific antibodies were initially identified by direct ELISA using the immunogen, and subsequently verified by western blot analysis and immunofluorescence using intact ALCAM. Selected clones were scaled up and inoculated into one liter bioreactors (Wilson Wolf Manufacturing

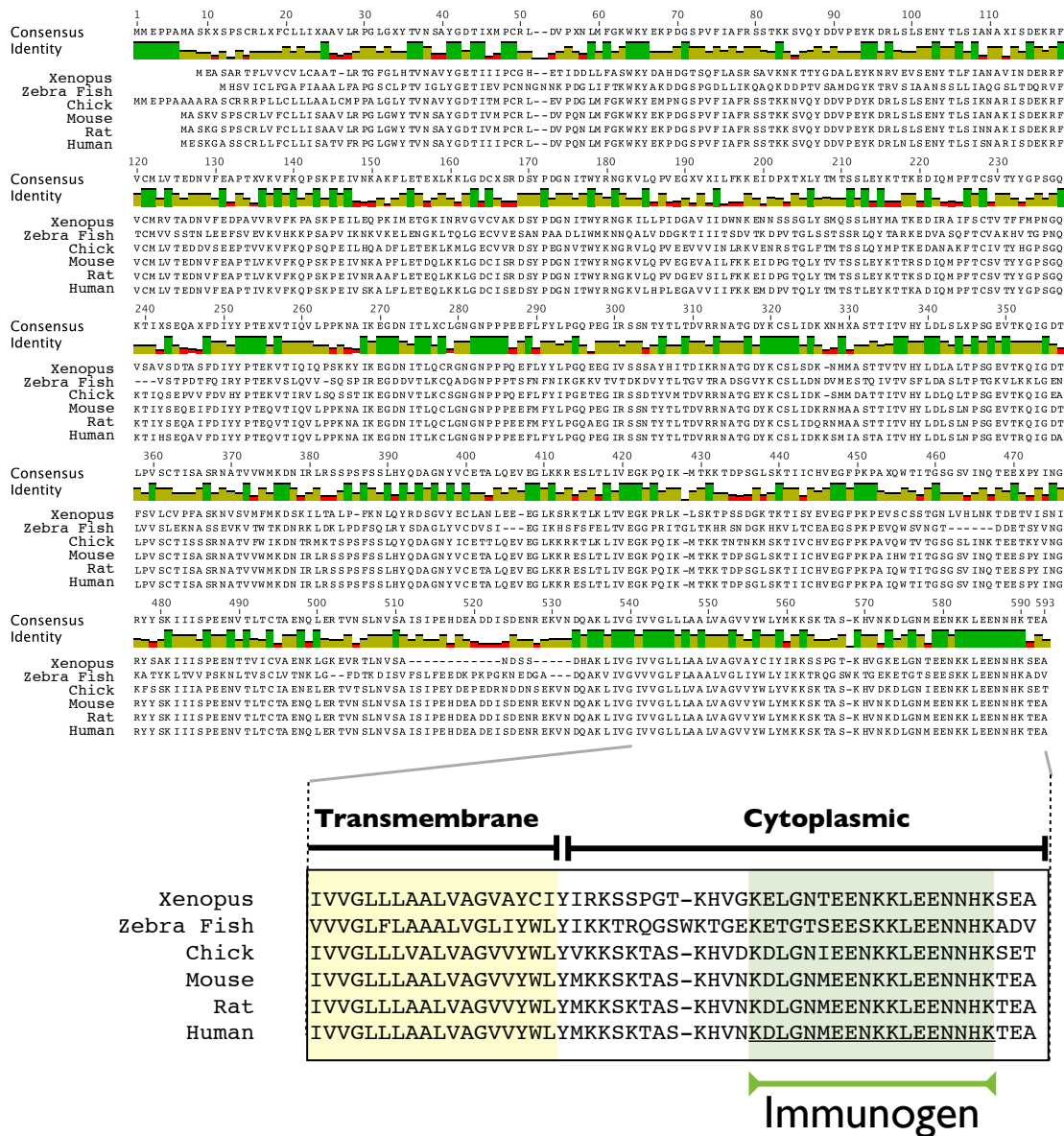


Figure 15. Multi-species sequence alignment was carried out using the Geneious™ bioinformatics software. Along the top of each alignment is the sequence identity plot comparing the sequence across species. Green peaks are 100% identity among species; yellow and red are lower identities. Immunogen sequence is located in the cytoplasmic tail consisting of a highly conserved 14 amino acid sequence.

Corporation) and grown for 3-4 weeks. Purified antibodies were obtained by affinity chromatography on Protein-G sepharose (GE Life Sciences) from bioreactor-generated supernatants.

Enzyme-linked Immunosorbent Assay (Direct ELISA). Flat-bottomed 96-well microtiter plates were coated with KLH-conjugated peptide at 10 µg/ml in Carbonate-Bicarbonate buffer pH 9.6 (15mM Na₂CO₃, 30mM NaHCO₃, 0.001% Thimerosal) for 4hr (37°C) or overnight (4°C). Coated plates were washed and blocked with 1% BSA in PBST (PBS + 0.1% Tween-20) using an ELx405 Select (Bio-Tek). Supernatant or diluted sera (100µl) was allowed to incubate at 37°C for 1hr before washing three times with PBST. Peroxidase-conjugated goat anti-mouse IgG Fc fragment specific secondary antibody (Jackson ImmunoResearch Labs) diluted 1:5000 in PBST/1% BSA was added to the wells and incubated 1 hr at 37°C. Plates were washed three times in PBST and bound antibodies were detected utilizing the colorimetric substrate ABTS (Sigma) and hydrogen peroxide according to vendor instructions). For whole-cell lysate ELISA, flat-bottomed high-binding 96-well plates were coated with 10µg of whole protein lysate in PBS and incubated overnight at room temperature. Coated plates were subsequently treated as described above for KLH-conjugated peptide.

(Sandwich ELISA). For the detection of human ALCAM in serum samples from colorectal cancer patients, 96-well microtiter plates (Costar 9018) were coated with 2 µg/ml of capturing antibody overnight at 4°C. Human serum samples were

diluted 1:80 in PBS/1%BSA and the ELISA reaction was performed as described by manufacturer protocol (R&D Systems).

Statistical analysis. Descriptive statistics were applied to show patient's basic characteristics stratified by ALCAM shedding score. Wilcoxon rank sum test and Kruskal-Wallis test were applied to exam the mRNA expression difference between normal tissues and cancer tissues or the ALCAM shedding percentage among normal patients and cancer patients in all different stages. Kaplan-Meier curve was used to estimate the survival probability for each group, with corresponding p-value and hazard ratio calculated from log-rank test. Receiver Operating Characteristic (ROC) curves were used to identify the optimal specificity and sensitivity for patient stratification. For survival analysis the patient population was dichotomized across a value of ALCAM shedding or intact ALCAM as defined by the ROC curves. For ALCAM shedding this was 0.75 and for intact ALCAM this was 0.15 For shedding the p-values of all statistical tests were two-sided and considered significant when $p < 0.05$ where * denotes $p < 0.05$, ** denotes $p < 0.01$ and *** denotes $p < 0.001$. All statistics were completed using either R, SPSS or GraphPad Prism. Multivariable analysis using logistic regression was performed on stage II patients (n=66; median follow-up, 70 months; median age of diagnosis, 67 years). The variables included were ALCAM shedding, age at time of diagnosis, race and gender with an incidence of 51.5% (34 events) for overall survival and 26.9% (18 events) for disease specific survival.

RESULTS

Correlation of ALCAM and ADAM17 expression with survival of colorectal cancer patients. In normal colorectal tissue, immunohistochemical staining for the extracellular domain of ALCAM using HPA10926 reveals the protein at areas of cell-cell contact within the epithelial cells of the colonic crypts and in hemopoietic cell populations of the stroma (Fig. 16A i and ii). In contrast to normal colon, the concomitant staining of colorectal cancer tissue reveals a very heterogeneous staining. Within the same tumor, some regions exhibit elevated ALCAM (Fig. 16A iii) while others exhibit irregular staining (iv) or lack ALCAM staining altogether (v). Similar heterogeneity of ALCAM staining is observed in a publicly available tissue microarray (proteintlas.org) (134)). ALCAM protein expression is detectable in 12/14 CRC cell lines (Fig. 16B and Fig. 17). Expression of the ALCAM mRNA in CRC cell lines among the NCI60 (Col) is intermediate between the low expressing leukemia (Leu) cell lines and the high expressing breast cancer (Br) cell lines (Fig. 16B).

To evaluate ALCAM mRNA expression in colorectal cancer, a single cohort consisting of 250 patients obtained through a multi-institutional collection (VUMC, UAMC and Moffitt Cancer Center) was analyzed. ALCAM mRNA is elevated in cancer patients (Fig. 16C, $p < 0.001$) and univariate analysis revealed that high ALCAM expression was in fact associated with significantly decreased survival (Fig. 1C, $p < 0.0001$). Similarly, expression of ADAM17 (the sheddase of ALCAM) was also significantly elevated in colorectal cancer (Fig. 16D, $p < 0.0001$). The

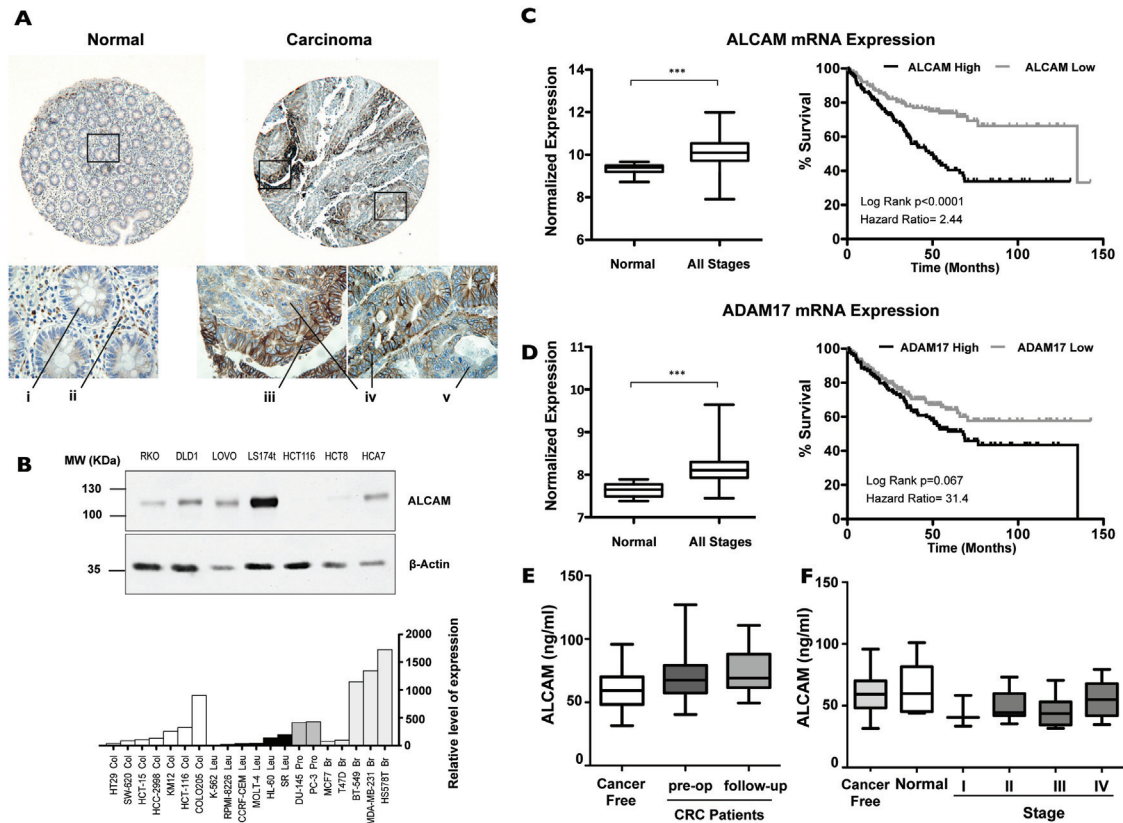


Figure 16. ALCAM expression in colorectal carcinoma and its correlation to patient outcome. A) Representative immunohistochemical staining for ALCAM in normal and tumor colon sections using an antibody directed to the extracellular domain of ALCAM (HPA010926). B) Expression of ALCAM in CRC cell lines evaluated by immunoblotting (left) and microarray analysis (right, GDS1761). Expression (mRNA) of ALCAM (C) and ADAM17 (D) in a cohort of 250 colorectal cancer patients was correlated to patient survival after dichotomizing the population across its mean expression into patients with “High ALCAM” and “Low ALCAM”. E) Using an ALCAM sandwich ELISA, circulating levels of shed ALCAM were evaluated in serum from cancer-free patients ($n=48$) and compared to serum from CRC patients at time of diagnosis (pre-op, $n=42$) and serum from patient at time of followup after treatment (post-op, $n=19$). F) CRC patients were stratified according to stage (I-IV) and compared to cancer-free patients ($n=48$) and healthy adults ($n=6$). Box plots show the mean, standard deviation and full range of the expression data. Survival is presented with Kaplan-Meier plots and log-rank test was used to evaluate significance.

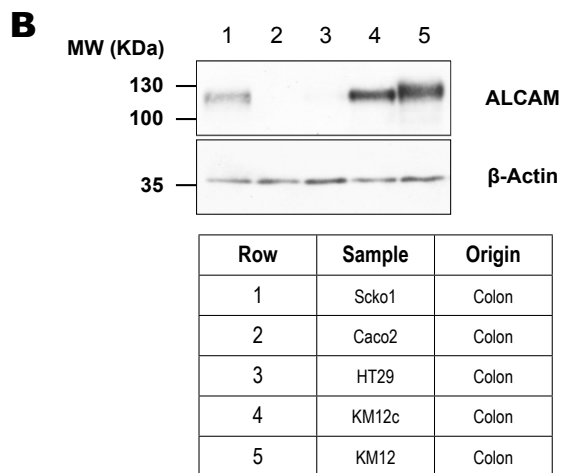
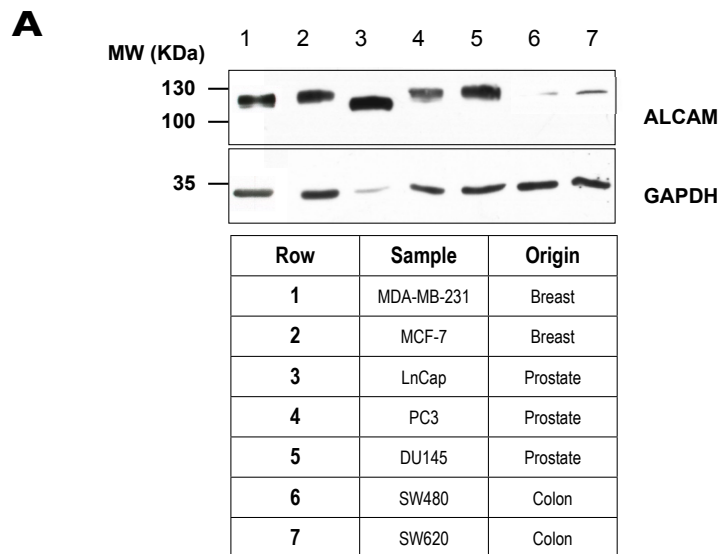


Figure 17. ALCAM expression in continuous cancer cell lines. Lysates from human cancer cell lines immunoblotted for ALCAM using an antibody specific for its extracellular domain.

association of ADAM17 expression with patient survival was not statistically significant ($p=0.067$), but its elevated expression in CRC together with its established ability to cleave ALCAM is sufficient to suggest that ADAM17 is available to cleave ALCAM and increase its shedding within the tumor microenvironment. Indeed, previous studies reported heterogeneous staining of ADAM17 in colorectal cancer (Merchant et al., 2008), which might be responsible for the variable detection of ALCAM extracellular domain within the tissue. The soluble extracellular domain can be detected in the serum of some cancer patients (90,112). However, ALCAM-specific ELISA of serum from CRC patients did not reveal a correlation between disease progression and increase in circulating ALCAM when comparing serum obtained from cancer free patients and serum obtained from CRC patients prior to, and after therapy (Fig. 16E). Detailed comparison of cancer free patients and normal healthy individuals versus increasing stages of CRC patients revealed no significant correlation with circulating levels of ALCAM (Fig. 16F).

The histological detection of membranous ALCAM had been found to correspond negatively with patient survival (20). Using an antibody to the extracellular domain of ALCAM, a histological evaluation of a 69-patient cohort was performed (Fig. 18). While the presence or absence of membrane staining did not correspond with overall or disease specific survival, the loss of detectable cytoplasmic ALCAM corresponded with very poor prognosis. However, only 8/69 patients (12%; Fig. 18, bottom right) were negative for cytoplasmic ALCAM while 39/69 (56%; Fig. 18, bottom left) lacked membranous ALCAM. This loss of ALCAM from

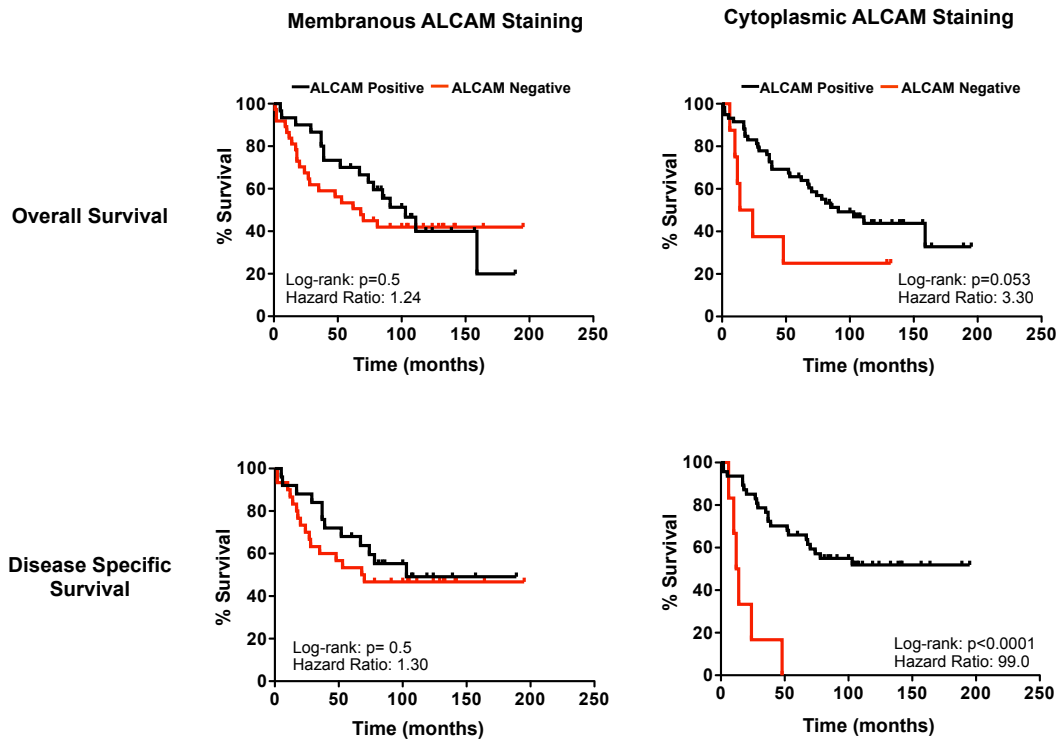


Figure 18. Lack of cytoplasmic ALCAM corresponds with poor patient outcome. Detection of ALCAM on the membrane vs in the cytoplasm. A tissue microarray of 75 CRC and 12 normal colonic tissues was stained by traditional IHC for the extracellular domain of ALCAM. Membranous and cytoplasmic staining was stained and scored by an independent pathologist in a blinded manner.

the membrane (with concomitant retention of cytoplasmic staining) is likely to be due to shedding of the ectodomain from the cell surface.

Production and validation of an antibody specific for the cytoplasmic domain of ALCAM. Since ALCAM shedding occurs on the surface of the tumor cells, we hypothesized that shedding might be detectable within the tumor tissue itself. In order to achieve this, we thought to develop an ALCAM dual-stain based on independent detection of the intracellular and extracellular domains with domain-specific antibodies (Fig. 19A). Using these antibodies in histological staining of normal and tumor tissue sections should enable the detection of ALCAM shedding *in situ* (Table 3). To accomplish this, a unique antibody directed to the cytoplasmic tail of ALCAM was generated using a 14 AA sequence from the cytoplasmic tail (Fig. 15) conjugated to KHL to immunize four A/J mice. Spleens from two seropositive mice were fused and 125 viable hybridomas selected from >8000 antigen-reactive clones were evaluated by comparing reactivity to native ALCAM and KLH using direct ELISA (Fig. 20A). ALCAM-specific hybridomas were validated by immunoblotting using whole cell lysate to confirm binding to intact ALCAM protein (Fig. 20A). Antibody specificity for ALCAM was verified by comparing reactivity with lysates from control and ALCAM knockdown cells (Fig. 20B) and mouse tissue from *wild type* and *ALCAM*^{-/-} mice (Fig. 19B). Antigen specificity was confirmed by competitive blocking using the immunizing peptide during immunoblotting (0.1 or 1 μ g/ml, Fig. 20C) and histological staining (1 μ g/ml, Fig. 19C). As expected, peptide competition with the immunizing peptide resulted

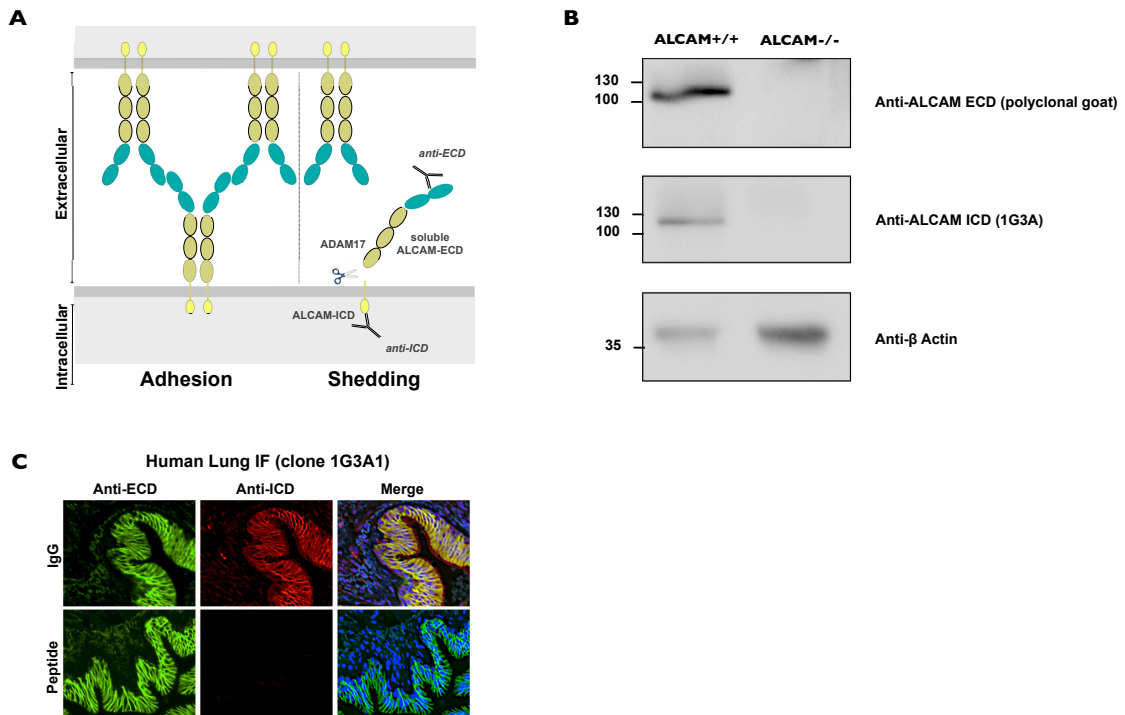


Figure 19. The specificity of anti-ALCAM ICD confirmed by analysis of ALCAM in ALCAM^{-/-} mice. A) Schematic representation of ALCAM and its organization as a cell-cell adhesion molecule. Individual domains are presented as ovals (extracellular IgG-like domain) or rectangles (intracellular domain). B) The antibody 1G3A1 specific for the cytoplasmic tail of ALCAM was used to immunoblot 40 μ g of liver extracts from wild type and ALCAM^{-/-} mice. C) ALCAM specificity of individual clones was evaluated by outcompeting antibody binding with the immunizing peptide in immunofluorescence staining of human lung tissue sections.

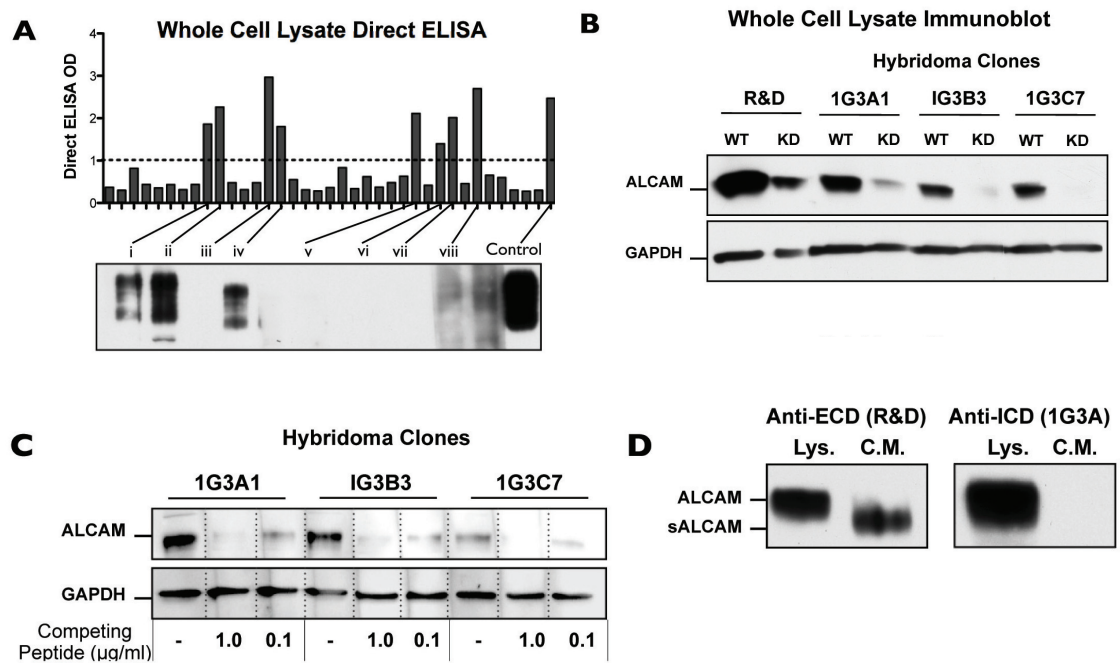


Figure 20. Screening and validation of an antibody specific to the cytoplasmic domain of ALCAM. A) B) Individual hybridoma clones reactive to the immunizing peptide were screened by direct ELISA using whole cell lysate from a cell line expressing high levels of ALCAM (PC3). A 1.0 OD was used to select clones for further validation by immunoblotting cutoff. Three high titre clones chosen for further validation were 1G3A1 (ii), 1G3B3 (iv), and 1G3CF (i). B) Hybridoma clones 1G3A1, 1G3B3, and 1G3CF were further for specificity to ALCAM by comparing their reactivity to ALCAM with a commercial antibody (directed against the extracellular domain) using lysates from parental PC3 cells and PC3 cells with shRNA-mediated knockdown of ALCAM. C) ALCAM specificity of individual clones was further evaluated by outcompeting antibody binding with the immunizing peptide in Immunoblots of whole cell lysates (PC3). D) Specificity of purified 1G3A1 against the cytoplasmic tail of ALCAM was confirmed by immunoblotting intact ALCAM (whole cell lysate; Lys.) and shed ALCAM (conditioned medium; C.M.) from PC3 cells.

in a loss of Intracellular ALCAM. The stable hybridoma 1G3A1 was selected as the most promising antibody based on its reactivity in ELISA, immunoblot, immunofluorescence and standard immunohistochemistry. Specificity of 1G3A1 for the cytoplasmic tail of ALCAM was defined by its ability to detect intact ALCAM in cell lysates but not shed ALCAM in conditioned medium (Fig. 20D). In contrast, the commercial antibody against the extracellular domain of ALCAM (R&D) detects intact as well as shed ALCAM which lacks the cytoplasmic domain.

Dual-staining for the intracellular and extracellular domains of ALCAM in normal and tumor tissue. Using the antibody 1G3A1 to specifically detect the cytoplasmic domain of ALCAM together with the commercial antibody HPA010926 specific for the extracellular domain, we developed a dual-staining procedure for ALCAM in human tissues (Fig. 21&22). Three-color staining (Nuclei: blue, Extracellular Domain: green, Intracellular Domain: red) was performed on tissues along the digestive tract including stomach (Fig. 21A) and colon (Fig. 21B). In normal tissues, detection of the extracellular and cytoplasmic domains of ALCAM coincided, thereby suggesting that ALCAM is expressed and present in its intact form (Fig. 21C, arrow). However, within tumor tissues the intracellular domain (Red) is often seen in the absence of the extracellular domain (Green) indicating that the extracellular domain of ALCAM was shed (Fig. 21C, arrow head). In gastric cancer, entire glandular structures appear to lack staining for the extracellular domain while others are fully positive (Fig. 21Ci). This all-or-none staining for the extracellular domain suggests that ALCAM-shedding is activated

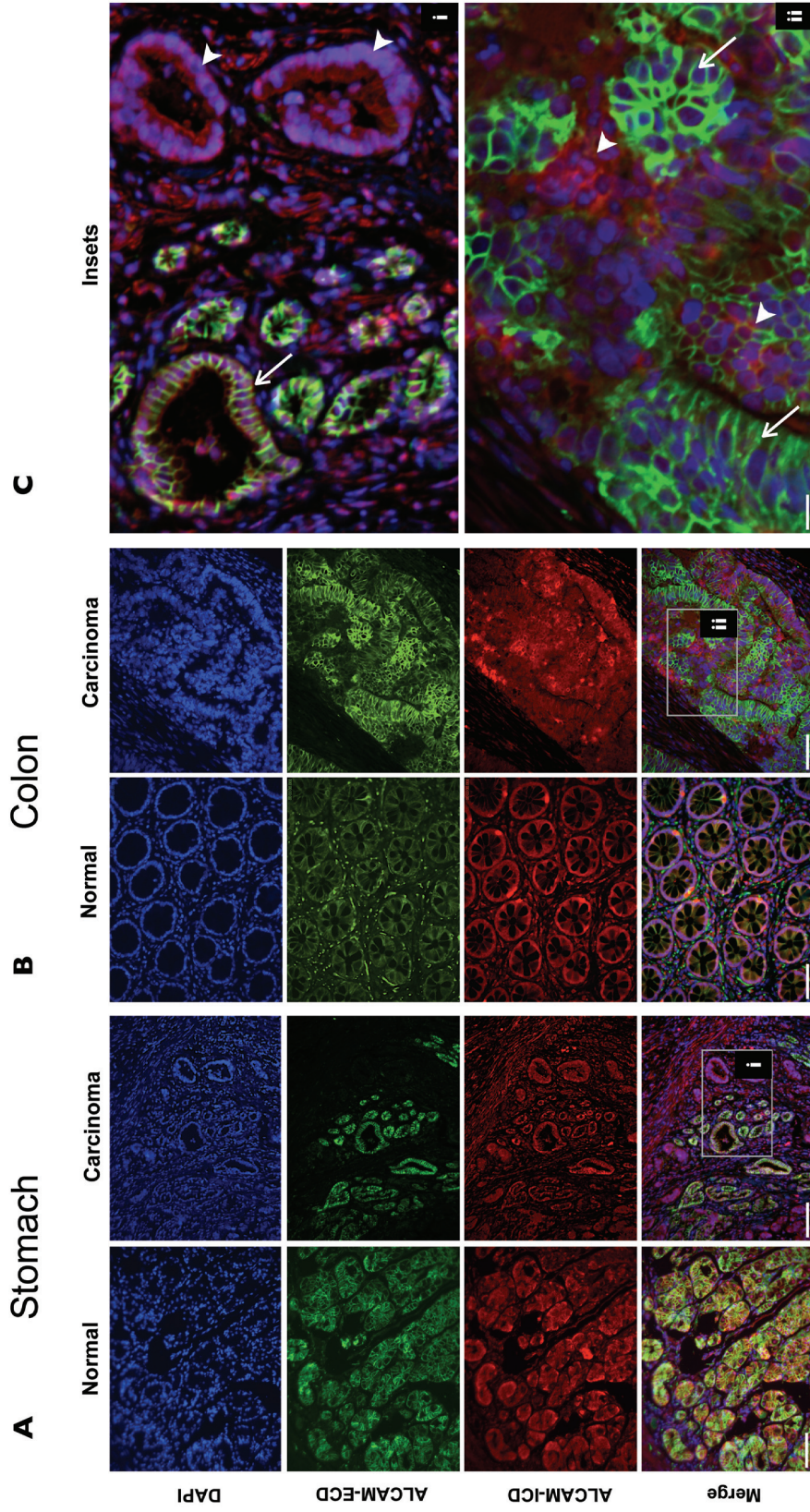


Figure 21. Detection of ALCAM shedding in cancers of the stomach and colon. The ALCAM dual stain composed of the antibody HPA010926 directed against the extracellular domain (green) and antibody 1G3A1 directed against the intracellular domain (red) was used to identify locations within the tissue that exhibited ALCAM shedding in cancers of the stomach (A) and colon (B), scale bar = 64µm. Images of nuclear stain (blue) were merged with images of HPA010926 (green) and 1G3A1 (red) staining. Insets (C) present magnified regions i and ii from stomach and colon carcinoma. Areas of ALCAM shedding are identified by the presence of 1G3A1 staining (red) and an absence of HPA010926 (green) staining. Arrow: intact ALCAM, Arrow Head: ALCAM shedding. Scale bar = 320µm.

at a macroscopic level within the tissue architecture of the stomach. In colorectal carcinoma tissue ALCAM staining is more heterogeneous with small populations of cells within the same histological structure exhibiting different levels of staining for the ALCAM extracellular domain (Fig. 21Cii). The irregular staining in CRC suggests that ALCAM shedding is occurring throughout the tumor but regulated at a cellular level.

Quantitative analysis of ALCAM shedding. Previous studies evaluating ALCAM as a biomarker for predicting colorectal cancer patient survival have published conflicting and inconclusive results (20,52,53,109,161,162). We postulate that this variability is due to ALCAM shedding, since these studies all evaluate ALCAM through detection of its extracellular domain. To visualize ALCAM shedding we used HPA010926 rabbit monoclonal antibody to detect the extracellular domain and 1G3A1 monoclonal mouse antibody (Fig. 20) to detect the intracellular domain. Shedding of ALCAM was defined for the selected tumor area as the presence of the intracellular domain of ALCAM and the absence of the extracellular domain of ALCAM (Fig. 22). Immunofluorescent staining for each domain was completed simultaneously on sections from paraffin-embedded colorectal cancer tissue which were digitally scanned and quantitatively assessed using ImageJ (Fig. 23). Shedding was defined as the loss of the extracellular domain and retention of the cytoplasmic domain. Shedding data is presented graphically in Fig. 22A and B. Quantitatively ALCAM shedding is the fraction of detectable ALCAM from which the extracellular domain is absent ($[\text{Total ALCAM} - \text{Intact ALCAM}] / \text{Total}$

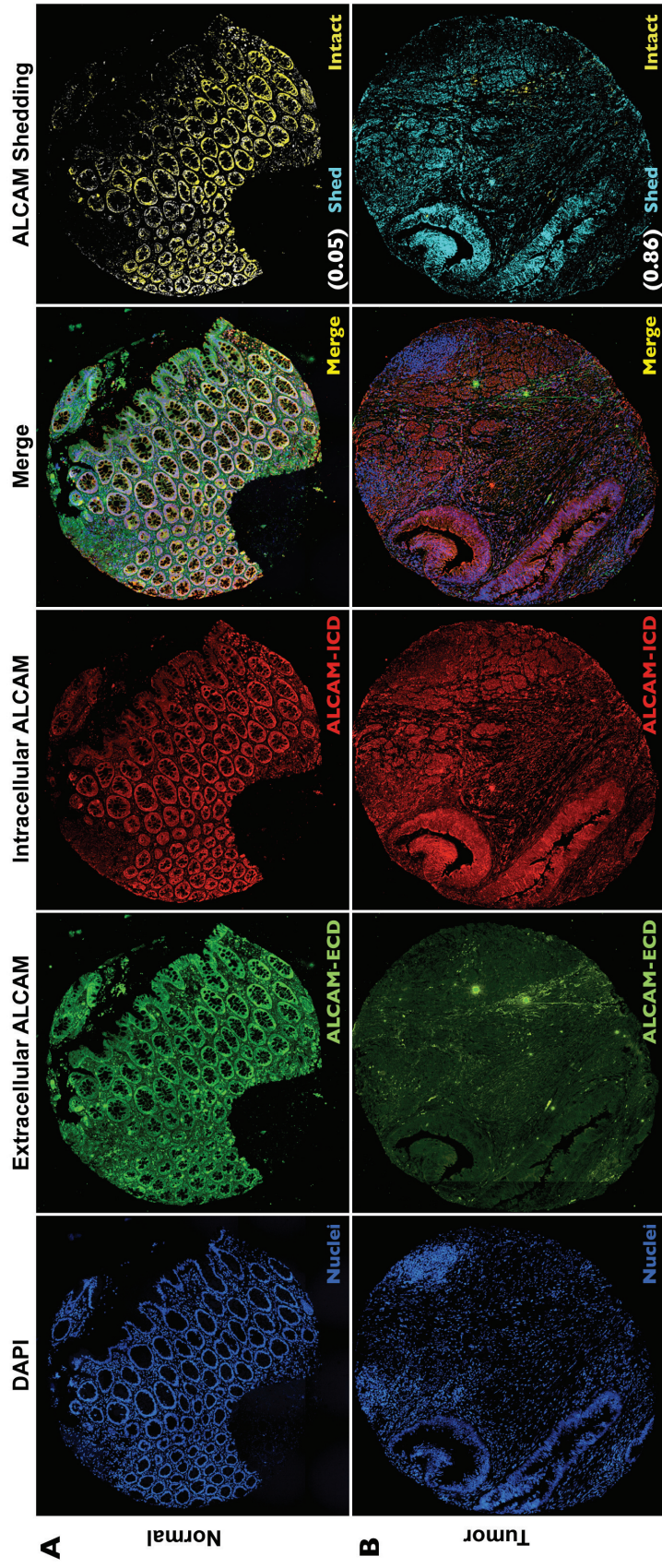


Figure 22. Quantitative analysis of ALCAM shedding in CRC. The ALCAM dual stain was used to detect the extracellular domain (green) and intracellular domain (red) of ALCAM in normal colonic mucosa (A) and colorectal cancer (B). Using computational analysis with ImageJ, intact ALCAM was defined by the co-localization of detectable intracellular domain (ICD) and extracellular domain (ECD). ALCAM shedding was defined as the detection of ALCAM-ICD in the absence of co-localized ALCAM-ECD. The results of this analysis presents ALCAM shedding quantitatively as the fraction of total detectable ALCAM from which the extracellular domain is absent. This is shown graphically in the last panel with the colors yellow and teal representing intact ALCAM and ALCAM shedding respectively.

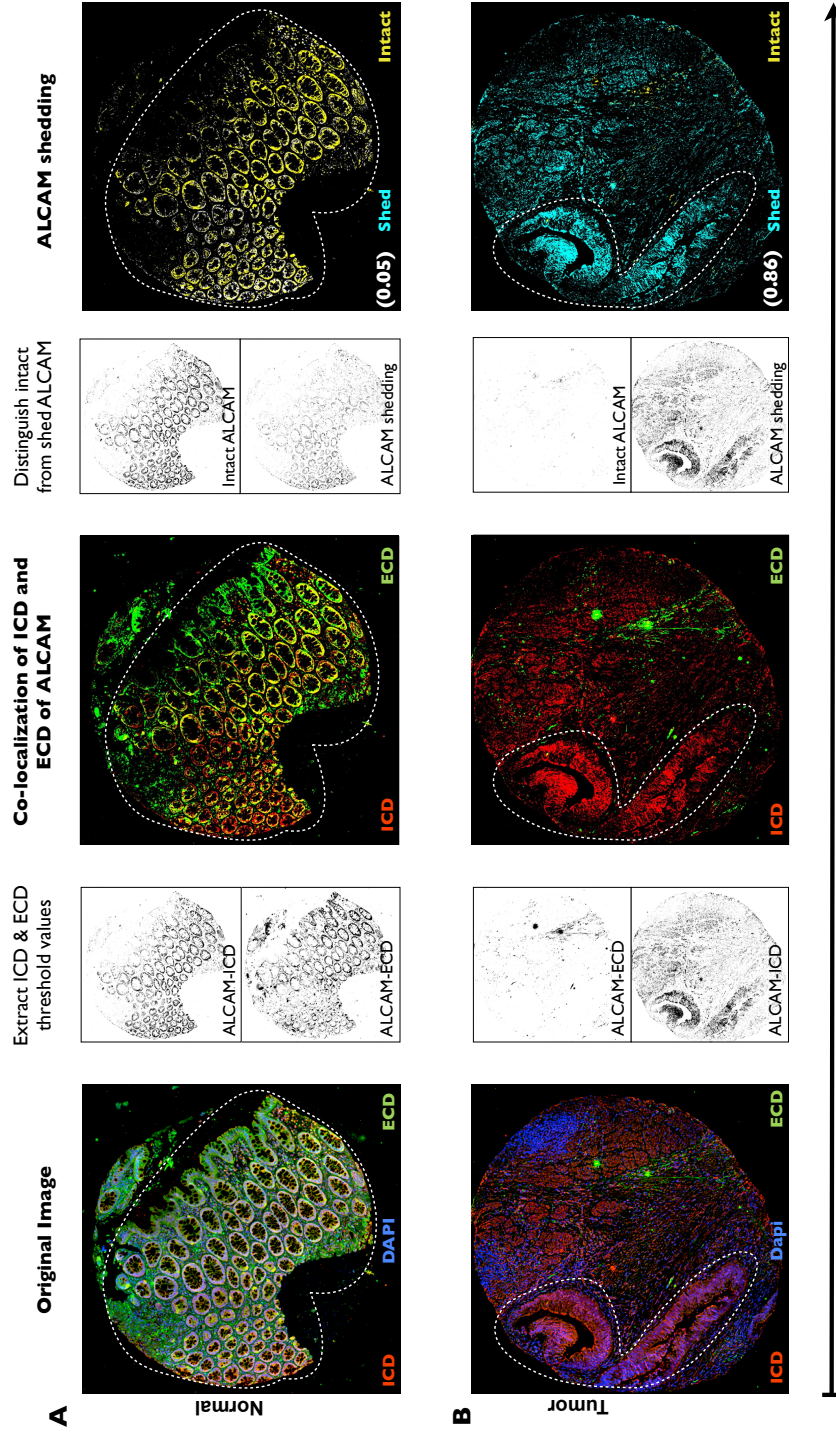


Figure 23. The image processing pipeline implemented using Fiji. Images obtained of normal (A) and tumor (B) tissues through scanning on the Ariol® platform were processed to obtain the fraction of ALCAM shed. The original images was separated into its individual color channels and threshold values were obtained for the red channel (ALCAM-ICD) and the green channel (ALCAM-ECD). A co-localization of these thresholded areas was used to distinguish intact ALCAM (both ALCAM-ICD and -ECD, yellow) from shed ALCAM (only ALCAM-ICD, teal). Quantitatively ALCAM shedding is defined as the fraction of detectable ALCAM from which the extracellular domain is absent.

ALCAM). In normal colonic mucosa, detection of the extracellular and intracellular domains overlap extensively, demonstrating the predominant presence of intact ALCAM (yellow) and little ALCAM shedding (teal) (Fig. 22A, last panel). Conversely, in tumor sections the intracellular domain of ALCAM remains detectable while the extracellular ALCAM is frequently absent, indicating that ALCAM is shed (Fig. 22B, last panel).

ALCAM shedding corresponds with reduced patient survival. Since ALCAM shedding is clearly elevated in tumors, we hypothesized that ALCAM shedding can be an accurate prognostic marker for colorectal cancer. To evaluate this, histological detection of ALCAM shedding was performed on specimens from 105 CRC patients and 12 healthy controls (see Table 4 for patient demographics). For each specimen, ALCAM shedding was quantified as described for Fig. 22. For each patient, the mean value across three specimens was used to evaluate the correlation between ALCAM shedding and patient survival. ALCAM shedding is clearly elevated in tissue from CRC (Fig. 24A). Shedding is already increased in some stage I CRC patients and is significantly increased for stage II, III and IV patients. Indeed ANOVA analysis confirms significant elevation across the increasing stages (mean fraction shed = 0.64, 0.73, and 0.89, for stage II, III, and IV, Fig. 24B). Moreover, ALCAM shedding was elevated in patients that died during the course of their disease. The presence of elevated ALCAM shedding in stage II patients is particularly interesting. This led us to hypothesize that patients with elevated ALCAM shedding have a worse outcome.

Characteristic	Total	Low ALCAM Shedding*	High ALCAM Shedding*
N (%)	105	50 (47.6)	55 (52.4)
Age at Dx [Range]	63.7[10-90]	61.5 [26-89]	65.6 [10-90]
AJCC Stage (%)			
I	8 (10.7)	4 (50)	4 (50)
II	66 (42.7)	35 (53)	31 (46.9)
III	25 (37.3)	10 (40)	15 (60)
IV	6 (9.3)	0 (0)	6 (100)
Sex (%)			
M	52 (49.3)	27 (52)	25 (48)
F	53 (50.7)	23 (43)	30 (57)
Average ALCAM Shedding Score [Range]	0.68 [0.011-0.99]	0.42 [0.011-0.75]	0.89 [0.77-0.99]
* Low and High ALCAM are dicotomized across the fraction of ALCAM that is shed being equal to 0.75.			

Table 4. Comparison of High and Low ALCAM Shedding colon cancer patients with respect to age, sex, and staging

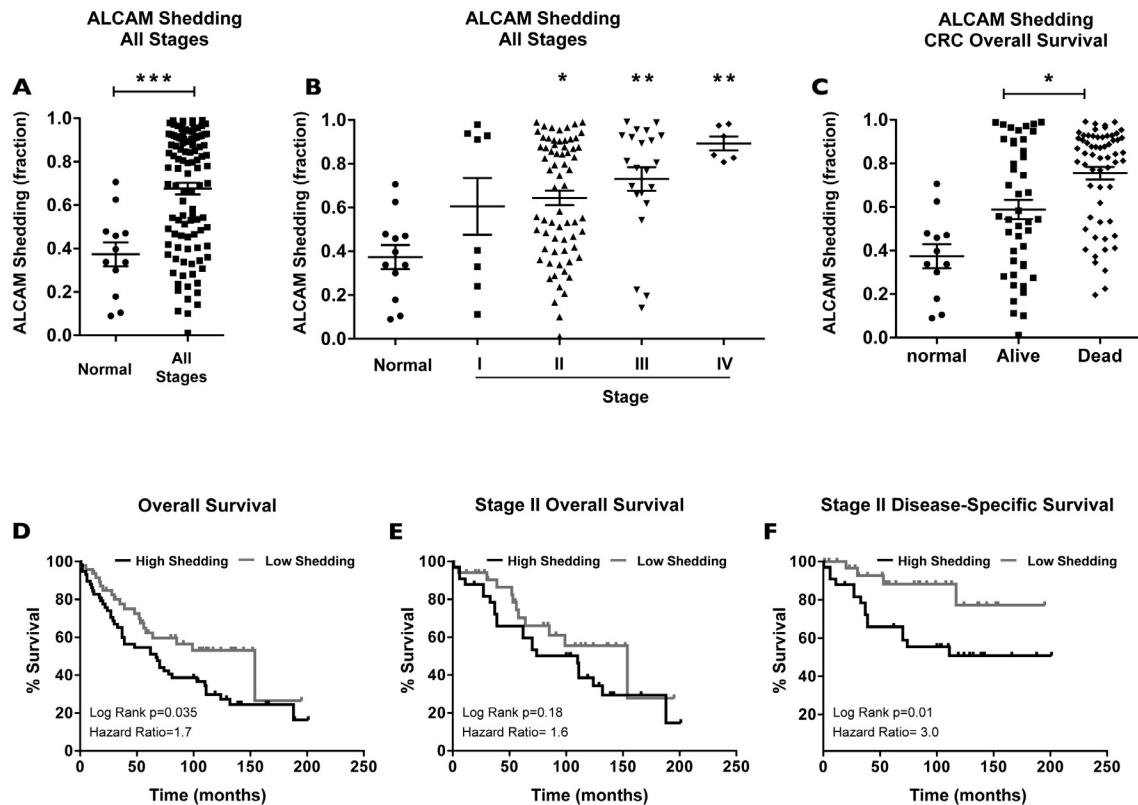


Figure 24. ALCAM shedding in CRC correlates with poor survival. ALCAM shedding was evaluated in tissue from 105 CRC patients and 12 healthy controls. Scatter plots demonstrate the differences in ALCAM shedding between normal colonic mucosa and CRC tumors as a single population (A), stratified across histological stage (B), or separated according to survival (C). Kaplan-Meier survival curves of CRC patients with high versus low ALCAM shedding were generated and log-rank tests performed to evaluate the correlation of ALCAM shedding with overall survival of patients at all stages (D), overall survival of stage II patients (E) or disease-specific survival of stage II patients (F). Scatter plots show the mean and SEM with statistical evaluation by Mann-Whitney for selected groups (A and C) or Kruskal-Wallis with Dunn's multiple comparison restricted to normal (B). Survival is presented as Kaplan-Meier plots with the log-rank test used to evaluate significance.

To evaluate the correlation between ALCAM shedding and patient outcome, survival analysis was performed by segregating CRC patients based on ALCAM expression (Fig. 24D) using a shed fraction of 0.75 to delineate “High” vs “Low” ALCAM shedding. When analyzing the full population of CRC patients, high ALCAM shedding correlated positively with worse overall survival ($p=0.035$, Figure 24D). To determine if ALCAM shedding can be prognostic for early stage disease, a univariate survival analysis was performed specifically to stage II patients. While ALCAM shedding does not correlate with overall survival in stage II patients (Fig. 24E), it correlates strongly with disease-related death showing significant survival benefit in the Stage II patients with low ALCAM shedding (Fig. 24F, $p=0.01$ HR=3.0).

Multivariable analysis was restricted to stage II patients since they were the emphasis of our investigation and the cohort biased to this population. Multivariable analysis with logistic regression of stage II patients found that ALCAM shedding and age at time of diagnosis were both independent predictors of overall survival after adjusting for gender and race (ALCAM shedding; adjusted odds ratio (OR), 9.972; 95% confidence interval (CI) 1.17-84.9 ; $p=0.035$. Age; OR, 1.079; 95% CI, 1.027-1.133; $p=0.003$). An analysis of disease-specific survival found that only ALCAM shedding was an independent predictor of survival after adjusting for age at time of diagnosis, race and gender (ALCAM shedding OR, 29.02; 95% CI, 2.165-389.08; $p=0.011$). Bootstrapping was performed as an internal validation to confirm these results and found that ALCAM shedding contin-

ued to be an independent predictor of survival in stage II patients (overall survival $p=0.002$; disease-specific survival $p=0.023$).

DISCUSSION

The main goal of this study was to determine if ALCAM shedding corresponds to patient outcome in colorectal cancer. As cancer treatments evolve towards individualized therapies, they rely increasingly on the availability of prognostic and predictive markers to determine the patient's status and facilitate treatment decisions. Some published studies evaluating ALCAM detection as a biomarker for CRC suggest clinical utility, but others have been inconclusive and contradictory (20,52,53,109,162). This ambiguity in the literature may be explained by ALCAM shedding via ADAM17-mediated cleavage (83,89). We propose that ALCAM shedding, rather than its expression, indicates disease progression. Our dual stain reveals both intra- and extracellular epitopes of ALCAM and clarifies its prognostic value in CRC. ALCAM shedding in tissues was defined as the detection of the intracellular epitope in the absence of the extracellular domain. Using this novel assay, we demonstrate a strong correlation between elevated ALCAM shedding and poor patient outcome. Importantly, ALCAM shedding correlates with poor outcome in early stage disease (Stage II, Fig. 24). Thus, ALCAM is not merely a biomarker for disease progression but may also allow for outcome stratification among patients with early stage disease.

ALCAM was originally identified in the context of at least five distinct biologies: leukocyte activation, neuronal guidance, bone development, stem cell

identification, and cancer progression (120). ALCAM expression is frequently elevated during oncogenesis. However, detection of the protein in tumor tissues is extremely variable. Knowing that ALCAM is shed by the protease ADAM17 (83), we speculated that in CRC, ALCAM is expressed and shed by ADAM17 into the circulation. Indeed, the irregular pattern of expression reported here for ALCAM was previously observed for ADAM17 in glandular tissue of early to advanced gastric cancer (164) and colorectal cancer patients (53). Unfortunately, serum levels of ALCAM in controls (cancer-free age + sex-matched individuals, 45-95ng/ml) overlap with circulating levels in CRC patients pre- or post-therapy (45-125 and 50-110ng/ml respectively, Fig. 16E). This compromises the accuracy and specificity of a blood test for ALCAM (Fig. 16) (165). Nevertheless, the lack of specificity for tumor-derived ALCAM detection in the circulation does not negate the fact that ALCAM shedding within the tumor tissue corresponds with disease progression.

The detection of ALCAM shedding within the tumor tissue itself greatly increases the specificity of ALCAM as a prognostic factor. Our primary aim was to devise a method to stratify at-risk patients using ALCAM shedding as an indicator of disease progression and poor patient outcome, and not as a diagnostic tool. Indeed, the strong correlation between ALCAM shedding and poor patient outcome in early stage disease suggests that molecular progression can occur in a cancer that appears histologically more benign.

An important disparity becomes apparent when we correlate clinical outcome (survival) with ALCAM gene transcription (mRNA), protein expression

(based on detection of intact ALCAM) and ALCAM shedding. Elevated ALCAM transcription is associated with poor outcome yet elevated levels of intact ALCAM protein (through detection of co-localized extracellular domain and intracellular domain) is associated with improved outcome (Fig. 25A vs. B). This disparity could be rectified if we consider that the extracellular domain of ALCAM is shed leaving the mistaken impression that ALCAM protein is lost during tumor progression. Indeed, our analysis of ALCAM shedding (summarized in Fig. 25C) demonstrates that ALCAM shedding rather than loss of expression corresponds with patient outcome. This observation can explain why five independent evaluations of ALCAM in CRC have given conflicting results (20,52,53,109,162).

Although ADAM17 is responsible for proteolytic cleavage of several tumor-associated proteins, few studies have analyzed ectodomain shedding for prognostic purposes. Only one other study attempted to look at shedding used monoclonal antibodies specific for the cleavable form of ErbB4 (166), but was unable to look at shedding directly. The dual staining of ALCAM we presented here is, then, a novel approach to detect molecular behavior (shedding) rather than the molecular identity. Indeed, our results suggest that detection of molecular behavior correlates more specifically with the disease than gene expression itself. Given that the disruption of ALCAM-ALCAM interactions promotes tumor cell motility and metastasis (94,167), ALCAM shedding may predict malignant progression at a molecular level. The clinical correlation between ALCAM shedding and patient outcome (Fig. 24) suggests that detection of disease progression at a molecular level can predict long-term patient outcome. The presence of this correla-

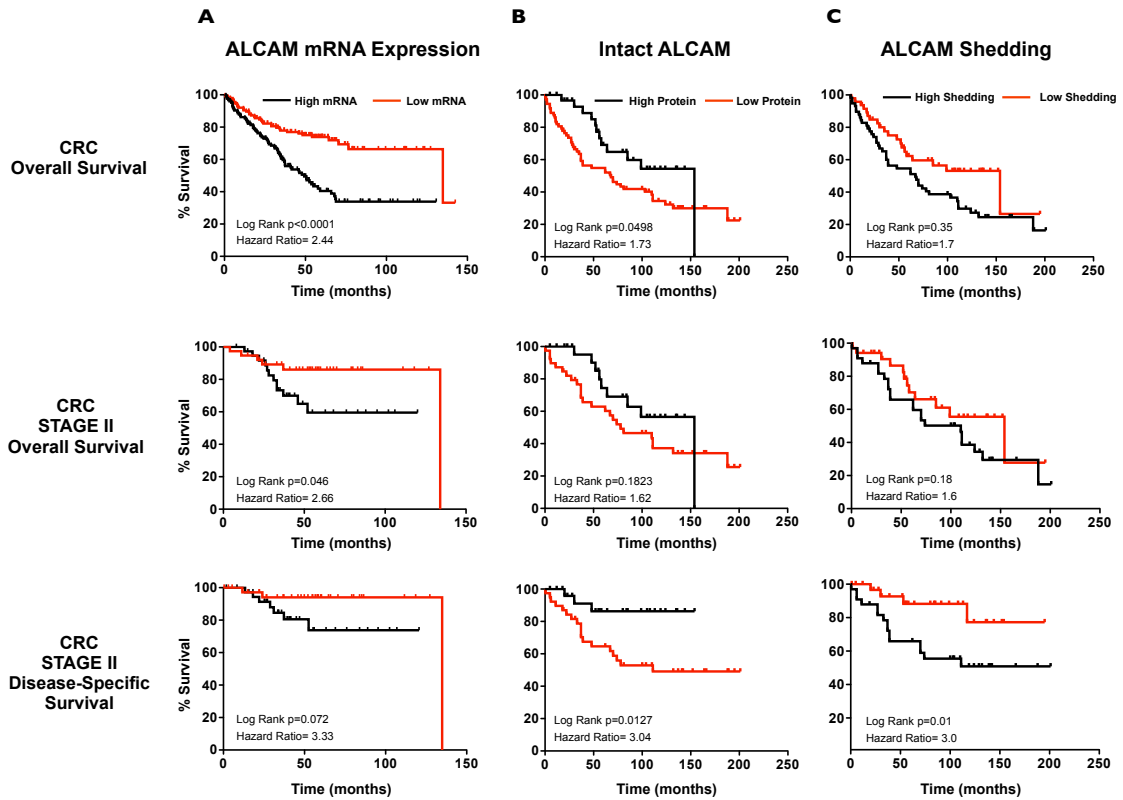


Figure 25. ALCAM mRNA, protein and shedding in colorectal cancer. Kaplan-Meier survival analysis contrasts CRC patients overall survival, stage II patient overall survival and disease-specific stage II CRC survival with high versus low ALCAM mRNA expression (A) protein expression (B) or ALCAM shedding (C). Survival is presented as Kaplan-Meier plots with the log-rank test used to evaluate significance.

tion in early stage disease (stage II, Fig. 24) emphasizes that this molecular progression is present prior to pathological and clinical progression. Detection of this molecular progression allows for stratification of patients according to their risk for poor long-term outcome. Considering that ALCAM is altered in a number of malignancies (96,107,122,168), the clinical correlation of ALCAM shedding to patient outcome is likely to extend beyond CRC to other cancers.

CHAPTER IV

CONCLUSIONS

Significance

The studies presented within this document demonstrate our work on the contribution of tumor-derived ALCAM to skeletal metastasis of prostate cancer and the clinical relevance of its proteolytic product on patient outcome and survival. We hypothesized that a reduction of homotypic ALCAM interactions would disrupt tumor cell adhesion and enhance prostate cancer metastasis. On the contrary, work from Chapter II leads us to conclude that expression of ALCAM is a critical component of tumor metastasis to bone and survival at the secondary site. The work herein points out the dichotomy that exists between ALCAM expression at the mRNA and protein level with adding another dimensional analysis of post-translational proteolytic regulation of ALCAM as it relates to tumor burden. These studies involving the regulation of ALCAM shedding by TGF β , in particular our *in vitro* data in Chapter II, highlight the notion that the cellular microenvironment can act as a key modulator of tumor cell behavior. Finally, the work in Chapter III highlights the use of intratumoral assessment of proteolytic cleavage as a novel approach to using ALCAM as a tumor biomarker in patient stratification. Future work will investigate the mechanisms through which ALCAM engages in the bone microenvironment, both in normal and pathological states. Moreover, investigations using the Rag1^{-/-}:ALCAM^{-/-} immunodeficient model in our lab will

help dissect the contribution of ALCAM-mediated interactions within the bone stroma to tumor cell behavior. Overall, this dissertation has contributed to understanding the multifactorial function of ALCAM in tumorigenesis and provides the evidence and necessary tools for future studies into the mechanism of ALCAM as a signaling adhesion molecule.

Preliminary Data and Future Directions

ALCAM as a mediator of apoptotic resistance

Although we demonstrate that loss of ALCAM decreases prostate tumor cell colonization in the bone, at least in-part, through enhanced apoptosis, the exact mechanism by which this happens remains unknown. One of the major hallmarks of cancer includes the ability of tumor cells to evade apoptosis or programmed cell death (169). Recent studies indicate changes in expression of cell adhesion molecules, including members of the IgSF, may impact apoptotic pathways in cancer cells (170). ALCAM is frequently dysregulated in cancer and has been posed to be protective of apoptosis in breast cancer (17,23,99,148). Apoptosis typically involves deregulation of the p53 tumor suppressor pathway, however, the apoptotic effect we observed was in the PC3 p53-null cell line (171). Modulation of apoptosis by cell adhesion molecules is not a novel observation. For example, human Jurkat T lymphocytes lacking the cell adhesion molecule, PECAM-1, are more sensitive to UV irradiation. Moreover, in this same study, transfection with a Lys89Ala variant of PECAM-1, which lacks homophilic binding capacity, results in enhanced apoptosis. Subsequent studies in murine lung tumor cells

have shown enhanced apoptosis upon functional inhibition of NCAM by anti-NCAM antibodies (172).

In addition to the function of the extracellular domain in cell adhesion, the intracellular domain of CAMs can be cleaved by gamma secretase and subsequently released to elicit intracellular signaling (173). Most recently, studies of the intracellular domain of L1 cell adhesion molecule (L1CAM) have demonstrated DNA damage checkpoint response through interaction of L1CAM intracellular domain with NBS1, a critical component of the MRN complex in early checkpoint response signaling (170). While there is no known function of the short 34 amino acid intracellular domain of ALCAM, we have observed nuclear localization of ALCAM in liver hepatocytes and confocal images of lung epithelial cells using the intracellular domain-specific monoclonal antibody (Fig. 26). To follow up on the increased apoptosis results in our ALCAM knockdown *in vivo* experiments (Fig 27), I completed a preliminary *in vitro* experiment to test if (1) intracellular ALCAM cleavage is necessary for protection from apoptosis and (2) determine if loss of ALCAM enhances apoptosis in response to TNF-alpha. Treatment with a gamma-secretase inhibitor in combination with TNF-alpha and cyclohexamide resulted in an increase in cleaved caspase-3 protein. These results suggest that the anti-apoptotic role of ALCAM could be mediated through cleavage of the intracellular domain. (Fig 27).

On the other hand, it is possible that the intracellular domain of ALCAM may not function directly to mediate its protective effects, rather it is through indirect regulation of anti-apoptotic genes. Signaling pathways that initiate down

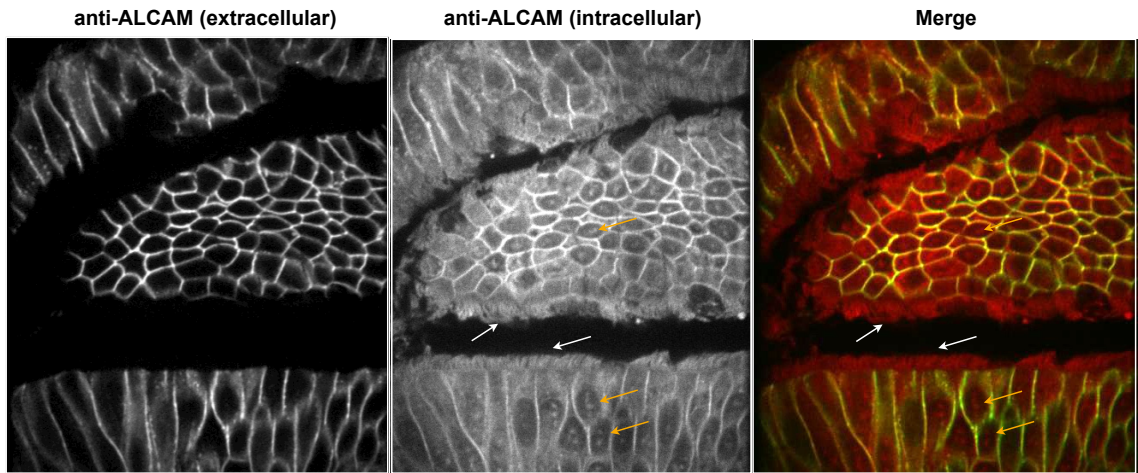


Figure 26. ALCAM cytoplasmic domain has a distinct distribution compared to the extracellular domain. Fluorescent staining of paraffin embedded lung tissue with antibodies against the extracellular and intracellular domain reveal a unique distribution of the cytoplasmic domain. In addition to the expected co-localization at areas of cell-cell contact, the cytoplasmic domain is visible at the apical surface (white arrow, where the extracellular domain is absent), throughout the cytoplasm, and in the nucleus (orange arrow).

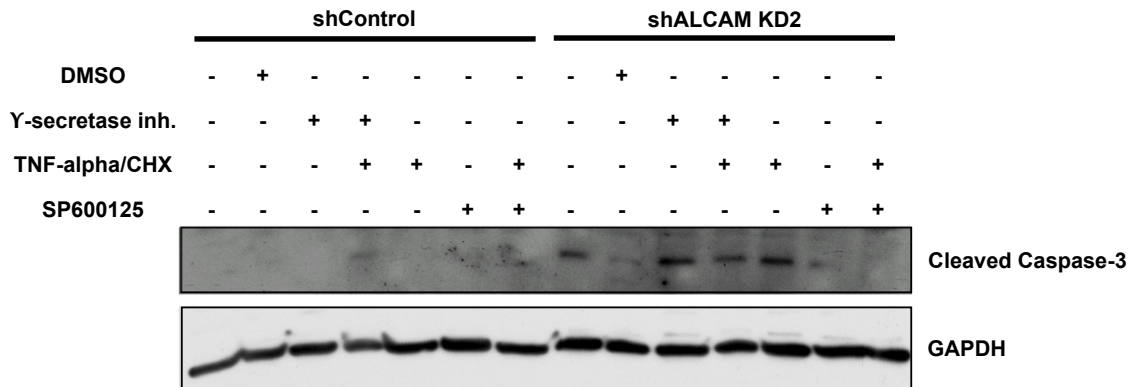


Figure 27. Reduced ALCAM expression results in enhanced apoptosis. PC3 cells stably expressing a short-hairpin RNA targeting ALCAM were found to have increased cleaved caspase-3 as detected by Western blot compared to parental PC3 expressing a scrambled short-hairpin RNA. Cells were treated for 4 hrs. with indicated compounds: diluent control (DMSO), 1 μ M InSolution gamma-secretase Inhibitor X, 20ng/ml TNF α /10 μ M cyclohexamide, 50 μ M SP600125 JNK Inhibitor.

stream activation of apoptosis have been classified into two categories: 1. the intrinsic pathway involving mitochondrial stress and 2. the extrinsic pathway involving TNF- α , TRAIL, and FAS-L in the engagement of death receptors (174). Upon activation of either pathway, there is downstream activation of caspases, a family of cysteine proteases that act as common cell death effector molecules. ALCAM is frequently dysregulated in cancer and has been posed to be protective of apoptosis in breast cancer (17,23,99,175). This hypothesis is supported by *in vitro* data, whereby ALCAM gene silencing in MCF-7 tumor cells resulted in increased markers of apoptosis, cleaved caspase-7 and PARP, in addition to decreased Bcl-2 expression (175). A known activator of apoptosis, tumor necrosis factor alpha (TNF- α), engages with TNFR1 to promote the recruitment of signal transduction molecules that perpetrate cellular apoptosis (176). TNF- α also induces activation of nuclear factor κ B (NF- κ B), which acts as a negative regulator of TNF- α -induced apoptosis. In breast cancer cell lines, MB-MDA-231 and MCF-7 cells, TNF- α increases Bcl-2 mRNA and protein and this induction was dependent on the p65 subunit of NF- κ B (177). In a preliminary experiment utilizing PC3 cells stably expressing a short hairpin RNA targeting ALCAM (shALCAM KD3), baseline levels of cleaved caspase-3 were elevated in comparison to PC3 shControl. Pretreatment of PC3 shALCAM KD2 cells with SP600125, a JNK inhibitor, in conjunction with TNF- α /cyclohexamide, resulted in decreased cleaved caspase-3 expression (Fig. 27). This result suggest that increases in TNF- α -mediated apoptosis in cells with reduced ALCAM expression is, in part, due to JNK activity, a known downstream effector of TNF- α -induced apop-

tosis. (Fig. 27) (178). Taken together, we can speculate that in prostate cancer cells, ALCAM expression confers resistance to TNF- α -induced apoptosis possibly through Bcl-2 overexpression.

Contribution of ALCAM to bone metastasis

Our data presented thus far demonstrate that tumoral ALCAM functions to increase prostate tumor metastasis and to protect from apoptosis in the bone microenvironment. As ALCAM is often thought to function in the context of its cell adhesive function, it was surprising that a silencing of ALCAM expression in prostate tumor cells led to a reduction in metastasis rather than enhanced metastasis. These suppositions are based on prior experiments by van Kempen and colleagues in which ectopic expression in BLM cells of an amino-truncated ALCAM construct, Δ N-ALCAM, lacking the ligand-binding domain and retaining the oligomerization domains, decreased cell adhesion and led to rapid metastasis in nude mice (94). While this study noted a reduction in primary tumor size of Δ N-ALCAM tumor cells, it was attributed to the rapid departure of tumor cells resulting from disruption in cell adhesion and not a defect in proliferation or apoptosis (94). An alternative explanation for reduced metastasis to bone in the intracardiac bone metastasis model is that ALCAM knockdown tumor cells have reduced capacity to process MMP-2. In a study using a transgenic model in which the SV40 large T antigen is overexpressed in prostatic neuroendocrine cells and MMP-2 is non-functional, MMP-2 “knockout” mice had no change in primary tumor development, however there was reduced lung metastasis and increased survival

(179). Considering *in vitro* and *in vivo* data showing BLM Δ N-ALCAM and anti-ALCAM siRNA-treated melanoma cells have severely impaired MMP-2 activation, one suspect MMP-2 activation is functionally impaired in our models of prostate tumorigenesis (93). These data support the notion that MMPs, specifically MMP-2, could account for no alteration in primary tumor growth, but enhanced metastasis (Fig 10C-F & 11).

Although elevated apoptosis was evident in the ALCAM knockdown tumor cells, tumor take was not diminished in our intratibial model. This observation suggests while our intracardiac experiments aimed to address the role of ALCAM in metastasis to bone, it was not possible to tease apart ALCAM's role in extravasation versus colonization and expansion at the secondary site. In studies of ALCAM requirement for trans-endothelial monocyte migration, treatment with blocking ALCAM antibodies resulted in inhibition of trans-endothelial migration of monocyte lines (150). Moreover, confocal analysis of ALCAM in activated monocytes revealed localization of ALCAM at endothelial junctions. In the presence of ALCAM-Fc or treatment with anti-ALCAM antibodies in *in vitro* trans-endothelial cell assays, THP1 monocytes have a 50% and 70% reduction in migration, respectively. Monocytes do not express CD6, the heterotypic binding molecule of ALCAM, thus it is reasonable to conclude that homotypic ALCAM-ALCAM interaction is responsible for ALCAM-mediated trans-endothelial migration in monocytes. Taken together with our PC3 intracardiac studies where ALCAM knockdown in the tumor cells result in a reduction in tumor incidence, these results suggest additional levels of complexity of ALCAM's function in tumor progression

in which the extracellular domain of ALCAM participates in tumor cell trans-endothelial migration.

While down regulation of ALCAM expression in PC3 prostate tumor cells was not sufficient to affect invasion or metastatic dissemination to soft tissue, metastasis to bone was decreased (Fig 10). Direct inoculation *in vivo* of ALCAM knockdown tumor cells into the tibia was did not result in a significant reduction in tumor incidence compared to the intracardiac tumor model (Fig. 11). Though proliferation and apoptosis studies determined smaller tumor occupancy in the ALCAM knockdown tumors, we cannot exclude the role of ALCAM in trans-endothelial migration to mediate osteotropism in our intracardiac model. Our current work using the orthotopic, intracardiac and intratibial models do not adequately address the extravasational component in tumor metastasis. We can speculate that there is a dual role for ALCAM in metastasis to bone. Though not quantitatively assessed, it was noted in our intracardiac injection experiments prior to tumor cell inoculation, that ALCAM KD cells had increased clustering. While the loss of ALCAM may affect trans-endothelial migration, it is also possible that compensatory increases in other related cell adhesion molecules, could result in increased clustering and decreased metastasis in our intracardiac model. *in vitro* (Fig. 4A), analysis of shed ALCAM, regardless of overall total cellular ALCAM expression, reveals that SDF-1, PDGF, and BMP2 induce ALCAM shedding from the cell surface (Fig. 30). Future studies using the bone specific isolates, BS159 & BS473, can help determine if bone metastatic cells are selectively responsive to shed ALCAM after treatment with these cytokines.

ALCAM as a marker of bone metastasis

To determine if TGF β is the predominant driver of ALCAM ectodomain shedding in the bone microenvironment, we performed longitudinal analysis of serum ALCAM in tumor-bearing mice. We tested serum levels of tumor-derived ALCAM pre- and post-treatment with a TGF β neutralizing antibody, 2G7, compared to matched control IgG2a (Fig. 28). The tumor size selection for treatment was based on previous experiments comparing tumor size with serum levels of shed ALCAM. Contrary to our hypothesis, acute inhibition of TGF β with 2G7 did not result in any significant changes in shed ALCAM (Fig. 28 B&C). This may be due to several factors including the possibility that ADAM17 activity is not exclusively activated in the bone microenvironment by TGF β . Subsequent *in vitro* analysis of ALCAM shedding by ELISA shows increased baseline ectodomain shedding of ALCAM in PC3 bone metastatic clones versus parental PC3 shControl (Fig. 29). In addition, BS-159 and BS-473, the highly aggressive *in vivo*-passaged PC3 bone-metastatic cell lines (Fig. 30), no longer increase ALCAM shedding in response to TGF β (Fig. 29C), confirming our results that *in vivo* inhibition of TGF β in bone metastasis is unable to abolish ALCAM shedding. In the bone microenvironment, it is possible TGF β is no longer the main driver of ALCAM shedding. It is possible there are other drivers of ALCAM expression and shedding. These include NFkappaB which, through upstream signaling of SDF-1, is a key chemokine in the promotion of osteolytic lesions and maintenance of HSC in endosteal niche (180,181). While our data in Chapter II have shown that TGF β is the predominant cytokine responsible

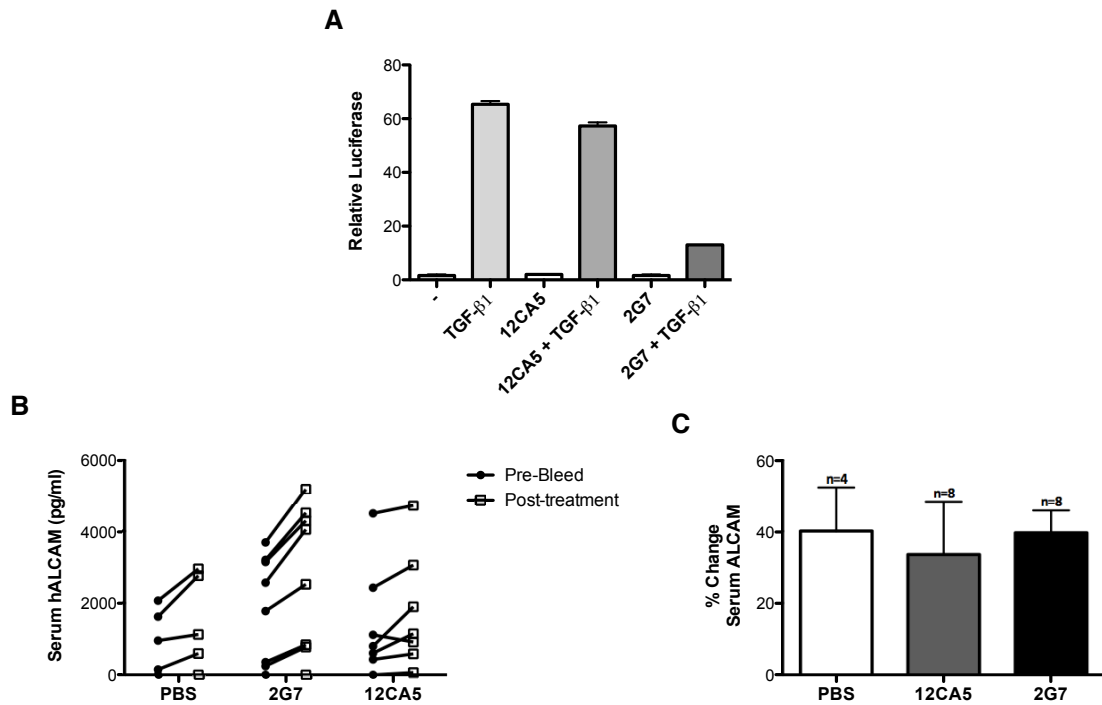


Figure 28. Inhibition of TGF β does not decrease circulating serum tumor-derived ALCAM (A) *In vitro* luciferase expression of mink lung epithelial cells stably expressing a plasminogen activator inhibitor-1/luciferase reporter (PAI-1/luciferase reporter; kind gift from the lab of Harold L. Moses) treated with the indicated combinations of 10ng/ml of TGF β , 2G7 neutralizing pan-TGF β IgG2, and control IgG2, 12CA5. Treatment with 2G7 had an blunted luciferase response to TGF β validating 2G7 effectiveness. **(B)** Serum human/tumor-derived ALCAM levels did not respond to inhibition of TGF β as measured by ELISA in PC3-luc tumor-bearing mice at 4 weeks post-intratumoral inoculation and 2 days post treatment with PBS (n=8), 2G7 (n=8), or 12CA5 Control IgG2 (n=8). **(C)** Quantitation of percent change in serum ALCAM from (B).

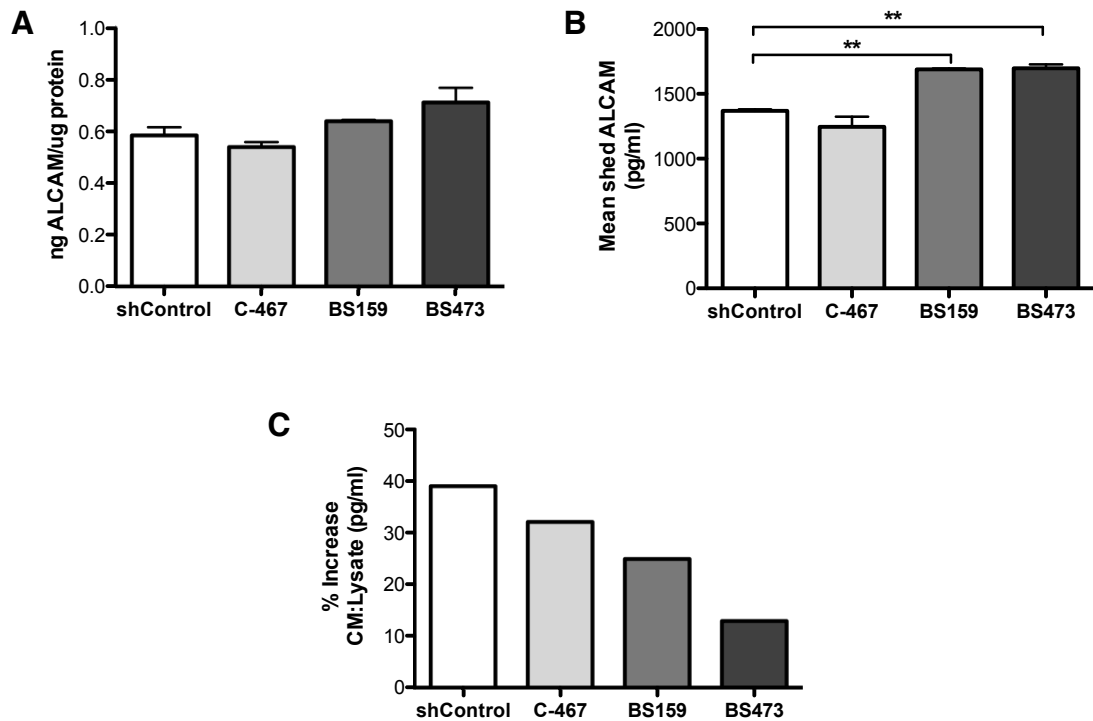


Figure 29. Elevated baseline ALCAM shedding and decreased sensitivity to TGF β in PC3 bone metastatic subclones. (A) Overall ALCAM total protein expression; ng ALCAM/ μ g total protein. Levels in PC3-luc shControl parental, PC3-luc chest tumor isolate (C-467), PC3-luc skeletal mets (BS159 & BS473) were measured by ELISA. **(B)** Quantitation of mean shed ALCAM levels (not normalized to overall ALCAM total protein expression) in conditioned media of PC3-luc shControl, C-467, BS159 and BS473 tumor cell lines. **(C)** Percent increase of shed ALCAM relative to total protein expression in cells treated with 10ng/ml of TGF β for 48hrs.

Soluble ALCAM - Conditioned Media

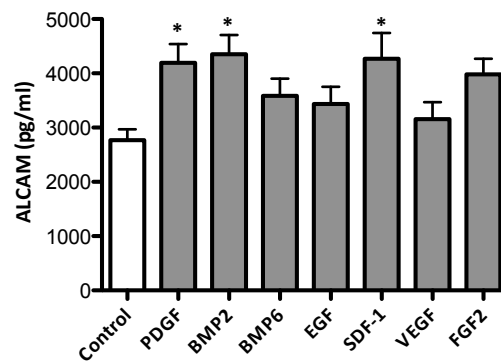
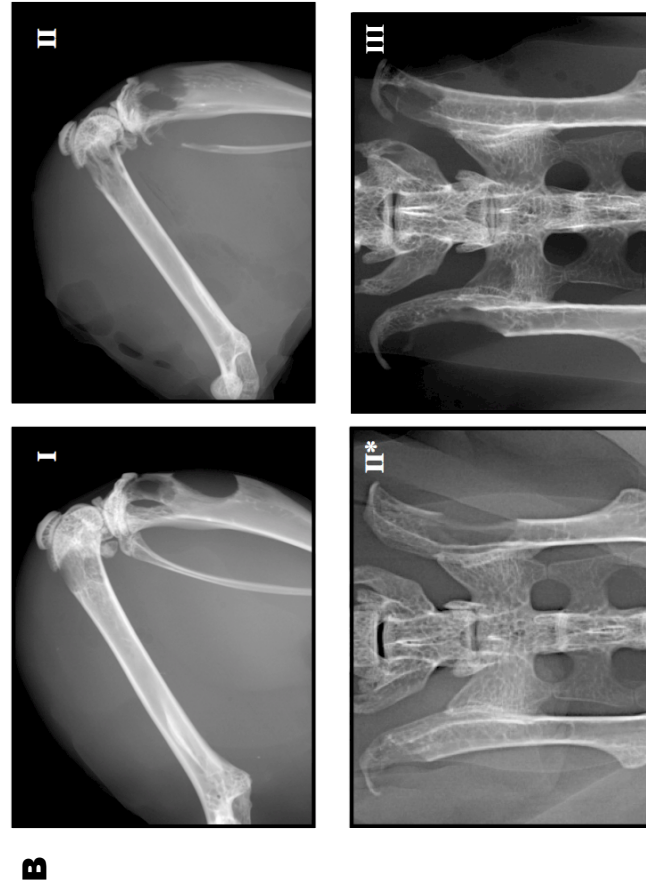
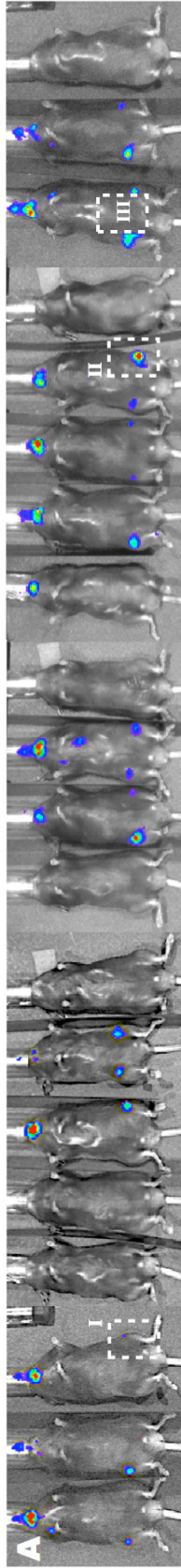


Figure 30. Bone microenvironment-associated soluble factors provoke ALCAM shedding *in vitro*. ELISA analysis of ALCAM shedding, pg/ml, in concentrated conditioned media of PC3 cells treated with indicated exogenous cytokines

for ALCAM shedding *in vitro* (Fig. 4A), analysis of shed ALCAM, regardless of overall total cellular ALCAM expression, reveals that SDF-1, PDGF, and BMP2 induce ALCAM shedding from the cell surface (Fig. 30). Future studies using the bone specific isolates, BS159 & BS473, can help determine if bone metastatic cells are selectively responsive to shed ALCAM after treatment with these cytokines.

In establishing an alternative immunodeficient model for bone metastasis (Fig. 31-32), we isolated several aggressive bone specific clones through sequential *in vivo* passaging in Rag1^{-/-} mice (Fig. 31-32). Upon isolation of BS159 10-week post-intracardiac injections of PC3-luc cells into Rag^{-/-} mice, cells were cultured and re-injected into Rag^{-/-} mice to produce the BS473 cell line. It is of note, that re-injection of BS159 into Rag^{-/-} mice resulted in accelerated and enhanced osteolytic tumor burden, with endpoint for the BS159 isolate reached at 4 weeks post-intracardiac injections versus 12 weeks for the parental line. Mean levels of shed ALCAM comparing parental PC3 shControl with the chest tumor isolate (C-467) and bone-specific isolates (BS159 & BS473), though not statistically significant, indicate a dose increase in ALCAM shedding specific to the aggressiveness of bone specific clones (Fig. 29C).

The majority of publications concerning ALCAM shedding in the clinical setting correlate serum levels with advanced stage disease; however, its temporal regulation following tumor inoculation suggested it may have a physiologic role in tumor progression. Furthermore tumor-derived ALCAM shedding, not host-derived (Fig. 33C) is significantly correlated with both lesion area and total number of bone le-



Summary of PC3 metastasis in Rag1^{-/-}

Site	Lesion Distribution		
	Incidence	Events	Aver.lesions/
Femur	13/14 (93%)	26	1.86
Tibia	13/14 (93%)	28	2
Fibula	3/14 (21%)	3	0.21
Humerus	12/14 (86%)	22	1.57
Skull/ Mandible	13/14 (93%)	13	0.93
Spine	3/14 (21%)	4	0.29
Pelvis	12/14 (86%)	19	1.36
Ribs	0/14 (0%)	0	0

Site	Incidence		
	Incidence	%	Aver.lesions/
Total	14/19	74	-
Long	14/14	100	5.64
Skull/ Mandible	13/14	93	0.93

Incidence= Ratio of mice with lesions, Events= total number of lesions, Frequency= number of lesions/mice with lesions.

Figure 31. Skeletal metastasis of PC3-luc in Rag1^{-/-} after intracardiac injection. (A) In vivo luciferase images of Rag1^{-/-} mice injected via intracardiac inoculation with PC3-luc BS159, bone-specific isolate, prostate tumor cells. **(B)** Representative x-ray images of osteolytic lesions in indicated mice from **(A)** 4-weeks post-injection **(C)** Summary of lesion distribution and incidence in Rag1^{-/-} bone metastasis model.

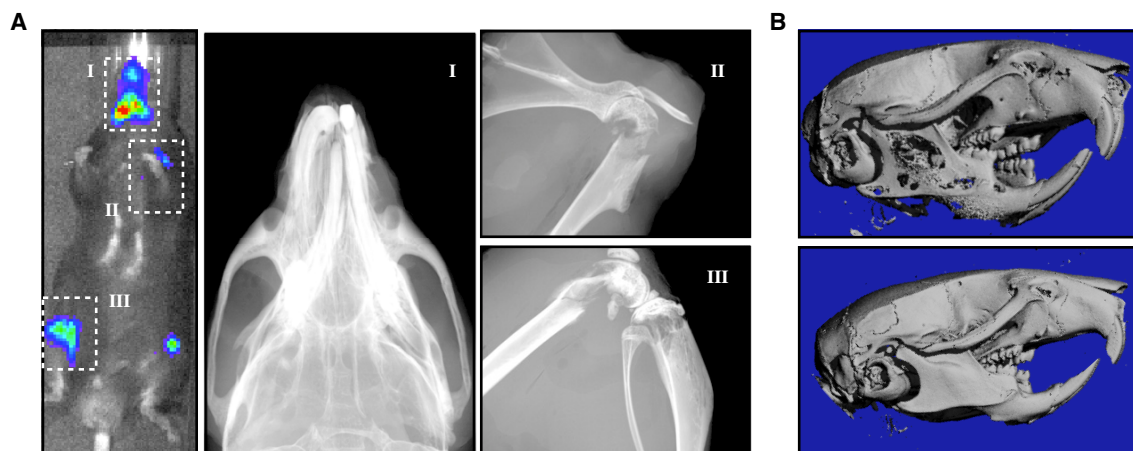


Figure 32. Analysis of bone lesions formed by PC3 in Rag1^{-/-} after intracardiac injection. (A) Representative luciferase image of PC3-luc tumor-bearing Rag1^{-/-}; matching x-ray images from lesions present in mandible (I), humerus (II) and femur and tibia (III). **(B)** Representative mandible microCT images of osteolytic tumor burden in PC3-luc tumor-bearing mice (top) versus control PBS-injected (bottom)

sions per animal (Fig. 33A&B). The endogenous levels of ALCAM shedding was enhanced in tumor cells residing in the bone versus the orthotopic site (Fig. 29B & 33D), suggesting a microenvironmental contribution to the proteolytic shedding of ALCAM during the tumor progression to bone.

In collaboration with Dr. Julie Sterling, we confirmed that tumor ALCAM shedding is elevated in mice bearing skeletal metastases (Fig. 34A). Though ALCAM shedding correlates with tumor burden, it is particularly indicative of tumors in bone. Treatment with Zoledronic Acid (ZA) prevents both tumor growth and circulating levels of tumor-derived ALCAM (Fig. 34B). We confirm that elevated ALCAM shedding correlates with tumor growth and not to general wound repair because mice recovering from a full-thickness skin wound (Fig. 7B) or acute LPS administration (Fig. 7C) do not exhibit elevated ALCAM levels. Collectively, these data suggest that ALCAM shedding may act as an clinically relevant marker of skeletal metastasis and response to therapy.

ALCAM endosteal niche competition

While we have convincing data that ALCAM expression is important in the osteotropism and survival of tumor cells in the bone, (Figure 12) further work is necessary to fully elucidate the mechanisms involved. Given the proclivity of prostate tumor cells to metastasize to bone and contribute to disease morbidity (Coleman, 2006), it would be beneficial to investigate ALCAM in the context of post-dissemination survival and niche occupancy of PCa cells and their ability to co-op the hematopoietic niche. Molecular crosstalk between HSCs and osteoblasts in-

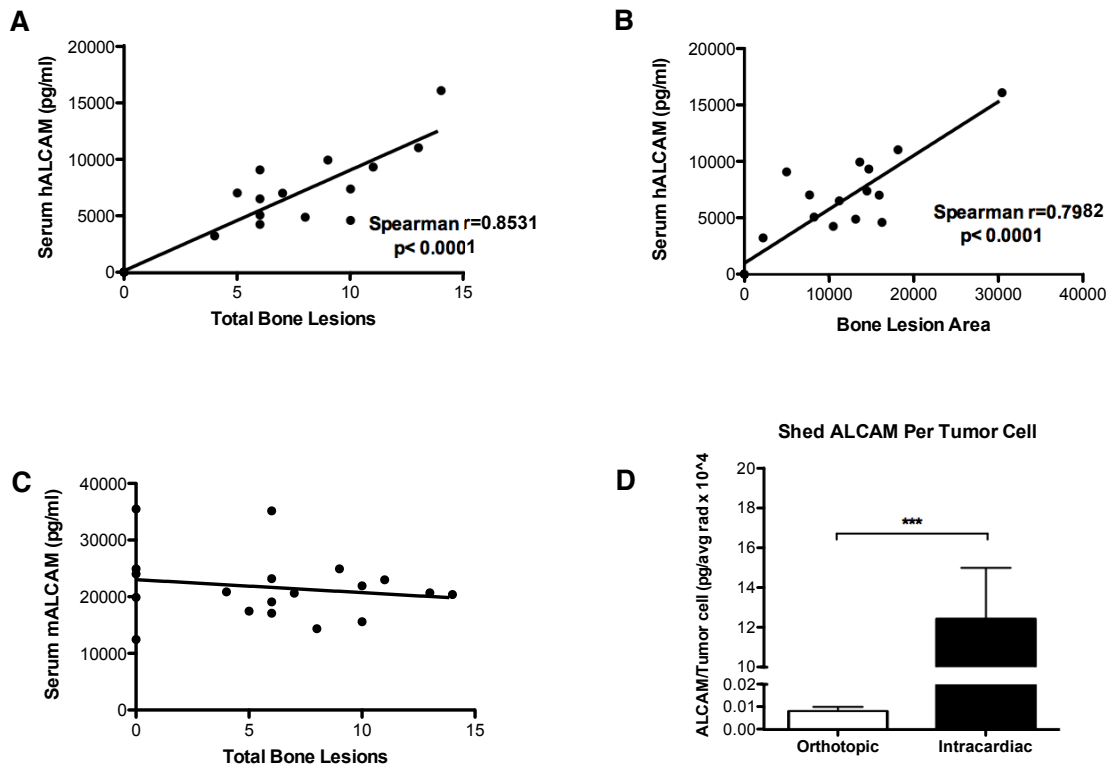


Figure 33: ALCAM shedding correlates with bone lesion number and area. Circulating ALCAM levels were monitored longitudinally in mice bearing PC3-luc tumor cells inoculated via intracardiac injection in Rag1^{-/-} mice. **(A)** Circulating levels of soluble tumor-derived ALCAM correlated with total number of bone lesions $R^2=0.7685$ **(B)** Circulating levels of soluble tumor-derived ALCAM correlated with total number bone lesion area $R^2=0.8146$ **(C)** Circulating levels of soluble host-derived ALCAM correlated with total number of bone lesions **(D)** Amount of shed ALCAM relative to cell number in PC3 cells orthotopically implanted into the prostate or injected via intracardiac route. *** $p < 0.001$ (Mann-Whitney test) Each point reflects mean of duplicate measurements \pm SD. Each line and corresponding R^2 represents a best fit linear regression analysis.

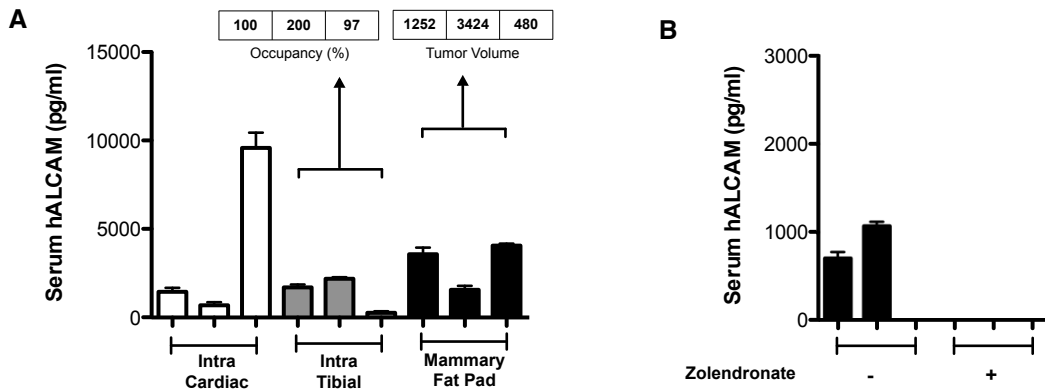


Figure 34. Shedding of tumor-derived ALCAM shedding is detectable and responsive to zolendronate in tumor bearing animals. (A) Tumor-derived serum ALCAM as measured by ELISA is readily detected in endpoint studies of mice bearing MDA231 tumors in an intracardiac, intratibial, and orthotopic (mammary fat pad) models. Tumor-derived ALCAM corresponds to tumor burden in both intracardiac (occupancy %) and mammary fat pad (tumor volume) models. **(B)** Serum tumor-derived ALCAM in an intracardiac model of MDA231 is indicative of treatment response with Zolendronate wherein treated animals lacked both serum ALCAM and detectable tumor-induced bone disease.

volves cell adhesion molecules that mediated extracellular matrix interactions, in addition to cell-cell interactions, both heterotypic and homotypic interactions. These interactions facilitate the maintenance of physical proximity of HSCs to the endosteal bone-marrow niche, but also participate in signaling that promotes HSC quiescence (180,182).

In the context of ALCAM, the terminal domain (D1) is required for homotypic interactions. In CHO cells transfected with full length ALCAM, the addition of exogenous soluble ALCAM reduces cell aggregation in a dose-dependent manner, suggesting that soluble ALCAM is able to compete and disrupt endogenous homotypic interactions (24). Recently, researchers subdivided osteoblast-enriched ALCAM (+) Sca (-) cells from bone marrow endosteal cells. These cells highly express multiple cell adhesion molecules and significantly upregulate homing and cell-adhesion related genes in HSCs (74). Initial observations have noted that circulating HSCs in prostate cancer patients have been an indicator of bone metastasis, and that prostate cancer cells inoculated into bone marrow remain dormant and resistant to drug treatment (183). HSCs continuously migrate from the bone marrow to the blood and back (184,185). However, in a seminal study by Shiozawa et al, the authors were able to show co-transplanted prostate cancer cells (PC3 & C42) and hematopoietic stem cells (HSCs) transplanted into NOD/SCID mice compete for the endosteal niche (186). Further experiments were completed using a novel vessel assay in which osteoblasts were depleted through transgene activation. In the absence of mature osteoblasts, PC3 prostate tumor cells directly inoculated into the vessels were unable to grow (186,187). This

was in part due to enhanced apoptosis, suggesting that prostate cancer growth is dependent on the presence of osteoblasts in the endosteal niche for colonization.

Preliminary investigations from our lab (data not shown) characterizing lineage differentiation in ALCAM^{-/-} mice indicate an increase, yet not significant, in adipocyte differentiation and decreased osteoblast number. While further investigation is warranted, these results suggest that ALCAM is important in the differentiation of osteoblasts, an important component of prostate cancer colonization to bone. Similar to the *in vivo* competition assay with HSCs and prostate cancer cells, one could expand to include the contribution of ALCAM in competition of the endosteal niche. In a study characterizing fetal and adult hematopoietic tissue, expression of ALCAM in CHO cells conferred homophilic adhesion that could be competed with a soluble recombinant ALCAM-Fc fusion protein. These data suggest a role for ALCAM in the adhesion of stem cells and progenitor cells to themselves or to other ALCAM⁺ supportive cells in the microenvironment (71). One could pose a model, as it is related to our *in vivo* studies with PC3 tumor cells which have high levels of ADAM17 expression and ectodomain shedding of the extracellular domain of ALCAM, substantial amounts of soluble ALCAM generated by tumor cells can disrupt HSC adhesion to endosteal niche thereby serving a dual role that includes: 1.) promoting tumor cell occupancy of endosteal stem cell niche and 2.) promote differentiation of HSC to osteoblastic and osteoclast for induction of vicious cycle.

We have characterized a bone metastasis model in Rag1^{-/-} immunodeficient mice, isolating bone specific, highly aggressive prostate and breast meta-

static clones (Fig. 31-23). One particular advantage of using this model is the reproductive robustness in breeding and maintaining homozygous mating pairs. In doing so, Rag1^{-/-}/ALCAM^{-/-} mice have been generated to study the impact of host-derived ALCAM on tumor cell metastasis to bone. In an effort to further understand the role of ALCAM in the HSC niche, we could potentially utilize Rag1^{-/-}/ALCAM^{-/-} mice to determine if a host-derived ALCAM is critical for HSC homing or colonization in the endosteal niche. Similar experiments can be done, whereby, wild type HSCs and prostate tumor cells are co-injected, and we can determine directly if there is decreased occupancy of HSCs in the endosteal niche and numbers of circulating HSCs. These future experiments will lead to a greater understanding of ALCAM's functional role in the tumor bone stem cell niche.

Concluding Remarks

The data presented within dissertation demonstrate the impact of ALCAM in prostate cancer progression and human colorectal cancer patient outcome through genetic, biochemical analyses, animal models and through using novel dual-immunohistochemistry of human tissue. Despite the clinical relevance and its role in diverse cellular processes, the precise function of ALCAM in prostate cancer is largely unknown. Our work presented herein, has advanced our understanding of ALCAM as a serum biomarker and functionally its role in metastasis. Furthermore, in our clinical studies, the detection of intratumoral regulation of ALCAM proteolytic cleavage can be a predictive measurement of patient outcome. The diversity of ALCAM functions in neuronal migration, immune modula-

tion and hematopoietic maintenance represent several pathways that can be exploited by tumor cells to promote metastasis and growth. We anticipate new insights into the dynamic relationship between the extracellular adhesive functions and intracellular signaling role will emerge in future mechanistic studies of ALCAM. While it is suspected that ALCAM function may be context and cell dependent, insight will lead to a broader application to investigating the intracellular signaling capacity of cell adhesion molecules. While the adhesive function is implied of cell adhesion molecules, subsequent regulation of intracellular localization and signaling have largely been understudied. Further investigation is warranted to understand the full contribution of ALCAM to cancer and our ability to co-opt this participation towards improved therapy.

REFERENCES

1. Siegel R, Naishadham D, Jemal A. Cancer statistics, 2012. *CA: A Cancer Journal for Clinicians*. 2012;62:10–29.
2. Friedl P, Wolf K. Tumour-cell invasion and migration: diversity and escape mechanisms. *Nat Rev Cancer*. 2003;3:362–74.
3. Sahai E. Illuminating the metastatic process. *Nat Rev Cancer*. 2007;7:737–49.
4. Polyak K, Weinberg RA. Transitions between epithelial and mesenchymal states: acquisition of malignant and stem cell traits. *Nat Rev Cancer*. 2009;9:265–73.
5. Palmer TD, Ashby WJ, Lewis JD, Zijlstra A. Targeting tumor cell motility to prevent metastasis. *Adv. Drug Deliv. Rev.* 2011;63:568–81.
6. Wai Wong C, Dye DE, Coombe DR. The Role of Immunoglobulin Superfamily Cell Adhesion Molecules in Cancer Metastasis. *Int J Cell Biol*. 2012;2012:1–9.
7. Juliano RL. Signal transduction by cell adhesion receptors and the cytoskeleton: functions of integrins, cadherins, selectins, and immunoglobulin-superfamily members. *Annu. Rev. Pharmacol. Toxicol.* 2002;42:283–323.
8. Cavallaro U, Christofori G. Cell adhesion and signalling by cadherins and Ig-CAMs in cancer. *Nat Rev Cancer*. 2004;4:118–32.
9. Kiss JZ, Muller D. Contribution of the neural cell adhesion molecule to neuronal and synaptic plasticity. *Rev Neurosci*. 2001;12:297–310.
10. Ditlevsen DK, Povlsen GK, Berezin V, Bock E. NCAM-induced intracellular signaling revisited. *J. Neurosci. Res.* 2008;86:727–43.
11. Yilmaz M, Christofori G. Mechanisms of Motility in Metastasizing Cells. *Molecular Cancer Research*. 2010;8:629–42.
12. Zecchini S, Bombardelli L, Decio A, Bianchi M, Mazzarol G, Sanguineti F, et al. The adhesion molecule NCAM promotes ovarian cancer progression via FGFR signalling. *EMBO Mol Med*. 2011;3:480–94.
13. Gratzinger D, Barreuther M, Madri JA. Platelet–endothelial cell adhesion molecule-1 modulates endothelial migration through its immunoreceptor

- tyrosine-based inhibitory motif. *Biochem Biophys Res Commun.* 2003;301:243–9.
14. Van Kilsdonk JW, Wilting RH, Bergers M, Van Muijen GN, Schalkwijk J, Van Kempen LC, et al. Attenuation of Melanoma Invasion by a Secreted Variant of Activated Leukocyte Cell Adhesion Molecule. *Cancer Research.* 2008;68:3671–9.
 15. Cayrol R, Wosik K, Berard JL, Dodelet-Devillers A, Ifergan I, Kebir H, et al. Activated leukocyte cell adhesion molecule promotes leukocyte trafficking into the central nervous system. *Nat Immunol.* 2007;9:137–45.
 16. Ofori-Acquah SF, King J, Voelkel N, Schaphorst KL, Stevens T. Heterogeneity of barrier function in the lung reflects diversity in endothelial cell junctions. *Microvasc Res.* 2008;75:391–402.
 17. Piazza T, Cha E, Bongarzone I, Canevari S, Bolognesi A, Polito L, et al. Internalization and recycling of ALCAM/CD166 detected by a fully human single-chain recombinant antibody. *Journal of Cell Science.* 2005;118:1515–25.
 18. Burkhardt M, Mayordomo E, Winzer K-J, Fritzsche F, Gansukh T, Pahl S, et al. Cytoplasmic overexpression of ALCAM is prognostic of disease progression in breast cancer. *Journal of Clinical Pathology.* 2006;59:403–9.
 19. Sawhney M, Matta A, Macha MA, Kaur J, Dattagupta S, Shukla NK, et al. Cytoplasmic accumulation of activated leukocyte cell adhesion molecule is a predictor of disease progression and reduced survival in oral cancer patients. *Int. J. Cancer.* 2009;124:2098–105.
 20. Weichert W, Knösel T, Bellach J, Dietel M, Kristiansen G. ALCAM/CD166 is overexpressed in colorectal carcinoma and correlates with shortened patient survival. *Journal of Clinical Pathology.* 2004;57:1160–4.
 21. Tanaka H, Matsui T, Agata A, Tomura M, Kubota I, McFarland KC, et al. Molecular cloning and expression of a novel adhesion molecule, SC1. *Neuron.* 1991;7:535–45.
 22. van Kempen LC, Nelissen JM, Degen WG, Torensma R, Weidle UH, Bloemers HP, et al. Molecular basis for the homophilic activated leukocyte cell adhesion molecule (ALCAM)-ALCAM interaction. *J Biol Chem.* 2001;276:25783–90.
 23. Tomita K, van Bokhoven A, Jansen CF, Bussemakers MJ, Schalken JA. Coordinate recruitment of E-cadherin and ALCAM to cell-cell contacts by alpha-catenin. *Biochem Biophys Res Commun.* 2000;267:870–4.

24. Ikeda K, Quertermous T. Molecular isolation and characterization of a soluble isoform of activated leukocyte cell adhesion molecule that modulates endothelial cell function. *J Biol Chem.* 2004;279:55315–23.
25. Weiner JA, Koo SJ, Nicolas S, Fraboulet S, Pfaff SL, Pourquié O, et al. Axon fasciculation defects and retinal dysplasias in mice lacking the immunoglobulin superfamily adhesion molecule BEN/ALCAM/SC1. *Mol. Cell. Neurosci.* 2004;27:59–69.
26. Buhusi M, Demyanenko GP, Jannie KM, Dalal J, Darnell EPB, Weiner JA, et al. ALCAM regulates mediolateral retinotopic mapping in the superior colliculus. *Journal of Neuroscience.* 2009;29:15630–41.
27. Bowen MA, Patel DD, Li X, Modrell B, Malacko AR, Wang WC, et al. Cloning, mapping, and characterization of activated leukocyte-cell adhesion molecule (ALCAM), a CD6 ligand. *J. Exp. Med.* 1995;181:2213–20.
28. Gimferrer I, Calvo M, Mittelbrunn M, Farnós M, Sarrias MR, Enrich C, et al. Relevance of CD6-mediated interactions in T cell activation and proliferation. *J Immunol.* 2004;173:2262–70.
29. Hassan NJ, Simmonds SJ, Clarkson NG, Hanrahan S, Puklavec MJ, Bomb M, et al. CD6 regulates T-cell responses through activation-dependent recruitment of the positive regulator SLP-76. *Molecular and Cellular Biology.* 2006;26:6727–38.
30. Singer NG, Richardson BC, Powers D, Hooper F, Lialios F, Endres J, et al. Role of the CD6 glycoprotein in antigen-specific and autoreactive responses of cloned human T lymphocytes. *Immunology.* 1996;88:537–43.
31. Zimmerman AW, Joosten B, Torensma R, Parnes JR, van Leeuwen FN, Figdor CG. Long-term engagement of CD6 and ALCAM is essential for T-cell proliferation induced by dendritic cells. *Blood.* 2006;107:3212–20.
32. Lee BP-L, Imhof BA. Lymphocyte transmigration in the brain: a new way of thinking. *Nat Immunol.* 2008;9:117–8.
33. Castro MAA, Oliveira MI, Nunes RJ, Fabre S, Barbosa R, Peixoto A, et al. Extracellular isoforms of CD6 generated by alternative splicing regulate targeting of CD6 to the immunological synapse. *J Immunol.* 2007;178:4351–61.
34. Hassan NJ, Barclay AN, Brown MH. Frontline: Optimal T cell activation requires the engagement of CD6 and CD166. *Eur. J. Immunol.* 2004;34:930–40.

35. Diekmann H, Stuermer CAO. Zebrafish neurolin-a and -b, orthologs of ALCAM, are involved in retinal ganglion cell differentiation and retinal axon pathfinding. *J. Comp. Neurol.* 2009;513:38–50.
36. Fraboulet S, Schmidt-Petri T, Dhouailly D, Pourquié O. Expression of DM-GRASP/BEN in the developing mouse spinal cord and various epithelia. *Mech. Dev.* 2000;95:221–4.
37. Hirata H, Murakami Y, Miyamoto Y, Tosaka M, Inoue K, Nagahashi A, et al. ALCAM (CD166) is a surface marker for early murine cardiomyocytes. *Cells Tissues Organs.* 2006;184:172–80.
38. Pourquié O, Corbel C, Le Caer JP, Rossier J, Le Douarin NM. BEN, a surface glycoprotein of the immunoglobulin superfamily, is expressed in a variety of developing systems. *Proceedings of the National Academy of Sciences of the United States of America.* 1992;89:5261–5.
39. Gessert S, Maurus D, Brade T, Walther P, Pandur P, Kühl M. DM-GRASP/ALCAM/CD166 is required for cardiac morphogenesis and maintenance of cardiac identity in first heart field derived cells. *Dev. Biol.* 2008;321:150–61.
40. Choudhry P, Joshi D, Funke B, Trede N. Alcam mediates Edn1 signaling during zebrafish cartilage morphogenesis. *Dev. Biol. Elsevier Inc;* 2011;349:483–93.
41. Ohneda O. ALCAM (CD166): its role in hematopoietic and endothelial development. *Blood.* 2001;98:2134–42.
42. Heffron DS, Golden JA. DM-GRASP is necessary for nonradial cell migration during chick diencephalic development. *Journal of Neuroscience.* 2000;20:2287–94.
43. Ott H, Diekmann H, Stuermer CA, Bastmeyer M. Function of Neurolin (DM-GRASP/SC-1) in guidance of motor axons during zebrafish development. *Dev. Biol.* 2001;235:86–97.
44. Jeannet R, Cai Q, Liu H, Vu H, Kuo Y-H. Alcam regulates long-term hematopoietic stem cell engraftment and self-renewal. *Stem Cells.* 2013;31:560–71.
45. Prat-Vidal C, Roura S, Farré J, Gálvez C, Llach A, Molina CE, et al. Umbilical cord blood-derived stem cells spontaneously express cardiomyogenic traits. *Transplant. Proc.* 2007;39:2434–7.
46. Liu F, Akiyama Y, Tai S, Maruyama K, Kawaguchi Y, Muramatsu K, et al. Changes in the expression of CD106, osteogenic genes, and transcription

- factors involved in the osteogenic differentiation of human bone marrow mesenchymal stem cells. *J. Bone Miner. Metab.* 2008;26:312–20.
47. Gonzalez R, Griparic L, Vargas V, Burgee K, Santacruz P, Anderson R, et al. A putative mesenchymal stem cells population isolated from adult human testes. *Biochem Biophys Res Commun.* 2009;385:570–5.
 48. Hua J, Yu H, Dong W, Yang C, Gao Z, Lei A, et al. Characterization of mesenchymal stem cells (MSCs) from human fetal lung: potential differentiation of germ cells. *Tissue Cell.* 2009;41:448–55.
 49. Risbud MV, Guttapalli A, Tsai T-T, Lee JY, Danielson KG, Vaccaro AR, et al. Evidence for skeletal progenitor cells in the degenerate human intervertebral disc. *Spine.* 2007;32:2537–44.
 50. Karaöz E, Doğan BN, Aksoy A, Gacar G, Akyüz S, Ayhan S, et al. Isolation and in vitro characterisation of dental pulp stem cells from natal teeth. *Histochem Cell Biol.* 2010;133:95–112.
 51. Dalerba P, Dylla SJ, Park I-K, Liu R, Wang X, Cho RW, et al. Phenotypic characterization of human colorectal cancer stem cells. *Proceedings of the National Academy of Sciences of the United States of America.* 2007;104:10158–63.
 52. Horst D, Kriegl L, Engel J, Kirchner T, Jung A. Prognostic Significance of the Cancer Stem Cell Markers CD133, CD44, and CD166 in Colorectal Cancer. *Cancer Invest.* 2009;27:844–50.
 53. Levin TG, Powell AE, Davies PS, Silk AD, Dismuke AD, Anderson EC, et al. Characterization of the Intestinal Cancer Stem Cell Marker CD166 in the Human and Mouse Gastrointestinal Tract. *Gastroenterology.* Elsevier Inc; 2010;139:2072–5.
 54. Stuelten CH, Mertins SD, Busch JI, Gowens M, Scudiero DA, Burkett MW, et al. Complex display of putative tumor stem cell markers in the NCI60 tumor cell line panel. *Stem Cells.* 2010;28:649–60.
 55. Burns FR, Kannen von S, Guy L, Raper JA, Kamholz J, Chang S. DM-GRASP, a novel immunoglobulin superfamily axonal surface protein that supports neurite extension. *Neuron.* 1991;7:209–20.
 56. Paschke KA, Lottspeich F, Stuermer CA. Neurolin, a cell surface glycoprotein on growing retinal axons in the goldfish visual system, is reexpressed during retinal axonal regeneration. *The Journal of Cell Biology.* 1992;117:863–75.

57. Corbel C, Cormier F, Pourquié O, Bluestein HG. BEN, a novel surface molecule of the immunoglobulin superfamily on avian hemopoietic progenitor cells shared with neural cells. *Exp Cell Res.* 1992;203:91–9.
58. Avci HX, Zelina P, Thelen K, Pollerberg GE. Role of cell adhesion molecule DM-GRASP in growth and orientation of retinal ganglion cell axons. *Dev. Biol.* 2004;271:291–305.
59. DeBernardo AP, Chang S. Native and recombinant DM-GRASP selectively support neurite extension from neurons that express GRASP. *Dev. Biol.* 1995;169:65–75.
60. Pollerberg GE, Mack TG. Cell adhesion molecule SC1/DMGRASP is expressed on growing axons of retina ganglion cells and is involved in mediating their extension on axons. *Dev. Biol.* 1994;165:670–87.
61. Ott H, Bastmeyer M, Stuermer CA. Neurolin, the goldfish homolog of DM-GRASP, is involved in retinal axon pathfinding to the optic disk. *J. Neurosci.* 1998;18:3363–72.
62. Riet Te J, Zimmerman AW, Cambi A, Joosten B, Speller S, Torensma R, et al. Distinct kinetic and mechanical properties govern ALCAM-mediated interactions as shown by single-molecule force spectroscopy. *Journal of Cell Science.* 2007;120:3965–76.
63. DeBernardo AP, Chang S. Heterophilic interactions of DM-GRASP: GRASP-NgCAM interactions involved in neurite extension. *The Journal of Cell Biology.* 1996;133:657–66.
64. Zimmerman AW, Nelissen JMDT, van Emst-de Vries SE, Willems PHGM, de Lange F, Collard JG, et al. Cytoskeletal restraints regulate homotypic ALCAM-mediated adhesion through PKC α independently of Rho-like GTPases. *Journal of Cell Science.* 2004;117:2841–52.
65. Tan F, Ghosh S, Mbeunkui F, Thomas R, Weiner JA, Ofori-Acquah SF. Essential role for ALCAM gene silencing in megakaryocytic differentiation of K562 cells. *BMC Mol. Biol.* 2010;11:91.
66. Nelissen JM, Peters IM, de Grooth BG, van Kooyk Y, Figdor CG. Dynamic regulation of activated leukocyte cell adhesion molecule-mediated homotypic cell adhesion through the actin cytoskeleton. *Mol. Biol. Cell.* 2000;11:2057–68.
67. Thelen K, Georg T, Bertuch S, Zelina P, Pollerberg GE. Ubiquitination and endocytosis of cell adhesion molecule DM-GRASP regulate its cell surface presence and affect its role for axon navigation. *J Biol Chem.* 2008;283:32792–801.

68. Wu S-L, Kim J, Bandle RW, Liotta L, Petricoin E, Karger BL. Dynamic profiling of the post-translational modifications and interaction partners of epidermal growth factor receptor signaling after stimulation by epidermal growth factor using Extended Range Proteomic Analysis (ERPA). *Mol. Cell Proteomics*. 2006;5:1610–27.
69. Delgado VMC, Nugnes LG, Colombo LL, Troncoso MF, Fernández MM, Malchiodi EL, et al. Modulation of endothelial cell migration and angiogenesis: a novel function for the “tandem-repeat” lectin galectin-8. *The FASEB Journal*. 2011;25:242–54.
70. Bruder SP, Horowitz MC, Mosca JD, Haynesworth SE. Monoclonal antibodies reactive with human osteogenic cell surface antigens. *Bone*. 1997;21:225–35.
71. Uchida N, Yang Z, Combs J, Pourquoié O, Nguyen M, Ramanathan R, et al. The characterization, molecular cloning, and expression of a novel hematopoietic cell antigen from CD34+ human bone marrow cells. *Blood*. 1997;89:2706–16.
72. Bruder SP, Ricalton NS, Boynton RE, Connolly TJ, Jaiswal N, Zaia J, et al. Mesenchymal stem cell surface antigen SB-10 corresponds to activated leukocyte cell adhesion molecule and is involved in osteogenic differentiation. *J. Bone Miner. Res.* 1998;13:655–63.
73. Cortés F, Deschaseaux F, Uchida N, Labastie MC, Frieria AM, He D, et al. HCA, an immunoglobulin-like adhesion molecule present on the earliest human hematopoietic precursor cells, is also expressed by stromal cells in blood-forming tissues. *Blood*. 1999;93:826–37.
74. Nakamura Y, Arai F, Iwasaki H, Hosokawa K, Kobayashi I, Gomei Y, et al. Isolation and characterization of endosteal niche cell populations that regulate hematopoietic stem cells. *Blood*. 2010;116:1422–32.
75. Choi S-C, Kim KD, Kim J-T, Kim JW, Lee HG, Kim J-M, et al. Expression of human NDRG2 by myeloid dendritic cells inhibits down-regulation of activated leukocyte cell adhesion molecule (ALCAM) and contributes to maintenance of T cell stimulatory activity. *J. Leukoc. Biol.* 2008;83:89–98.
76. Delorme B, Charbord P. Culture and characterization of human bone marrow mesenchymal stem cells. *Methods Mol. Med.* 2007;140:67–81.
77. Stewart K, Monk P, Walsh S, Jefferiss CM, Letchford J, Beresford JN. STRO-1, HOP-26 (CD63), CD49a and SB-10 (CD166) as markers of primitive human marrow stromal cells and their more differentiated progeny: a comparative investigation in vitro. *Cell Tissue Res.* 2003;313:281–90.

78. Arai F. Mesenchymal Stem Cells in Perichondrium Express Activated Leukocyte Cell Adhesion Molecule and Participate in Bone Marrow Formation. *Journal of Experimental Medicine*. 2002;195:1549–63.
79. Chitteti BR, Cheng Y-H, Poteat B, Rodriguez-Rodriguez S, Goebel WS, Carlesso N, et al. Impact of interactions of cellular components of the bone marrow microenvironment on hematopoietic stem and progenitor cell function. *Blood*. 2010;115:3239–48.
80. Kristiansen G, Pilarsky C, Wissmann C, Stephan C, Weissbach L, Loy V, et al. ALCAM/CD166 is up-regulated in low-grade prostate cancer and progressively lost in high-grade lesions. *Prostate*. 2003;54:34–43.
81. Mezzanzanica D, Fabbi M, Bagnoli M, Staurenco S, Losa M, Balladore E, et al. Subcellular Localization of Activated Leukocyte Cell Adhesion Molecule Is a Molecular Predictor of Survival in Ovarian Carcinoma Patients. *Clinical Cancer Research*. 2008;14:1726–33.
82. Zheng X, Ding W, Xie L, Chen Z. [Expression and significance of activated leukocyte cell adhesion molecule in prostatic intraepithelial neoplasia and adenocarcinoma]. *Zhonghua Nan Ke Xue*. 2004;10:265–8.
83. Bech-Serra JJ, Santiago-Josefat B, Esselens C, Saftig P, Baselga J, Arribas J, et al. Proteomic Identification of Desmoglein 2 and Activated Leukocyte Cell Adhesion Molecule as Substrates of ADAM17 and ADAM10 by Difference Gel Electrophoresis. *Molecular and Cellular Biology*. 2006;26:5086–95.
84. Gööz M. ADAM-17: the enzyme that does it all. *Crit. Rev. Biochem. Mol. Biol*. 2010;45:146–69.
85. Tsakadze NL, Sithu SD, Sen U, English WR, Murphy G, D'Souza SE. Tumor necrosis factor-alpha-converting enzyme (TACE/ADAM-17) mediates the ectodomain cleavage of intercellular adhesion molecule-1 (ICAM-1). *J Biol Chem*. 2006;281:3157–64.
86. Garton KJ, Gough PJ, Philalay J, Wille PT, Blobel CP, Whitehead RH, et al. Stimulated shedding of vascular cell adhesion molecule 1 (VCAM-1) is mediated by tumor necrosis factor-alpha-converting enzyme (ADAM 17). *J Biol Chem*. 2003;278:37459–64.
87. Kalus I, Bormann U, Mzoughi M, Schachner M, Kleene R. Proteolytic cleavage of the neural cell adhesion molecule by ADAM17/TACE is involved in neurite outgrowth. *Journal of Neurochemistry*. 2006;98:78–88.
88. Maretzky T, Schulte M, Ludwig A, Rose-John S, Blobel C, Hartmann D, et al. L1 is sequentially processed by two differently activated metalloproteases

and presenilin/gamma-secretase and regulates neural cell adhesion, cell migration, and neurite outgrowth. *Molecular and Cellular Biology*. 2005;25:9040–53.

89. Rosso O, Piazza T, Bongarzone I, Rossello A, Mezzanzanica D, Canevari S, et al. The ALCAM shedding by the metalloprotease ADAM17/TACE is involved in motility of ovarian carcinoma cells. *Mol. Cancer Res*. 2007;5:1246–53.
90. Miccichè F, Da Riva L, Fabbi M, Pilotti S, Mondellini P, Ferrini S, et al. Activated leukocyte cell adhesion molecule expression and shedding in thyroid tumors. *PLoS ONE*. 2011;6:e17141.
91. Degen WG, van Kempen LC, Gijzen EG, van Groningen JJ, van Kooyk Y, Bloemers HP, et al. MEMD, a new cell adhesion molecule in metastasizing human melanoma cell lines, is identical to ALCAM (activated leukocyte cell adhesion molecule). *Am. J. Pathol*. 1998;152:805–13.
92. Choi S, Kobayashi M, Wang J, Habelhah H, Okada F, Hamada J, et al. Activated leukocyte cell adhesion molecule (ALCAM) and annexin II are involved in the metastatic progression of tumor cells after chemotherapy with Adriamycin. *Clin. Exp. Metastasis*. 2000;18:45–50.
93. Lunter PC, van Kilsdonk JWJ, van Beek H, Cornelissen IMHA, Bergers M, Willems PHGM, et al. Activated leukocyte cell adhesion molecule (ALCAM/CD166/MEMD), a novel actor in invasive growth, controls matrix metalloproteinase activity. *Cancer Research*. 2005;65:8801–8.
94. van Kempen LCLT, Meier F, Egeblad M, Kersten-Niessen MJF, Garbe C, Weidle UH, et al. Truncation of activated leukocyte cell adhesion molecule: a gateway to melanoma metastasis. *J Invest Dermatol*. 2004;122:1293–301.
95. Ofori-Acquah SF, King JA. Activated leukocyte cell adhesion molecule: a new paradox in cancer. *Transl Res*. 2008;151:122–8.
96. Kahlert C, Weber H, Mogler C, Bergmann F, Schirmacher P, Kenngott HG, et al. Increased expression of ALCAM/CD166 in pancreatic cancer is an independent prognostic marker for poor survival and early tumour relapse. *Br J Cancer*. 2009;101:457–64.
97. Wiiger MT, Gehrken HB, Fodstad Ø, Maelandsmo GM, Andersson Y. A novel human recombinant single-chain antibody targeting CD166/ALCAM inhibits cancer cell invasion in vitro and in vivo tumour growth. *Cancer Immunol. Immunother*. 2010;59:1665–74.

98. Ihnen M, Wirtz RM, Kalogeras KT, Milde-Langosch K, Schmidt M, Witzel I, et al. Combination of osteopontin and activated leukocyte cell adhesion molecule as potent prognostic discriminators in HER2- and ER-negative breast cancer. *Br J Cancer*. 2010;103:1048–56.
99. Kristiansen G, Pilarsky C, Wissmann C, Kaiser S, Bruemendorf T, Roepcke S, et al. Expression profiling of microdissected matched prostate cancer samples reveals CD166/MEMD and CD24 as new prognostic markers for patient survival. *J. Pathol*. 2005;205:359–76.
100. Davies SR, Dent C, Watkins G, King JA, Mokbel K, Jiang WG. Expression of the cell to cell adhesion molecule, ALCAM, in breast cancer patients and the potential link with skeletal metastasis. *Oncol Rep*. 2008;19:555–61.
101. Davies S, Jiang WG. ALCAM, activated leukocyte cell adhesion molecule, influences the aggressive nature of breast cancer cells, a potential connection to bone metastasis. *Anticancer Res*. 2010;30:1163–8.
102. Ihnen M, Köhler N, Kersten JF, Milde-Langosch K, Beck K, Höller S, et al. Expression levels of Activated Leukocyte Cell Adhesion Molecule (ALCAM/CD166) in primary breast carcinoma and distant breast cancer metastases. *Dis. Markers*. 2010;28:71–8.
103. Tachezy M, Zander H, Marx AH, Stahl PR, Gebauer F, Izbicki JR, et al. ALCAM (CD166) Expression and Serum Levels in Pancreatic Cancer. Kolligs FT, editor. *PLoS ONE*. 2012;7:e39018.
104. Corrias MV, Gambini C, Gregorio A, Croce M, Barisione G, Cossu C, et al. Different subcellular localization of ALCAM molecules in neuroblastoma: Association with relapse. *Cell. Oncol*. 2010;32:77–86.
105. Ishigami S, Ueno S, Arigami T, Arima H, Uchikado Y, Kita Y, et al. Clinical implication of CD166 expression in gastric cancer. *J Surg Oncol*. 2011;103:57–61.
106. van Kempen LC, van den Oord JJ, van Muijen GN, Weidle UH, Bloemers HP, Swart GW. Activated leukocyte cell adhesion molecule/CD166, a marker of tumor progression in primary malignant melanoma of the skin. *Am. J. Pathol*. 2000;156:769–74.
107. Hong X, Michalski CW, Kong B, Zhang W, Raggi MC, Sauliunaite D, et al. ALCAM is associated with chemoresistance and tumor cell adhesion in pancreatic cancer. *J Surg Oncol*. 2010;101:564–9.
108. Kulasingam V, Zheng Y, Soosaipillai A, Leon AE, Gion M, Diamandis EP. Activated leukocyte cell adhesion molecule: a novel biomarker for breast cancer. *Int. J. Cancer*. 2009;125:9–14.

109. Tachezy M, Zander H, Gebauer F, Marx A, Kaifi JT, Izbicki JR, et al. Activated leukocyte cell adhesion molecule (CD166)-Its prognostic power for colorectal cancer patients. *Journal of Surgical Research*. Elsevier Ltd; 2012;:1–6.
110. Tachezy M, Effenberger K, Zander H, Minner S, Gebauer F, Vashist YK, et al. ALCAM (CD166) expression and serum levels are markers for poor survival of esophageal cancer patients. *Int. J. Cancer*. 2011.
111. Vaisocherová H, Faca VM, Taylor AD, Hanash S, Jiang S. Comparative study of SPR and ELISA methods based on analysis of CD166/ALCAM levels in cancer and control human sera. *Biosens Bioelectron*. 2009;24:2143–8.
112. Witzel I, Schröder C, Müller V, Zander H, Tachezy M, Ihnen M, et al. Detection of Activated Leukocyte Cell Adhesion Molecule in the Serum of Breast Cancer Patients and Implications for Prognosis. *Oncology*. 2012;82:305–12.
113. Hansen AG, Freeman TJ, Arnold SA, Starchenko A, Jones-Paris CR, Gilger MA, et al. Elevated ALCAM shedding in colorectal cancer correlates with poor patient outcome. *Cancer Research*. 2013.
114. Coleman RE. Clinical features of metastatic bone disease and risk of skeletal morbidity. *Clin. Cancer Res*. 2006;12:6243s–6249s.
115. Mehra R, Kumar-Sinha C, Shankar S, Lonigro RJ, Jing X, Philips NE, et al. Characterization of bone metastases from rapid autopsies of prostate cancer patients. *Clin. Cancer Res*. 2011;17:3924–32.
116. Mundy GR. Metastasis to bone: causes, consequences and therapeutic opportunities. *Nat Rev Cancer*. 2002;2:584–93.
117. Pound CR, Partin AW, Eisenberger MA, Chan DW, Pearson JD, Walsh PC. Natural history of progression after PSA elevation following radical prostatectomy. *JAMA*. 1999;281:1591–7.
118. Jin J-K, Dayyani F, Gallick GE. Steps in prostate cancer progression that lead to bone metastasis. *Int. J. Cancer*. 2011;128:2545–61.
119. Pokutta S, Weis WI. Structure and mechanism of cadherins and catenins in cell-cell contacts. *Annu. Rev. Cell. Dev. Biol*. 2007;23:237–61.
120. Hansen A, Swart GW, Zijlstra A. ALCAM. UCSD Nature Molecule Pages [Internet]. 2011. Available from: <http://www.signaling-gateway.org/molecule/query?afcsid=A004126&type=abstract>

121. King JA, Ofori-Acquah SF, Stevens T, Al-Mehdi A-B, Fodstad Ø, Jiang WG. Breast Cancer Res 2004 King. Breast Cancer Res. 2004;6:R478.
122. Minner S, Kraetzig F, Tachezy M, Kilic E, Graefen M, Wilczak W, et al. Low activated leukocyte cell adhesion molecule expression is associated with advanced tumor stage and early prostate-specific antigen relapse in prostate cancer. Hum. Pathol. 2011;42:1946–52.
123. Akhurst RJ, Derynck R. TGF-beta signaling in cancer--a double-edged sword. Trends Cell Biol. 2001;11:S44–51.
124. Derynck R, Akhurst RJ, Balmain A. TGF-beta signaling in tumor suppression and cancer progression. Nat Genet. 2001;29:117–29.
125. Li X, Placencio V, Iturregui JM, Uwamariya C, Sharif-Afshar A-R, Koyama T, et al. Prostate tumor progression is mediated by a paracrine TGF- β /Wnt3a signaling axis. Oncogene. 2008;27:7118–30.
126. Park J-I, Lee M-G, Cho K, Park B-J, Chae K-S, Byun D-S, et al. Transforming growth factor-beta1 activates interleukin-6 expression in prostate cancer cells through the synergistic collaboration of the Smad2, p38-NF-kappaB, JNK, and Ras signaling pathways. Oncogene. 2003;22:4314–32.
127. Ashby WJ, Wikswo JP, Zijlstra A. Magnetically attachable stencils and the non-destructive analysis of the contribution made by the underlying matrix to cell migration. Biomaterials. 2012;33:8189–203.
128. Lin AH, Luo J, Mondschein LH, Dijke ten P, Vivien D, Contag CH, et al. Global analysis of Smad2/3-dependent TGF-beta signaling in living mice reveals prominent tissue-specific responses to injury. J Immunol. 2005;175:547–54.
129. Jameson J. A Role for Skin gamma delta T Cells in Wound Repair. Science. 2002;296:747–9.
130. Li H, Jiang M, Honorio S, Patrawala L, Jeter CR, Calhoun-Davis T, et al. Methodologies in Assaying Prostate Cancer Stem Cells. Methods in Molecular Biology. Totowa, NJ: Humana Press; 2009. pages 85–138.
131. Park SI, Kim SJ, McCauley LK, Gallick GE. Preclinical Mouse Models of Human Prostate Cancer and Their Utility in Drug Discovery. Hoboken, NJ, USA: John Wiley & Sons, Inc; 2011.
132. Varambally S, Yu J, Laxman B, Rhodes DR, Mehra R, Tomlins SA, et al. Integrative genomic and proteomic analysis of prostate cancer reveals signatures of metastatic progression. Cancer Cell. 2005;8:393–406.

133. Nakagawa T, Kollmeyer TM, Morlan BW, Anderson SK, Bergstralh EJ, Davis BJ, et al. A tissue biomarker panel predicting systemic progression after PSA recurrence post-definitive prostate cancer therapy. *PLoS ONE*. 2008;3:e2318.
134. Uhlen M, Oksvold P, Fagerberg L, Lundberg E, Jonasson K, Forsberg M, et al. Towards a knowledge-based Human Protein Atlas. Nature Publishing Group. Nature Publishing Group; 2010;28:1248–50.
135. Kim IY, Ahn HJ, Zelner DJ, Shaw JW, Sensibar JA, Kim JH, et al. Genetic change in transforming growth factor beta (TGF-beta) receptor type I gene correlates with insensitivity to TGF-beta 1 in human prostate cancer cells. *Cancer Research*. 1996;56:44–8.
136. Soond SM, Everson B, Riches DWH, Murphy G. ERK-mediated phosphorylation of Thr735 in TNFalpha-converting enzyme and its potential role in TACE protein trafficking. *Journal of Cell Science*. 2005;118:2371–80.
137. Wang SE, Xiang B, Guix M, Olivares MG, Parker J, Chung CH, et al. Transforming Growth Factor Engages TACE and ErbB3 To Activate Phosphatidylinositol-3 Kinase/Akt in ErbB2-Overexpressing Breast Cancer and Desensitizes Cells to Trastuzumab. *Molecular and Cellular Biology*. 2008;28:5605–20.
138. Ott GR, Asakawa N, Lu Z, Anand R, Liu R-Q, Covington MB, et al. Potent, exceptionally selective, orally bioavailable inhibitors of TNF-alpha Converting Enzyme (TACE): novel 2-substituted-1H-benzo[d]imidazol-1-yl)methyl)benzamide P1' substituents. *Bioorg Med Chem Lett*. 2008;18:1577–82.
139. Wang Y, Xue H, Cutz J-C, Bayani J, Mawji NR, Chen WG, et al. An orthotopic metastatic prostate cancer model in SCID mice via grafting of a transplantable human prostate tumor line. *Lab Invest*. 2005;85:1392–404.
140. Karan D, Lin FC, Bryan M, Ringel J, Moniaux N, Lin M-F, et al. Expression of ADAMs (a disintegrin and metalloproteases) and TIMP-3 (tissue inhibitor of metalloproteinase-3) in human prostatic adenocarcinomas. *Int J Oncol*. 2003;23:1365–71.
141. Baselga J, Rothenberg ML, Tabernero J, Seoane J, Daly T, Cleverly A, et al. TGF-beta signalling-related markers in cancer patients with bone metastasis. *Biomarkers*. 2008;13:217–36.
142. Jin R, Sterling JA, Edwards JR, Degraff DJ, Lee C, Park SI, et al. Activation of NF-kappa B Signaling Promotes Growth of Prostate Cancer Cells in Bone. *PLoS ONE*. 2013;8:e60983.

143. Wang J, Gu Z, Ni P, Qiao Y, Chen C, Liu X, et al. NF-kappaB P50/P65 hetero-dimer mediates differential regulation of CD166/ALCAM expression via interaction with microRNA-9 after serum deprivation, providing evidence for a novel negative auto-regulatory loop. *Nucleic Acids Res.* 2011;39:6440–55.
144. Domingo-Domenech J, Mellado B, Ferrer B, Truan D, Codony-Servat J, Sauleda S, et al. Activation of nuclear factor-kappaB in human prostate carcinogenesis and association to biochemical relapse. *Br J Cancer.* 2005;93:1285–94.
145. Domingo-Domenech J, Oliva C, Rovira A, Codony-Servat J, Bosch M, Filella X, et al. Interleukin 6, a nuclear factor-kappaB target, predicts resistance to docetaxel in hormone-independent prostate cancer and nuclear factor-kappaB inhibition by PS-1145 enhances docetaxel antitumor activity. *Clin. Cancer Res.* 2006;12:5578–86.
146. Lessard L, Bégin LR, Gleave ME, Mes-Masson A-M, Saad F. Nuclear localisation of nuclear factor-kappaB transcription factors in prostate cancer: an immunohistochemical study. *Br J Cancer.* 2005;93:1019–23.
147. Lessard L, Karakiewicz PI, Bellon-Gagnon P, Alam-Fahmy M, Ismail HA, Mes-Masson A-M, et al. Nuclear localization of nuclear factor-kappaB p65 in primary prostate tumors is highly predictive of pelvic lymph node metastases. *Clin. Cancer Res.* 2006;12:5741–5.
148. Jezierska A, Matysiak W, Motyl T. ALCAM/CD166 protects breast cancer cells against apoptosis and autophagy. *Med. Sci. Monit.* 2006;12:BR263–73.
149. Nguyen DX, Bos PD, Massagué J. Metastasis: from dissemination to organ-specific colonization. *Nat Rev Cancer.* 2009;9:274–84.
150. Masedunskas A, King JA, Tan F, Cochran R, Stevens T, Sviridov D, et al. Activated leukocyte cell adhesion molecule is a component of the endothelial junction involved in transendothelial monocyte migration. *FEBS Lett.* 2006;580:2637–45.
151. Buijs JT, Stayrook KR, Guise TA. The role of TGF- β in bone metastasis: novel therapeutic perspectives. *BoneKey Reports.* Nature Publishing Group; 2012;1:1–10.
152. Siegel R, Ward E, Brawley O, Jemal A. Cancer statistics, 2011. *CA: A Cancer Journal for Clinicians.* 2011;61:212–36.
153. Compton CC. Colorectal Carcinoma: Diagnostic, Prognostic, and Molecular Features. *Mod Pathol.* 2003;16:376–88.

154. Quasar Collaborative Group, Gray R, Barnwell J, McConkey C, Hills RK, Williams NS, et al. Adjuvant chemotherapy versus observation in patients with colorectal cancer: a randomised study. *Lancet*. 2007;370:2020–9.
155. Figueredo A. Adjuvant Therapy for Stage II Colon Cancer: A Systematic Review From the Cancer Care Ontario Program in Evidence-Based Care's Gastrointestinal Cancer Disease Site Group. *Journal of Clinical Oncology*. 2004;22:3395–407.
156. Midgley R, Kerr DJ. Adjuvant chemotherapy for stage II colorectal cancer: the time is right! *Nat Clin Pract Oncol*. 2005;2:364–9.
157. Johnston PG. Stage II colorectal cancer: to treat or not to treat. *Oncologist*. 2005;10:332–4.
158. Eschrich S. Molecular Staging for Survival Prediction of Colorectal Cancer Patients. *Journal of Clinical Oncology*. 2005;23:3526–35.
159. Smith JJ, Deane NG, Wu F, Merchant NB, Zhang B, Jiang A, et al. Experimentally Derived Metastasis Gene Expression Profile Predicts Recurrence and Death in Patients With Colon Cancer. *Gastroenterology*. Elsevier Inc; 2010;138:958–68.
160. Ogino S, Nosho K, Irahara N, Shima K, Baba Y, Kirkner GJ, et al. Prognostic Significance and Molecular Associations of 18q Loss of Heterozygosity: A Cohort Study of Microsatellite Stable Colorectal Cancers. *Journal of Clinical Oncology*. 2009;27:4591–8.
161. Gerger A, Zhang W, Yang D, Bohanes P, Ning Y, Winder T, et al. Common cancer stem cell gene variants predict colon cancer recurrence. *Clin. Cancer Res*. 2011;17:6934–43.
162. Lugli A, Iezzi G, Hostettler I, Muraro MG, Mele V, Tornillo L, et al. Prognostic impact of the expression of putative cancer stem cell markers CD133, CD166, CD44s, EpCAM, and ALDH1 in colorectal cancer. *Br J Cancer*. Nature Publishing Group; 2010;103:382–90.
163. Piao D, Jiang T, Liu G, Wang B, Xu J, Zhu A. Clinical implications of activated leukocyte cell adhesion molecule expression in breast cancer. *Mol Biol Rep*. 2012;39:661–8.
164. Zhang T-C, Zhu W-G, Huang M-D, Fan R-H, Chen X-F. Prognostic value of ADAM17 in human gastric cancer. *Med Oncol*. 2011.
165. Smedbakken L, Jensen JK, Hallen J, Atar D, Januzzi JL, Halvorsen B, et al. Activated Leukocyte Cell Adhesion Molecule and Prognosis in Acute Ischemic Stroke. *Stroke*. 2011;42:2453–8.

166. Hollmén M, Määttä JA, Bald L, Sliwkowski MX, Elenius K. Suppression of breast cancer cell growth by a monoclonal antibody targeting cleavable ErbB4 isoforms. *Oncogene*. 2009;28:1309–19.
167. Swart GWM. Activated leukocyte cell adhesion molecule (CD166/ALCAM): developmental and mechanistic aspects of cell clustering and cell migration. *European Journal of Cell Biology*. 2002;81:313–21.
168. Ihnen M, Müller V, Wirtz RM, Schröder C, Krenkel S, Witzel I, et al. Predictive impact of activated leukocyte cell adhesion molecule (ALCAM/CD166) in breast cancer. *Breast Cancer Res Treat*. 2008;112:419–27.
169. Hanahan D, Weinberg RA. Hallmarks of cancer: the next generation. *Cell* [Internet]. 2011;144:646–74. Available from: <http://dx.doi.org/10.1016/j.cell.2011.02.013>
170. Cheng L, Wu Q, Huang Z, Guryanova OA, Huang Q, Shou W, et al. L1CAM regulates DNA damage checkpoint response of glioblastoma stem cells through NBS1. *EMBO J*. Nature Publishing Group; 2011;30:800–13.
171. Scott SL, Earle JD, Gumerlock PH. Functional p53 increases prostate cancer cell survival after exposure to fractionated doses of ionizing radiation. *Cancer Research*. 2003;63:7190–6.
172. Campodónico PB, de Kier Joffé EDB, Urtreger AJ, Lauria LS, Lastiri JM, Puricelli LI, et al. The neural cell adhesion molecule is involved in the metastatic capacity in a murine model of lung cancer. *Mol. Carcinog*. 2010;49:386–97.
173. Riedle S, Kiefel H, Gast D, Bondong S, Wolterink S, Gutwein P, et al. Nuclear translocation and signalling of L1-CAM in human carcinoma cells requires ADAM10 and presenilin/gamma-secretase activity. *Biochem. J*. 2009;420:391–402.
174. Elmore S. Apoptosis: a review of programmed cell death. *Toxicol Pathol*. 2007;35:495–516.
175. Jezierska A, Olszewski WP, Pietruszkiewicz J, Olszewski W, Matysiak W, Motyl T. Activated Leukocyte Cell Adhesion Molecule (ALCAM) is associated with suppression of breast cancer cells invasion. *Med. Sci. Monit*. 2006;12:BR245–56.
176. Lowe SW, Lin AW. Apoptosis in cancer. *Carcinogenesis*. 2000;21:485–95.
177. Wang Y, Wang X, Zhao H, Liang B, Du Q. Clusterin confers resistance to TNF-alpha-induced apoptosis in breast cancer cells through NF-kappaB activation and Bcl-2 overexpression. *J Chemother*. 2012;24:348–57.

178. Verheij M, Bose R, Lin XH, Yao B, Jarvis WD, Grant S, et al. Requirement for ceramide-initiated SAPK/JNK signalling in stress-induced apoptosis. *Nature*. 1996;380:75–9.
179. Littlepage LE, Sternlicht MD, Rougier N, Phillips J, Gallo E, Yu Y, et al. Matrix metalloproteinases contribute distinct roles in neuroendocrine prostate carcinogenesis, metastasis, and angiogenesis progression. *Cancer Research*. 2010;70:2224–34.
180. Sugimura R, Li L. Bone Metastasis Targets The Endosteal Hematopoietic Stem Cell Niche. *IBMS BoneKEy*. 2011;8:381–4.
181. Wang J, Loberg R, Taichman RS. The pivotal role of CXCL12 (SDF-1)/CXCR4 axis in bone metastasis. *Cancer Metastasis Rev*. 2006;25:573–87.
182. Taichman RS. Blood and bone: two tissues whose fates are intertwined to create the hematopoietic stem-cell niche. *Blood*. 2005;105:2631–9.
183. Patel LR, Camacho DF, Shiozawa Y, Pienta KJ, Taichman RS. Mechanisms of cancer cell metastasis to the bone: a multistep process. *Future Oncol*. 2011;7:1285–97.
184. GOODMAN JW, HODGSON GS. Evidence for stem cells in the peripheral blood of mice. *Blood*. 1962;19:702–14.
185. Wright DE, Wagers AJ, Gulati AP, Johnson FL, Weissman IL. Physiological migration of hematopoietic stem and progenitor cells. *Science*. 2001;294:1933–6.
186. Shiozawa Y, Pedersen EA, Havens AM, Jung Y, Mishra A, Joseph J, et al. Human prostate cancer metastases target the hematopoietic stem cell niche to establish footholds in mouse bone marrow. *J Clin Invest*. 2011;121:1298–312.
187. Song J, Kiel MJ, Wang Z, Wang J, Taichman RS, Morrison SJ, et al. An in vivo model to study and manipulate the hematopoietic stem cell niche. *Blood*. 2010;115:2592–600.